THE CHARACTERISTICS OF THERMAL RESPOND DURING MICROWAVE ABLATION PROCESS USING SLOT ANTENNA IN LIVER TISSUE: BIOHEAT MODEL EMBEDDED WITH LARGE BLOOD VESSELS & POROUS LIVER MODEL

BY

MR. WUTIPONG PREECHAPHONKUL

A DISSERTATION SUBMITTED IN PARTIAL FULFILLMENT OF THE REQUIREMENTS FOR THE DEGREE OF DOCTOR OF PHILOSOPHY PROGRAM IN ENGINEERING

FACULTY OF ENGINEERING

THAMMASAT UNIVERSITY

ACADEMIC YEAR 2020

THE CHARACTERISTICS OF THERMAL RESPOND DURING MICROWAVE ABLATION PROCESS USING SLOT ANTENNA IN LIVER TISSUE: BIOHEAT MODEL EMBEDDED WITH LARGE BLOOD VESSELS & POROUS LIVER MODEL

BY

MR. WUTIPONG PREECHAPHONKUL

A DISSERTATION SUBMITTED IN PARTIAL FULFILLMENT OF THE REQUIREMENTS FOR THE DEGREE OF DOCTOR OF PHILOSOPHY PROGRAM IN ENGINEERING

FACULTY OF ENGINEERING

THAMMASAT UNIVERSITY

ACADEMIC YEAR 2020

THAMMASAT UNIVERSITY

FACULTY ENGINEERING

DISSERTATION

BY

MR WUTIPONG PREECHAPHONKUL

ENTITLED

THE CHARACTERISTICS OF THERMAL RESPOND DURING MICROWAVE ABLATION PROCESS USING SLOT ANTENNA IN LIVER TISSUE: BIOHEAT MODEL EMBEDDED WITH LARGE BLOOD VESSELS & POROUS LIVER MODEL

was approved as partial fulfillment of the requirements for the degree of Doctor of Philosophy Program in Engineering

on March 16, 2021

Chairman

(Associate Professor Wiroj Limtrakarn, Ph.D.)

Member and Advisor

(Professor Phadungsak Rattanadecho, Ph.D.)

Member

(Associate Professor Watit Pakdee, Ph.D.)

Member

(Assistant Professor Sappinandana Akamphon, Ph.D.)

Member

(Assistant Professor Pornthip Keangin, Ph.D.)

Dean

(Associate Professor Thira Jearsiripongkul, Dr. - ing.)

Dissertation Title	THE CHARACTERISTICS OF THERMAL RESPOND DURING MICROWAVE ABLATION PROCESS USING SLOT ANTENNA IN DEFORMABLE LIVER TISSUE: BIOHEAT MODEL EMBEDDED WITH LARGE BLOOD VESSELS & POROUS LIVER
Author	MR. WUTIPONG PREECHAPHONKUL
Degree	Doctor of Philosophy
Major Field/Faculty/University	Engineering Faculty engineering Thammasat University
Dissertation Advisor	Professor Phadungsak Rattanadecho, Ph.D.
Academic Year	2020

ABSTRACT

Microwave ablation (MWA) is a minimally invasive cancer treatment technique that induces thermal injury into the tumor by using microwave energy. This treatment applies microwave energy to the tumor by using the microwave antenna. The microwave energy is absorbed and converted to heat generation in the unwanted tissue. The goal of this treatment is to generate heat damaged by microwave energy in the tumor and unwanted heat to the surrounding tissue. The advantages of this treatment are rapid, effective, and non-toxic side effects. However, microwave ablation has dangerous when used incorrect conditions during treatment. Therefore, the studies of correct conditions are necessary. The modeling for heat transport in the biological tissue was applied in the therapeutics application for preventing injury and analyzing the effectiveness of the treatment process. However, the specific treatment area and comparative studies of the heating models were not investigated systematically. This dissertation presented the numerical analysis of specific absorption rate and heat transfer in liver cancer during MWA treatment by using a coaxial slot antenna. The mathematical model is considered coupled with the electromagnetic wave propagation

and heat transfer in the biological tissue. The coupled nonlinear set of these equations is solved using the finite element method (FEM). The influence of the large vessel locality was systematically investigated on the specific absorption rate and heat transfer in the 3D liver cancer domain. The results show the volumetric of damaged tissue in the model with a vertical blood vessel is lower than the model with a horizontal vessel. Furthermore, this result presented the asymmetrical temperature distribution, which indicated the necessity for the 3D assumption.

Moreover, this dissertation presented the comparative performance of the thermal model during the MWA process. The comparative thermal models implemented in this work were the bioheat model, the porous media model with constant velocity, and the Darcy-Brinkman porous model in the liver cancer model during the MWA process. The results show the Darcy-Brinkman porous model has a flexible use than the porous model with constant velocity and the bioheat model. The Darcy-Brinkman porous model was effective in various situations of predictions as compared to other models, since the role of conduction and the role of convection were combined. The value of the dissertation provides an indication of limitations that must be considered in administering microwave ablation therapy.

Keywords: Microwave ablation (MWA), heat transfer, Bioheat, Porous media, 3D Numerical simulation, FEM, Comparative thermal model, Local thermal equilibrium (LTE), Liver cancer, Thermal ablation

ACKNOWLEDGEMENTS

I would like to express my deepest gratitude to my advisor, Prof.Dr.Phadungsak Rattanadecho, of the Department of Mechanical Engineering, Thammasat University, for giving me the opportunity to work with him, and his invaluable guidance.

I also would like to appreciate my committees Assoc.Prof.Dr.Wiroj Limtrakarn, Assoc.Prof.Dr.Watit Pakdee, Asst.Prof.Dr.Sappinandana Akamphon, and Asst.Prof.Dr.Pornthip Keangin for accepting to participate as members in my graduate committees. Their comments are helpful throughout the period of my study.

My sincere thanks always remain with all members of the Research Center of Microwave Utilization in Engineering (R.C.M.E.), and many others for always being there, especially Mr. Niti Shaichompu, Mr. Chayanon Serttikul, Miss Thanaporn Jullabuth, Mr. Navapol Rodsomjit, Mr. Vanakorn Mongkol, as well as for constant entertaining moments we shared throughout the years.

I gratefully thank for the support from family, especially Mrs. Nam-ngern Preechaphonkul, who is supporting me in everything.

Furthermore, I gratefully acknowledge Thammasat university and Thailand Science Research and Innovation (under the Royal Golden Jubilee Ph.D. Program (RGJ) grant number PHD/0055/2558) for the financial support.

Mr. Wutipong Preechaphonkul

TABLE OF CONTENTS

	Page
ABSTRACT	-1-
ACKNOWLEDGEMENTS	-3-
LIST OF TABLES	-8-
LIST OF FIGURES	-9-
LIST OF ABBREVIATIONS	-11-
CHAPTER 1 INTRODUCTION	1
1.1 Introduction to the liver cancer treatment and modeling	1
1.2 Introduction to the microwave	7
1.3 Introduction to the microwave ablation	8
1.4 Research objectives	10
1.5 Scope of research	10
1.6 Expected benefits	11
1.7 Research procedure	11
CHAPTER 2 REVIEW OF LITERATURE	13
2.1 Introduction to the liver cancer treatment and modeling	13
2.2 Introduction to the microwave	27
CHAPTER 3 THEORIES AND MATHERMATICAL MODEL	34

3.1The modeling of electromagnetic wave propagation 34
3.2 The modeling of heat transfer in the biological tissue using simplified approach 37
3.2.1 Pennes bioheat model 37
3.2.2 Wulff continuum model 37
3.2.3 Klinger continuum model 38
3.2.4 The Continuum model of Chen and Holmes 39
3.2.5 Weinbaum, Jiji, and Lemons (WJL) Bioheat Model 42
3.2.6 The Weinbaum and Jiji (WJ) Bioheat Model 43
3.2.7 The heat transfer of large vessel flow 44
3.2 The modeling of heat transfer in the biological tissue using porous media approach 45
3.2.1 Local thermal equilibrium (LTE) model 47
3.2.2 Local thermal non-equilibrium (LTNE) model 48
3.2.3 Flow convection in biological tissues 49

CHAPTER 4 3D NUMERICAL ANALYSIS OF FOCUSED MICROWAVE ABLATION FOR THE TREATMENT OF PATIENTS WITH LOCALIZED LIVER CANCER EMBEDDED WITH A VERTICAL AND HORIZONTAL BLOOD VESSEL 51

4.1 Introduction 51
4.2 Problem statement 53
4.3 The formulation and the mathematical model 55
4.3.1 The physical model 56
4.3.2 The electromagnetic wave propagation analysis 56
4.3.3 The heat transfer in the living tissue analysis 59
4.3.4 The heat transfer and blood flow analysis of blood vessel 62
4.3.5 The thermal damaged tissue analysis 64
4.3.6 Initial condition 64

4.4 Calculation procedure 64
4.5 Results and discussion 66
4.5.1 The verification of the model 66
4.5.2 The electromagnetic wave propagation analysis 67
4.5.3 The heat transfer analysis 69
4.5.4 The damaged tissue analysis 72
4.6 Conclusion 74

CHAPTER 5 THE COMPARATIVE OF THE PERFORMANCE FOR PREDICTED THERMAL MODELS DURING MICROWAVE ABLATION PROCESS USING A SLOT ANTENNA 76

5.1 Introduction 76
5.2 Modeling and formulation 79
5.2.1 Problem description 80
5.2.2 Equations of electromagnetic wave propagation analysis 81
5.2.2.1 Governing equation and assumptions of electromagnetic wave propagation analysis 82
5.2.2.2 Boundary conditions of electromagnetic wave propagation analysis 84
5.2.3 Equations of heat transfer and blood flow analysis 85
5.2.3.1 Governing equation and assumptions of heat transfer and blood flow analysis 85
5.2.3.2 Boundary conditions of heat transfer and blood flow analysis 88
5.2.4 Initial condition 90
5.3 Calculation procedure 90
5.4 Results and discussion 91
5.4.1 The verification of the model 91

5.4.2 The comparative of the performance of thermal models 94
electromagnetic wave propagation analysis
5.5 Conclusion 100

CHAPTER 6 OVERALL CONCLUSIONS AND 103
RECOMMENDATIONS FOR FUTURE WORK

REFERENCES 108

APPENDICES

APPENDIX A 125

BIOGRAPHY 133

LIST OF TABLES

Tables	Page
2.1 Summarizes studies of heat transfer in the biological tissue based on the simplified approach	23
2.1 Summarizes studies of heat transfer in the biological tissue based on the simplified approach	32
4.1 Dimensions and dielectric properties of single slot MCA	58
4.2 The dielectric and thermal properties of the tissue	63
5.1 Dimensions and dielectric properties of single slot MCA	85
5.2 The dielectric and thermal properties of the tissue	86
5.3 Comparisons of RMSE of the liver tissue temperature between the presented model and Yang et al.	98

LIST OF FIGURES

Figures	Page
1.1 Estimated number of cancer cases in 2020 by World Health organization (WHO); (a) number of cancer new cases, (b)) number of death cases by cancer	1
1.2 The cancer treatment by percutaneous ethanol ablation	4
1.3 The experimental study of the MWA process in the bovine liver obtained by the Center of Excellence in Electromagnetic Energy Utilization in Engineering (CEEE) lab, Thammasat university	7
1.4 The liver cancer with the MWA treatment concept to the 3D mathematical modeling; (a) The liver cancer with the MWA treatment, (b) The control volume mathematical modeling of the liver cancer with the MWA treatment.	8
1.5 Electromagnetic spectrum	9
1.6 The equipments of the MWA system at Office of Advanced Science and Technology, Thammasat University; (a) the microwave generator (Acculis, AngioDynamics, 60-140 W, 2.45 GHz), (b) microwave antenna (Accu2i PMTA Applicator)	11
1.7 Research procedures	15
3.1 Schematic view of biological tissue	49
4.1 The liver cancer with the MWA treatment concept to the 3D mathematical model.	57
4.2 The physical domain and boundary conditions of the liver cancer embedded with a single blood vessel model; (a) the model with a vertical vessel, (b) the model with a horizontal vessel.	59
4.3 Grid independence test	70
4.4 The validation results of the calculated tissue temperature to the tissue temperature obtained by Yang et al.	71

4.5 The SAR distribution at the cross-section plane with microwave power of 10 W, and frequency of 2.45 GHz; (a) the model with a vertical vessel, (b) the model with a horizontal vessel. 72

4.6 SAR profile at the insertion depth line between the model embedded with a vertical and horizontal vessel with microwave power of 10 W, and frequency of 2.45 GHz. 73

4.7 Temperature and velocity fields at the cross-section plane with microwave power of 10 W, frequency of 2.45 GHz, and heating time of 10 min; (a) the model with a vertical vessel, (b) the model with a horizontal vessel. 74

4.8 The comparison of the transient temperature at the selected points between model with a vertical and horizontal vessel with microwave power of 10 W, frequency of 2.45 GHz 74

4.9 The transient temperature difference of the selected points between model with a horizontal and vertical vessel with microwave power of 10 W, and frequency of 2.45 GHz 75

4.10 The fraction of damaged tissue distribution and velocity arrow at the cross- section plane with microwave power of 10 W, frequency of 2.45 GHz, and heating time of 10 min; (a) the model with a vertical vessel, (b) the model with a horizontal vessel. 77

4.11 The comparison volumetric of damaged tissue between the model with a vertical and horizontal vessel, with microwave power of 10 W, frequency of 2.45 GHz 78

5.1 The physical domain and boundary conditions of porous liver cancer model with MWA; (a) The physical domain, (b) The boundary conditions 87

5.2 Grid independence test 97

5.3 The validation results of the calculated tissue temperature to the tissue temperature obtained by Yang et al. 98

5.4 The temperature distribution and velocity vector of the difference liver cancer models with MWA for a heating time of 1, 3, and 5 min, the microwave power of 10 W, and frequency of 2.45 GHz. 99

5.5 The SAR distribution of the difference liver cancer models at the insertion depth line with MW power of 10 W, and frequency of 2.45 GHz. 101

5.6 The temperature distribution of the difference liver cancer models at the insertion depth line with MW power of 10 W, and frequency of 2.45 GHz. 102

5.7 The temperature distribution of the difference liver cancer models along at the monitoring points for a heating time of 1, 3, 5 min with the MW power of 10 W, and frequency of 2.45 GHz. 103

5.8 The percentage of the damaged area in the difference liver cancer models with the MW power of 10 W and the MW frequency of 2.45 GHz. 104

5.9 The RMSE of the comparative temperatures with the different thermal models implemented in the liver cancer model with MW ablation for the MW power of 10 W and the MW frequency of 2.45 GHz 105

7.1 The granted award from International Exhibition and Invention of Geneva 2019 140

LIST OF ABBREVIATIONS

Symbols/Abbreviations	Terms
A	frequency factor (1/s)
a_{tb}	specific surface area between the blood and the tissue (m^2/m^3)
$\vec{B}$	magnetic flux density vector (Wb/m^2)
C	arbitrary constant
c	speed of light in free space (m/s)
C_p	specific heat capacity (J/kg· ºC)
$\vec{D}$	electric flux density vector (C/m^2)
d_p	diameter of tissue cells (m)
$\vec{E}$	electric field intensity vector (V/m)
E_a	activation energy (J/mol)
$\vec{e}$	unit vector of cylindrical coordinates
f	electromagnetic wave frequency (Hz)
g	standard gravity (m/s^2)
$\vec{H}$	magnetic field intensity vector (A/m)
h_{tb}	the blood to tissue interfacial heat transfer coefficient (W/m^2·ºC)
$\vec{J}$	density of free currents (A/m^2)
k	wave propagation constant (m^{-1})
k_{th}	thermal conductivity (W/m·ºC)
$\hat{n}$	unit vector on normal conditions
P	Pressure (Pa)
P_{in}	microwave power input (W)
Q	heat source (W/m^3)
q	density of free charges (C/m^3)
R	universal gas constant (J/mol.K)

r	dielectric radius (m)
Re	real part of complex number
T	temperature (ºC)
t	time (s)
u	blood velocity (m/s)
$\vec{V}$	blood velocity vector (m/s)
x	x-coordinate (m)
y	y-coordinate (m)
Z	wave impedance (Ω)
z	z-coordinate (m)

Greek symbols

β	coefficient of thermal expansion (1/K)
ε	permittivity (F/m)
θ_p	fraction of necrotic tissue
κ	permeability (m^2)
λ	wavelength (m)
λ^*	tortuosity
ρ	density (kg/m^3)
σ_{el}	electrical conductivity (S/m)
μ	dynamic viscosity (Pa.s)
ϕ	porosity of porous media
Ω	cumulative tissue damage
ω	blood perfusion rate (1/s)

Subscripts

b	blood phase
eff	effective
ext	external

inner	inner
met	metabolic
outer	outer
r	relative
r, z, ϕ	component of cylindrical coordinates
t	tissue
0	free space, initial condition
1, 2	domains, which contacted

CHAPTER 1
INTRODUCTION

1.1 Introduction to the liver cancer treatment and modeling

Based on the World Health Organization (WHO) report on cancer, cancer is the second leading cause of death globally. In 2018, the people about 9.6 million people died from cancer or one in six global deaths due to cancer. Many people have suffered from cancer. In this report, cancer cases are growing globally, and approximately 70% of cancer deaths occurred in low- and middle-income countries. In the high-income countries where the health systems are robust, the survival rate of cancer is improving. In the high-income countries where the health systems are robust, the survival rate of cancer is improving. That because many patients have access to early detection and quality of cancer treatment. On the other hand, the health systems of the low- and middle-income countries are least prepared to manage the cancer burden. Large numbers of cancer patients of these countries could not have access to timely quality diagnosis and treatment. Therefore, cancer is one of the most important problems facing this world today.

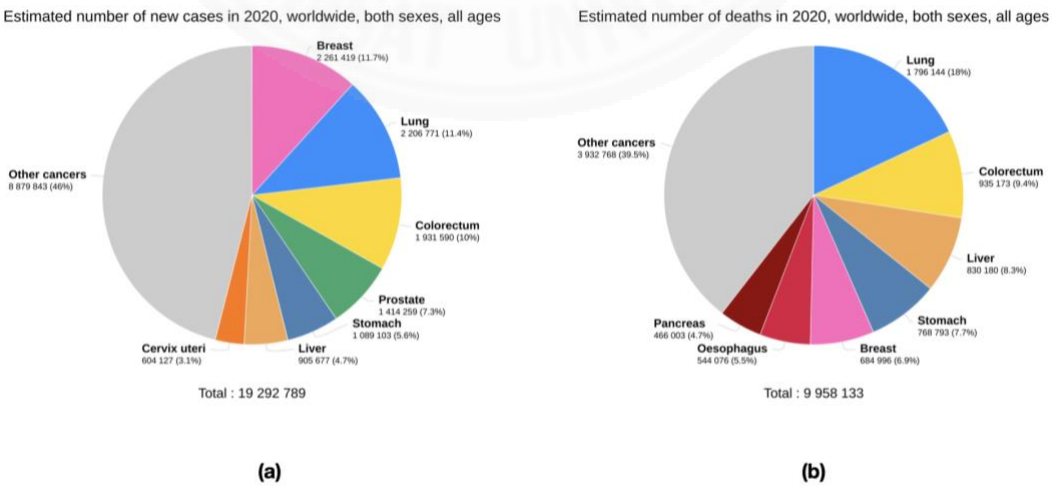

Fig. 1.1 Estimated number of cancer cases in 2020 by World Health Organization (WHO); (a) number of cancer new cases, (b)) number of death cases by cancer

Liver cancer is the sixth most common cancer incidence worldwide (Ananthakrishnan et al., 2006), but it is the second leading cause of death by cancers (Sia et al., 2018). Liver cancer is one of few cancers' disease increasing new incidence cases and the greatest increase in mortality during the past 2 decades (Llovet et al. 2016). Liver cancer is generally classified as a primary or secondary liver cancer. Primary liver cancer begins in the cells of the liver transformation of normal cells into diseased tissue (tumor cell) in a multistage process that generally progresses from a pre-cancerous lesion to a malignant tumor (Ananthakrishnan et al., 2006). Secondary liver cancer begins primary liver cancer or tumor at the liver organ spreading out of the liver to another part of the body. Liver cancer consists of a heterogeneous group of malignant tumors with different histological characteristics and an unfavorable prognosis that range from hepatocellular carcinoma (HCC) and intrahepatic cholangiocarcinoma (iCCA) to mixed hepatocellular cholangiocarcinoma (HCC- CCA), fibrolamellar HCC (FLC), and the pediatric neoplasm hepatoblastoma (Bosman et al., 2010; Lozano et al., 2012). In all of the liver cancer categories, the HCC is most of the common liver cancer. Approximately 90% of liver cancer cases are HCC types, with nearly 800,000 new cases annually (Llovet et al. 2016). The iCCA is the second most common liver cancer, with the highest incidence in Southeast Asia and low incidence in Western countries (Bridgewater et al., 2014). The information from both the Surveillance, Epidemiology, and End Results (SEER) and Eurocare occur that primary liver cancer has the lowest overall survival rate worldwide among the 11 most common cancers. The mortality rate with liver cancer approximately less than 10% 5-year survival (Parkin et al., 2005). Furthermore, the liver cancer burden is increasing globally, and Torre et al. was projection there could be 1 million cases by 2030 (Torre et al., 2015). In the untreated cases, liver cancer has a mortality rate of 100% at 5 years (McGahan & Dodd lII, 2001). Therefore, the liver cancer is necessary to treated.

Liver cancer is treated with many types of treatment. Cancer treatment uses surgery resection, radiation, medications, and other therapies to treat cancer, shrink cancer, stop cancer progression, and improve life quality. Types of cancer treatments depend on the particular situation. The patients may receive one treatment or a combination of treatments, such as surgical resection with chemotherapy or radiation

therapy. The treatment options will depend on several factors, such as the type and stage of cancer, the general health of patients, genetic, sizes, numbers, and position of cancer. Surgical resection is the first considered option for cancer treatment (Bruix et al., 2004), the achievement of this method about 60 to 70% 5-year survival in well-selected patients (Bruix et al., 2001; Bruix, 2005). This treatment is limited for patients with a single tumor and well-preserved liver function, who have neither abnormal bilirubin nor clinically relevant portal hypertension (Lencioni & Crocetti, 2007). Liver transplantation is a cancer treatment that benefits patients who have decompensated cirrhosis and one tumor smaller than 5 cm or up to three tumors smaller than 3 cm each. In this treatment, the inherent limitations are required a highly skilled surgical team and living donation, which donor short age greatly limits its applicability. Chemotherapy is one option for unresectable or medically untreatable patients, but it is not entirely satisfactory in terms of survival rate outcomes (Lencioni & Crocetti, 2007).

The coming of image-guided technology such as ultrasound, computed tomography (CT) or magnetic resonance imaging (MRI) was used in the health care system, which leads to the possibility of new treatment methods. Later, alternative cancer treatment methods were developed and presented as optional for patients who cannot treat by surgery. The different treatment methods have different therapy mechanisms, which led to different survival rates, complications, and reoccurrence. The percutaneous ethanol injection is a local ablative method for patients that are not surgical candidates. In this method, the alcohol is injected directly into the tumor through the thin needle guided by ultrasound or computed tomography (Ansari & Andersson, 2012). In this method, the alcohol is injected directly into the tumor through the thin needle guided by ultrasound or computed tomography, as shown in Fig. 1.2. The alcohol injection was induced tumor destruction by dehydration and protein denaturation (Ebara et al., 2005). Although the percutaneous ethanol injection is less invasive and may be associated with reduced postoperative pain and fewer complications, the other ablative methods are more accurate and effective than the percutaneous ethanol injection methods. Furthermore, the limitations of this method cannot be applied to tumor size over 3 cm and the leaked of alcohol during treatment method (Ansari & Andersson, 2012).

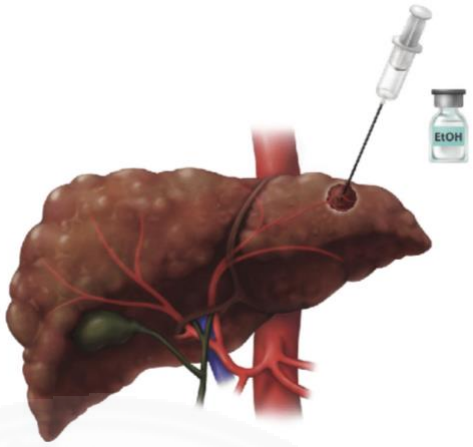

Fig. 1.2 The cancer treatment by percutaneous ethanol ablation (Voizard et al., 2019)

Cryosurgery also called cryoablation, or cryotherapy is a minimally invasive cancer treatment method that uses extreme cold to deep freezing and destruction tumor, including cancer cell. This treatment method is inserted the cryoprobe into the tumor area by using imaging guidance. The cryofluid as such as liquid nitrogen or high-pressure argon gas are fed into a cryoprobe that creating deep freezing that is area at contact with tumor (Yiu et al., 2007). The benefits of this treatment method are less invasive and may be associated with reduced postoperative pain, fewer complications, shorter hospital stay, and reduced costs (Ebara et al., 2005; Nabaei & Karimi, 2018; Shao et al., 2018). However, this treatment shortcoming is the surrounding tissue may be injured during the treatment process, and the cryosurgery cannot guarantee completely lethal damage to the entire tumor domain (Baust et al., 1997; Di et al., 2012).

Radiofrequency ablation (RFA) is a minimally invasive cancer treatment method that induces the thermal injury into the tumor using the electromagnetic energy with the frequency range of 350–500 kHz (Sabiston et al., 2001). RFA is a lower risk of complications when comparative with cryosurgery treatment (Wu et al., 2015). This treatment method is inserted the RFA electrodes directly into the tumor by using imaging guidance. The temperature of disease tissue surrounding the electrodes is increased by electrical energy and causes resistive heating (Curley et al., 2000). When the tumor temperatures exceed 50°C for more than 3 minutes, intracellular protein

denaturation and melting of lipid bilayers result in direct tumor cell is death. (McGahan et al., 1990; Rossi et al., 1990; Sanchez et al., 1993; Lounsberry, 1995). Although RFA is an effective cancer treatment method, it has limitations. For the larger tumor (usually defined to be larger than 3-5 cm in diameter) and the specific area near the large blood vessels, this treatment may not be suitable for the entirety encompassing the tumor volume (Brace, 2009; Ahmed & Goldberg, 2011).

Microwave ablation (MWA) is a minimally invasive cancer treatment method that induces thermal injury into the tumor, as same as RFA. MWA has applied the microwave energy into the diseased tissue or tumor area through the microwave antenna. The microwave would be absorbed and converted to the local heat generation in the tumor area (Keangin et al., 2011, Rattanadecho & Keangin, 2013). The tissue temperature rises to 52 ºC for a heating time of 1 min, or the instantaneous tissue temperature exceeds 54 ºC, the cell will be killed immediately (Dong et al., 1998; Goldberg et al., 2000; Whelan et al. 2005; Prakash et al., 2008; Prakash et al., 2012; Wu et al., 2013). Although MWA and RFA can heat the tumor to cytotoxic levels, the mechanisms of MWA and RFA are quite different. The primary distinction between RFA and MWA is that RFA heating occurs in the area with high current density, while MWA is heating around the slot of an antenna (Brace, 2009). That because the mechanism of heating methods is different. MWA induced the heating by electromagnetic field mechanism as opposed to the electrical current mechanism used in RFA (Poulou et al., 2015). The benefits of MWA are short ablation time, a short recovery period, less postoperative pain, and fewer complications that may be related to a minimally invasive treatment method. Comparative with RFA, MWA is a faster treatment time, higher flexible treatment, a larger zone of ablation, and a complete tumor kill (Wright et al., 2005; Liang & Wang, 2007; Izzo et al., 2019).

MWA has powerful treatment method and many advantages compared with conventional treatment for localized liver cancer. However, MWA has dangerous when used incorrect conditions during treatment, such as the heat spread over the boundaries of the tumor area. When the heat spread over the boundaries of the tumor, the temperature of healthy tissue is rising (Poulou et al., 2015). The increase of the healthy tissue temperature is resulting in the protein denaturation process, which is dangerous on the healthy tissue. Therefore, the studies of correct conditions are necessary.

Although MWA was an interesting and effective treatment method, the experimental and study in the humans liver could not be studied because it was due to humanity and the risk of unethical. Some group researchers have been experimenting with animals (Strickland et al., 2002; Hines-Peralta et al., 2006; Wu et al., 2013; Saccomandi et al., 2015; Lopresto et al., 2017; Marcelin et al., 2018).

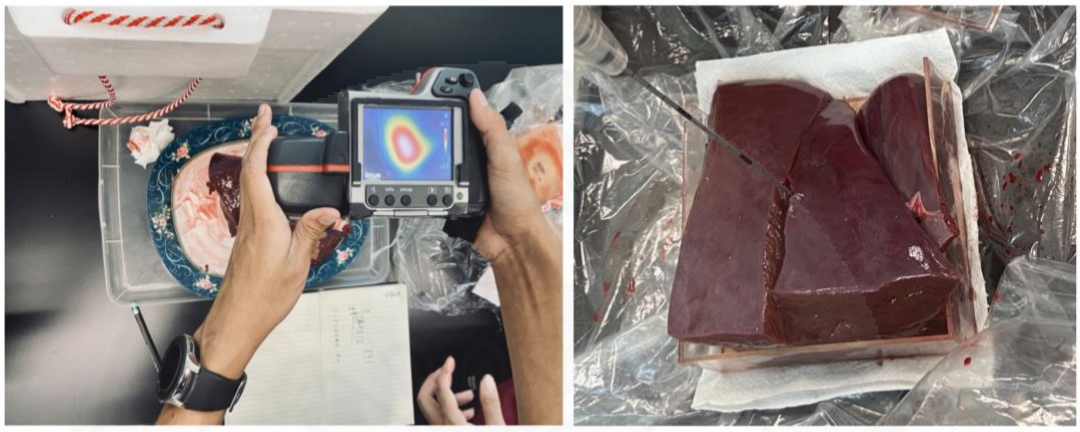

Fig. 1.3 The experimental study of the MWA process in the bovine liver obtained by the Center of Excellence in Electromagnetic Energy Utilization in Engineering (CEEE) lab, Thammasat university.

Fig. 1.3 shows the sample experimental results of the MWA process in the bovine liver obtained by the Center of Excellence in Electromagnetic Energy Utilization in Engineering (CEEE) lab, Thammasat university. This experiment using a microwave generator (Acculis, AngioDynamics, 60-140 W, 2.45 GHz) and connected the microwave antenna, which microwave ablation system operated at the Office of Advanced Science and Technology, Thammasat University. The experimental results are measuring by the fiber optic thermometer and infrared camera.

However, these experimental studies had limitations compared to experimenting with a nearly realistic human liver. The numerical simulation could be applied to study the treatment. It has been the advantage of needing only a short period, the low economic cost, humanity, and could be set up with conditions near to those of a real human liver (Keangin & Rattanadecho, 2013).

Several years ago, many researchers developed mathematical models for predicting the temperature distribution in the living tissue. The most widely heating model was introduced by Pennes, which has become well known as Pennes' bioheat model (Pennes, 1948). In the original, the Pennes' bioheat model was designed for predicting the temperature distribution in the human forearm. Due to the Pennes bioheat simplification, many studies have established and developed the mathematical of extending and modifying the Pennes' bioheat model (Wulff, 1974; Klinger, 1974; Chen & Holmes, 1980). Description of the bioheat and the modified bioheat can be found in literature (Pennes, 1948; Wulff, 1974; Klinger, 1974; Chen & Holmes, 1980; Weinbaum et al., 1984; Jiji et al., 1984; Charny et al., 1990; Arkin et al., 1994). For MWA treatment, the temperature distribution in biological tissue during the treatment process was indicated to treatment achieve. Therefore, the mathematical model based on the bioheat approach was developed for predicting the temperature distribution in the biological tissue during the MWA process (Yang et al., 2007; Keangin et al. 2011; Wang et al., 2015; Wu et al., 2016; Xu et al., 2019; Minbashi et al., 2020). However, liver cancer with MWA treatment models was developed based on two dimensions (2D) or 2D axial symmetry assumption. This assumption was reduced the complexities of realistic problem to the simplified problem. Although the 2D assumption benefits computation, this assumption could not be applied to the diversity of treatment cases, especially in the treatment area nearby the large blood vessels. In this limitation, the three dimensions (3D) problem has introduced.

Although the bioheat approach could be modified to improve accuracy and efficiency, the bioheat models have some limitations. This model cannot handle several physical effects, in particular, the directional of blood flow and convective heat transfer mechanism. Some researchers proposed the porous media model applied in the biological tissue for improved model accuracy and efficiency. The realistic, the biological tissue includes the cell, blood vessel, and interstitial space, which can be defined as the solid phase and fluid phase in the biological domain (Mahjoob & Vafai, 2009). Therefore, the biological tissue could assume a porous structure (Roetzel & Xuan, 1998; Nakayama & Kuwahara, 2008). Thus, the porous media theory can be applied in biological tissue (Mahjoob & Vafai, 2009; Rattanadecho & Keangin, 2013). The advantages of utilizing a porous media model in biological tissue has few

assumptions as compared to different established bioheat transfer models. Therefore, the porous media theory was applied to the liver cancer treatment with MWA process (Keangin & Rattanadecho, 2013; Keangin et al., 2013; Rattanadecho & Keangin, 2013). The comparison of the thermal models during the MWA process on the heat transfer affects the performance and effectiveness of the temperature prediction in the liver cancer model. Therefore, the fundamental of the different heating implemented could be selected as the suitable heat models for the right condition and situation.

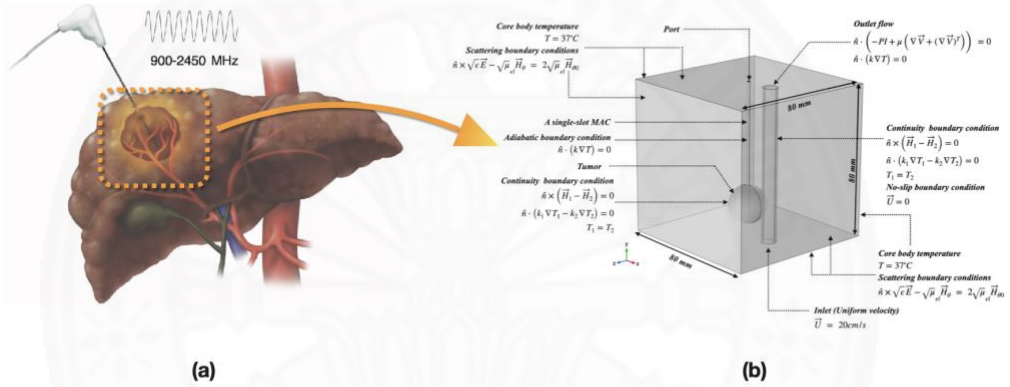

Fig. 1.4 The liver cancer with the MWA treatment concept to the 3D mathematical modeling; (a) The liver cancer with the MWA treatment (Voizard et al., 2019), (b) The control volume mathematical modeling of the liver cancer with the MWA treatment.

This dissertation was proposed the numerical simulation of the liver cancer treatment with the MWA process using a slot antenna. The characteristics of thermal response as same as heat transfer during the MWA process were investigated, which indicated to treatment achieve. This dissertation focuses on the treatment area near the large vascular (vessel), in which cannot be applied 2D axial symmetry assumption. Therefore, the 3D problem assumption was considered. Fig. 1.4 shows the 3D mathematical model in this study, which is converted from a practical treatment concept. In addition, the effect of vessel distancing on heat transfer of the deformed liver cancer model was investigated. The complex multi-physicals during the MWA

process were considered with the governing equation systematically. Furthermore, the performancing comparative of the predicted heating models as bioheat model and porous model was systematically comparison. The fundamental understanding of this study could be a guideline for effective treatment.

1.2 Introduction to the microwave

The microwave is a form of electromagnetic waves within a frequency range of 300 MHz to 300 GHz. The microwaves can be self-propagated in the vacuum or matter as same as the other electromagnetic waves. These waves are comprised and synchronized oscillations of electric and magnetic fields. In wave propagation, the electric and magnetic fields oscillate in phases perpendicular to each other and perpendicular to the wave direction. The electromagnetic wave is classified into several types according to the wave frequency. In the ordering, the high frequencies to the low frequencies as shown in Fig. 1.5.

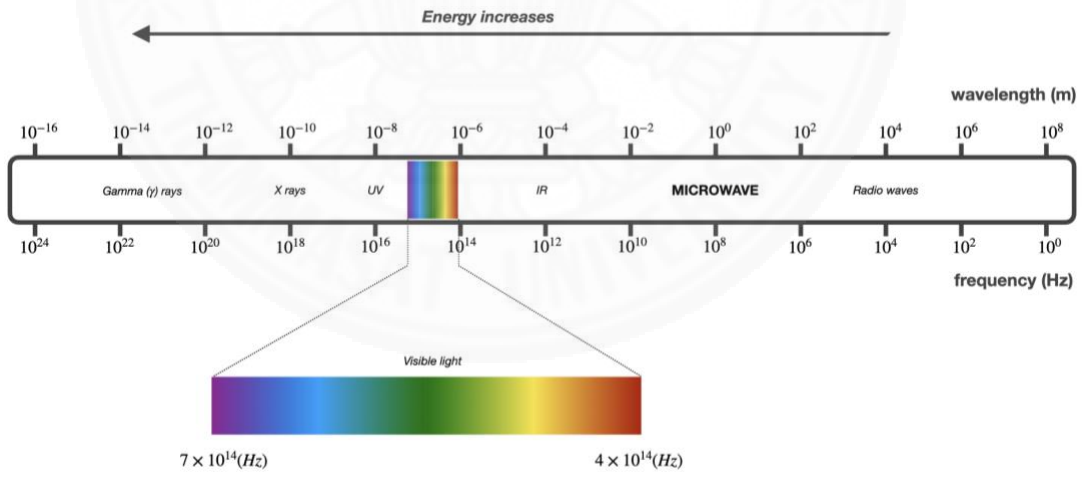

Fig. 1.5 Electromagnetic spectrum

Jame Clerk Maxwells produced the first complete set of equations governing electricity and magnetism, expressed in terms of fields, which has become well known as Maxwell's equations (Maxwell, 1890). Subsequently, Maxwell's equations were confirmed by Heinrich Hertz through experiments with radio waves

(Baird et al., 2013). Maxwell's theory predicted that coupled electric and magnetic fields could travel through space, which has become well known as an electromagnetic wave. Maxwell concluded that light itself is the electromagnetic wave of a short wavelength, but no one could prove this until Hertz's experiment confirmed it.

The microwave is one of the most popular electromagnetic waves and is widely used in many applications, such as spacecraft, communication, navigation, radar, or heating. The microwave heating application is contrasted to conventional heating. In microwave heating, the microwave penetrates the surface is converted into thermal energy within the material. This process is several advantages as rapid heating, selective heating, less material decomposition, non-pollution, or high-efficiency heating (Rattanadecho & Klinbun, 2011). For the many advantages, microwave heating has applied in many industrial processes and households. The accomplishments of microwave heating occurred in many applications, such as drying, melting, pasteurization, sterilization (Datta, 2001; Rattanadecho, 2002; Chatterjee et al., 2007; Keangin et al., 2013). The microwave is a rapid heating, selective heating, and highly efficient heating. Therefore, microwave heating was introduced to the therapeutic application.

1.3 Introduction to the microwave ablation

Microwave ablation (MWA) is a minimally invasive cancer treatment technique that induces thermal injury into the tumor, as same as RFA. This treatment technique has applied the microwave energy into the diseased tissue or tumor area through the microwave antenna. The microwave would be absorbed and converted to the local heat generation in the tumor area (Keangin et al., 2011, Rattanadecho & Keangin, 2013). When the tissue temperature exceeded the lethal temperature, the cancer cell will be destroyed. The benefits of this treatment technique are short ablation time, a short recovery period, less postoperative pain, and fewer complications that may be related to a minimally invasive treatment technique (Keangin et al., 2011). Comparative with RFA, MWA is a faster treatment time, higher flexible treatment, a larger zone of ablation, and a complete tumor kill (Wright et al., 2005; Liang & Wang, 2007; Izzo et al., 2019).

MWA is using the heat from microwave energy to kill cancer cells. The microwave energy transmitted by the microwave antenna creates heat in the tumor tissue without damaging surrounding tissue. In this process, the polar molecules (primarily the water) in the tissue are continuously forced to realign with the oscillating electric field continuously. The molecules vibrate and rotate, resulting in heat to a temperature high enough to cause cell death (Phadungsak & Keangin, 2013). MWA is to create direct heating in the tissue around the antenna. The mechanism of MWA heating differs from RFA heating. In RFA treatment process, heat created by resistive heating when the electrical current passes the ionic tissue. In the RFA treatment process, resistive heating is created when the electrical current passes the ionic tissue medium (Lubner et al., 2010). In the comparative, MWA is a technique that more flexible treatment and highly efficient heating than RFA.

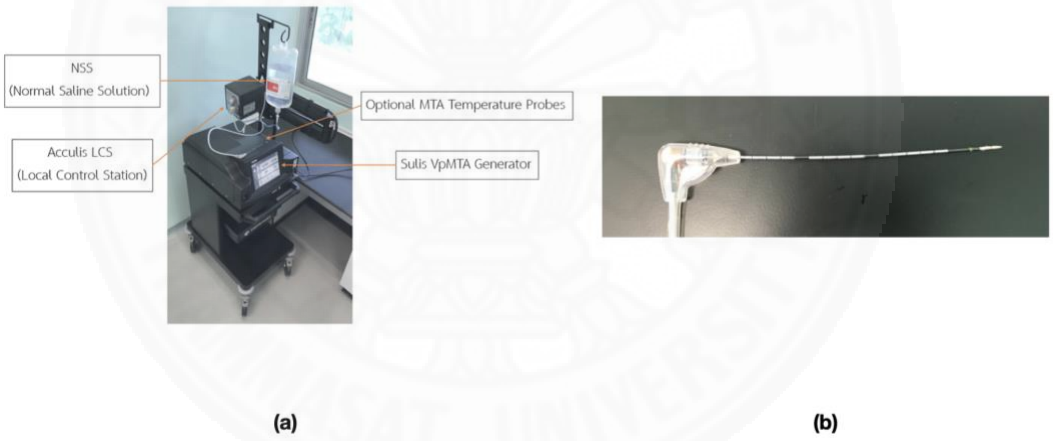

Fig. 1.6 the equipments of the MWA system at Office of Advanced Science and Technology, Thammasat University; (a) the microwave generator (Acculis, AngioDynamics, 60-140 W, 2.45 GHz), (b) microwave antenna (Accu2i PMTA Applicator)

The basic components of the MWA system consist of three components; the microwave generator, the microwave distribution system; the microwave antenna. The microwave generator is a device for creating microwave energy with a magnetron or solid-state source (Rattanadecho et al., 2007; Lubner et al., 2010). The generator created the microwave energy with specific microwave power and frequency to be

suitable for treatment conditions, as shown in Fig. 1.6(a). The microwave frequency of 915 MHz and 2.45 GHz are generally microwave frequencies for treatment application, as allowed by the federal communications commission (Hines-Peralta et al., 2006; Oshima et al., 2008; Brace, 2009). The microwave distribution system is a system connecting the generator to the microwave antenna. The microwave energy from the microwave generation is transmitted to the microwave antenna by the commonly accomplished coaxial cable transmission line. Coaxial cables were designed for excellent wave propagation characteristics, reducing the diameter and power loss. Therefore, coaxial cables were small and flexible, and resistance cable heating during the treatment process. Fig. 1.6(b) shows a sample of the microwave coaxial antenna. Fig. 1.6 shows the components of the MWA system at the Office of Advanced Science and Technology, Thammasat University.

The microwave antenna is a critical component of this treatment system. This part contract is contacted with the living tissue, inserted into the human body, and active in the heating zone. Many factors are required for a microwave antenna designed, such as safety for the human body, efficiency for transferring microwave energy, resistant heat during the treatment process. Moreover, an antenna is required as robust and as small as possible for minimally invasive treatment. The most common microwave antenna is straight and needle-like (Shock et al., 2004; Meredith et al., 2005; Yu et al., 2006). In many conditions, the antenna has been designed in many types. The advantages of the coaxial antenna are remarkable than the other antenna, such as small diameter and good handling of the microwave to a specific area (Strickland et al., 2002; Hines-Peralta et al., 2006; Wolf et al., 2008; Lubner et al., 2010). Therefore, this study uses a microwave coaxial antenna to transmit microwave energy during the MWA process.

Although MWA has a powerful treatment technique and many advantages compared with conventional treatment or alternative as RFA for localized liver cancer, this treatment has dangerous when used incorrect conditions during treatment, such as the heat spread over the boundaries of the tumor area. When the heat spread over the boundaries of the tumor, the temperature of healthy tissue is rising (Poulou et al., 2015). The increase of the healthy tissue temperature is resulting in the protein denaturation

process, which is dangerous on the healthy tissue. Therefore, the studies of correct conditions are necessary, which may improve the efficiency of this treatment.

1.4 Research objectives

1.4.1 To develop the couple numerical model of electromagnetic wave propagation, heat transfer, and blood flow in the biological tissue by using 3D simplified approach and porous media approach.

1.4.2 To study characteristics of specific absorption rate, heat transfer, and damaged tissue in the 3D biological tissue near large vascular subjected to the heating by microwave energy.

1.4.3 To study comparative heating models performance implemented to the liver cancer model during the MWA process.

1.5 Scope of research

1.5.1 Analysis of the specific absorption rate, heat transfer, damaged tissue in the liver cancer near large vessel during MWA treatment process by varying the two locality of blood vessel.

1.5.2 Analysis the performance of the heating model implemented to the liver cancer model during the MWA process.

1.6 Expected benefits

1.6.1 The developed the model will enable us to get more practical prediction of the heat transfer in liver cancer during MWA treatment process.

1.6.2 Obtain results can be applied to a wide range of problems related to therapeutic application during MWA treatment process.

1.6.3 This work will give us an understanding of the characteristics of specific absorption rate, heat transfer, and damaged tissue in the biological tissue near large vascular to the heating by microwave energy.

1.7 Research procedure

The study and research procedure consist of the following steps

1.7.1 Review literatures

1.7.2 Study the fundamental of electromagnetic wave propagation, heat transport, blood flow, and damaged tissue in biological tissue.

1.7.3 Developed the mathematical model and numerical scheme that considered electromagnetic wave propagation, heat transfer, damaged tissue, and tissue deformation of the liver cancer during MWA treatment process.

1.7.4 Compare the simulation results of the tissue temperature against the experimental results obtained from the literatures in order to verify the accuracy of the developed numerical model.

1.7.5 Study effect of large blood vessel locations on the specific absorption rate, heat transfer, and damaged tissue in liver cancer during MWA treatment process.

1.7.6 Study the performance of the heating model implemented to the liver cancer model during the MWA process.

1.7.7 Explain and discuss the effects of the physical parameters and comparative heating model on the specific absorption rate, heat transfer, and damaged tissue in liver cancer during MWA treatment process.

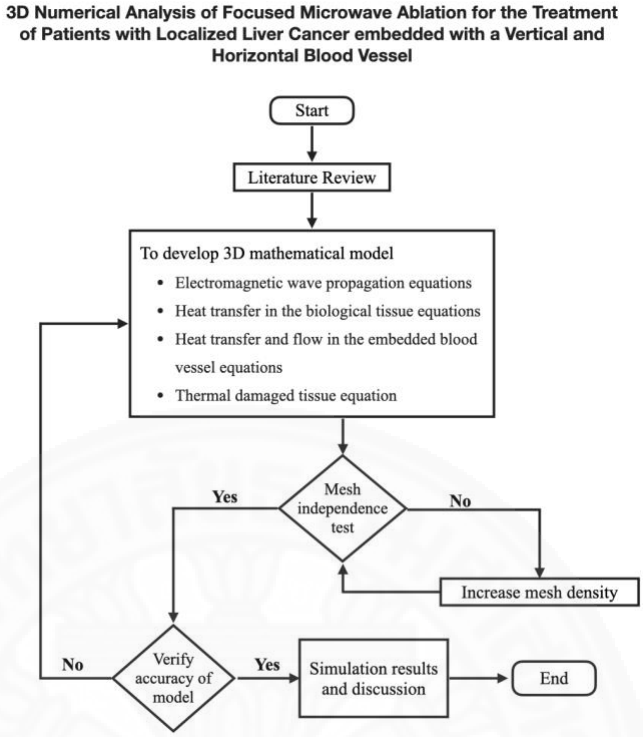

(a)

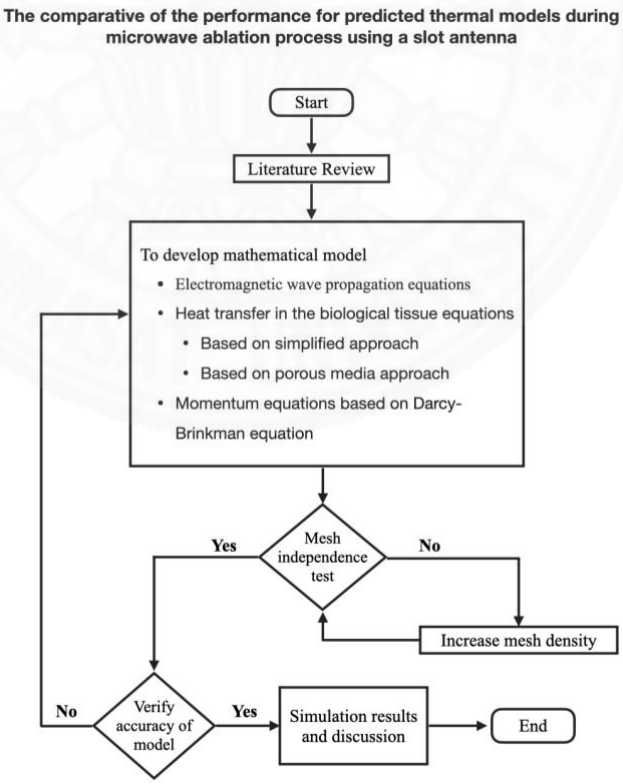

(b)

Fig. 1.7 Research procedures; (a) 3D numerical analysis, (b) comparative performance of predicted thermal model.

CHAPTER 2
REVIEW OF LITERATURE

This dissertation proposed to study the phenomenon of electromagnetic wave propagation, heat transfer, blood flow, damaged tissue, and tissue deformation of the MWA treatment in the 3D liver cancer tissue and the effect of the large vascular location nearby the treatment area on the specific absorption rate, temperature distribution, blood velocity, and necrotic of damaged tissue. The performancing comparative of the bioheat and porous media models was implemented to the liver cancer model during the MWA process was investigated. Therefore, the previous studies are briefly recalled as follows.

2.1 The studies of heat transfer in the biological tissue based on simplified approach

In the past, the theory of heat transfer in the biological tissue was diversified developed. Predicting the temperature distribution in the human body is a famous study because there are many benefits and applications, such as the comfortable design or therapeutics in medical, etc. However, a remarkable study of heat transfer in the biological tissue was introduced by Pennes in 1948 (Pennes, 1948). He proposed the equation describing the temperature distribution in the human forearm, which has become well known as the Pennes bioheat equation or bioheat equation. Pennes tried to predict the temperature distribution in the human forearm by using the energy balance based on heat conduction. However, temperature prediction had not corresponded to the temperature of experimental measurement. Therefore, he developed the bioheat equation for describing the heat transfer in the biological tissue. The bioheat equation was developed based on heat diffusion and added blood perfusion term and metabolism term in the energy conservation equation. The metabolism term represented the heat generation by the metabolism of the cell, and the blood perfusion term represented the energy exchange between tissue and the capillaries system. Pennes assumed the significant heat contribution between tissue and vascular systems at the

capillaries. Due to the Pennes bioheat simplification, many studies have established and developed the mathematical of the extending and modifying the bioheat model (Wulff, 1974; Klinger, 1974; Chen & Holmes, 1980; Weinbaum et al.,1984; Jiji et al., 1984).

Later, several researchers have questioned the physiological and physical phenomena validity of the assumption underlying the Pennes bioheat equation, especially heat transfer by flowing blood (Arkin et al. 1994). Wulff claimed that the heat transfer in the biological tissue is affected by the net blood flux within the biological tissue. Wulff developed and suggested the model with the directional blood term rather than the scalar perfusion term by Pennes (Wulff, 1974). Subsequently, Klinger proposed the heat transfer in the biological tissue caused by the blood flow inside the vessels. He suggested a blood convection term by considering the velocity of blood flow inside the vessels rather than the perfusion term by Pennes (Klinger, 1978). Wulff and Klinger's suggestion is consistent in improving the Pennes bioheat model by representing the directional blood term inserted the scalar blood perfusion term. Later, Chen and Holmes evacuated the thermal equilibrium length of the individual vessel with the semi-quantitative model. Results showed the thermal equilibration of the blood with the tissue occurs not in the capillaries (Chen & Holmes, 1980). The conclusions by Chen and Holmes were not supported the underlying assumptions of Pennes bioheat model. Subsequently, Chato investigated the heat transfer between the tissue and the vessel, which various vessels' geometry (Chato, 1980). He pointed out the magnitude of heat transfer at the large vessel and small vessel, such as the capillaries. However, the heat transfer between the tissue and the intermediate vessel was inconclusive. Chen and Holme pointed out that the intermediate vessel's significant heat transfer, which indicated the shortcomings assumptions of the Pennes bioheat model (Chen & Holmes, 1980). Later, Weinbaum and colleagues proposed the modified bioheat model based on completely different vascular. This study considered the heat transfer in the tissue and countercurrent vascular based on based on anatomical observations (Weinbaum et al., 1984). The mathematical model used the three equations and neglecting axial conduction. The modified bioheat by Weinbaum Jiji and Lemons (Weinbaum et al., 1984) was the effective model but required the most detail about the vascular structure (arkin et al., 1994). Therefore, this model was difficult to apply to most tissue. Based on the shortcoming of the modified bioheat by Weinbaum Jiji and Lemons, Weinbaum

and Jiji developed the modified bioheat with the one equation (Weinbaum & Jiji, 1985). This model adjusted the thermal conductivity to the effective conductivity for the presence of the simplified model. However, the modified bioheat by Weinbaum and Jiji was criticized the assumption (Wissler, 1987). Although the bioheat model is underlying the concern assumption, this model also has many benefits, especially the model simplified and useable for predicting the temperature. Hence, the bioheat model was used to describe the heat transfer in the biological tissue in many applications, especially thermal treatment.

Although the bioheat model was described the heat transfer in the homogeneous tissue, some studies were approached the bioheat in the nonhomogeneous tissue. Mechling et al. was carried out the numerical simulation to predict the hyperthermia treatment by using the microwave antenna in the brain tissue (Mechling et al., 1992). Later, Tzou developed a dual phase-lag model based on the Fourier's law of heat conduction (Tzou, 1995). However, this model gave erroneous results with non-homogeneous inner structure as in the case of biological tissues (Andreozzi, 2019).

Although many studies were used bioheat to study heat transfer in the biological tissue, a few studies have been applied the interaction between the heat transfer in the biological tissue and electromagnetic fields. The electromagnetic field interaction with the heat transfer in the biological tissue was defined by the specific absorption rate (SAR). This term was indicated the energy absorption per unit mass when exposed electromagnetic field. This mechanism interaction was improved the mathematical model to advanced. The advanced model application was predicted the heat transfer in the biological tissue when exposed to the electromagnetic field, such as radiofrequency ablation or microwave ablation. In 1998, Skinner et al. proposed the comparison treatment sources study between microwave ultrasound and laser in the thermal ablation process in three tissue sites; breast, brain, and liver (Skinner et al., 1998). This study was focused on the heat pattern in two geometries of tissue as spherical and cylindrical, and considered the SAR propagation in this tissue. Later, Fujimoto et al. investigated the correlation between the peak of SAR and the maximum temperature in the head model due to a dipole antenna (Fujimoto et al., 2006). This study calculated the SAR propagation in the human heads and converted it to the heat

generation by using the finite difference time domain (FDTD) method. Furthermore, several studies focused on the interaction between electromagnetic wave propagation and heat transfer in the biological tissue, which can be found in the literatures (Hirata et al., 2000; Wessapan et al., 2011; Wessapan & Rattanadecho, 2016; Wessapan & Rattanadecho, 2018).

Although the several studies focused on the interaction between electromagnetic wave propagation and heat transfer in the biological tissue, the previous studies mentioned above were not considered the characteristic heat transfer in the biological tissue by using microwave heating, as same as MWA treatment. However, there are some groups of research focused on the thermal treatment via the microwave. Camart et al. proposed the microwave antenna design, which affected heat pattern during treatment process. This study used numerical computation by an N points Gaussian quadrature formula for the electric field around the antenna and represented the SAR distribution (Carmart et al., 1992). The SAR distribution was converted to heat generation term in the bioheat equation. The effect of microwave antenna design presented on the temperature profile via solved the bioheat equation. After that, Saito et al. proposed the heat characteristic for composed the two coaxial-slot antennas (Saito et al., 2000). In this study, the SAR propagation and temperature distribution were solved by the numerical technique via the FDTD method. Afterward, Pisa et al. studied the power density and temperature distribution in cancer therapy when using the sleeve-slot antennas (Pisa et al., 2003). This study was calculated the SAR distribution with the FDTD method and converted it to the heat generation term in the bioheat equation. In 2007, Yang et al. developed and proposed the modified bioheat for predicting the high temperature in the MWA process (Yang et al., 2007). This study focused on liver cancer treatment via the MWA technique. The evaporation term was considered and developed to effective specific heat term in the bioheat equation. In this study, the numerical model was validated with the experiment on the bovine liver. This result showed the temperature distribution based on the modified bioheat model was more accurate than the model based on the Pennes bioheat. Phasukkit et al. configured the triple antennas for hepatic ablation treatment by using numerical and experimental studies (Phasukkit et al., 2009). This study developed the numerical modeling based on the finite element method (FEM), the SAR distribution was solved to identify the

volumetric heating term in the bioheat equation. In the studies of the heat transfer in the biological tissue during the MWA process in mentioned above, the electromagnetic wave propagation in the biological tissue considered based on SAR equation.

Although the benefits of this method could be simplified and quickly calculated, the electromagnetic wave propagation was not independently investigated. In addition, this equation considered the SAR characteristic was constant distribution, which inconsistent with the facts of treatment. Hence, there are the studies of the electromagnetic wave propagation in the biological tissue based on the Maxwell's equations. Wessapan et al. proposed the SAR and heat transfer in the biological tissue when exposed to the electromagnetic field at a frequency of 915 MHz and 2450 MHz (Wessapan et al., 2011). In this study, the FEM is used to analyze the transient problems. The electromagnetic field was investigated based on Maxwell's equations, and the heat transfer in the biological tissue was investigated based on the bioheat model. Furthermore, Other studies could be obtained from literature (Becker et al., 2007; Özen et al., 2008; Wessapan et al., 2011; Wessapan et al., 2012; Wessapan & Rattanadecho, 2016; Wessapan & Rattanadecho, 2018). Therefore, there are some studies developed the mathematical model based on Maxwell's equations for predicting the SAR distribution in the biological tissue. Keangin et al. investigated the heat transfer in the liver tissue during MWA treatment when using a single and double slot antenna (Keangin et al., 2011). This study developed the mathematical model was considered coupled with electromagnetic wave propagation equations and heat transfer in the biological tissue based on bioheat equation. This study focused the temperature and SAR distribution in the liver tissue when using a single and double slot antenna. Later, Wang et al. proposed the heat transfer and electromagnetic wave propagation in the liver cancer during MWA treatment when using multi-slot antenna (Wang et al., 2015). This study developed the numerical model by using FEM. This study developed the numerical model by using FEM. The mathematical model was considered coupled with the electromagnetic wave propagation equations and the heat transfer in the biological tissue based on the bioheat equation. This study focused on the number of slots and antenna design as same as Keangin study, and the different points were the number and dimensions of the slot-antenna. Later, Wu et al. evaluated the frequency microwave of the MWA treatment model (Wu et al., 2016). In this study, the mathematical model was

considered coupled with the electromagnetic wave propagation and heat transfer in the biological tissue based on the bioheat approach. This study focused on the temperature distribution and SAR distribution when using high microwave frequencies in MWA treatment. In 2020, Minbashi et al. investigated the effects of the input power of a microwave antenna on liver cancer tissue when injection of magnetic nanoparticles (Minbashi et al., 2020). The mathematical model was considered coupled with the electromagnetic wave propagation and heat transfer in the biological tissue based on the bioheat approach. This study focused on the temperature distribution when using vary microwave power in the liver tissue by injection of magnetic nanoparticles.

Furthermore, there are some studies focused on the thermomechanical of biological tissue when exposed the heating process (Shen et al., 2005; Yang et al., 2008; Xu et al., 2008). In the MWA treatment process, the temperature of biological tissue in the treatment area has quickly increased, which caused tissue deformation. Therefore, Keangin et al. proposed the heat transfer in the deformed liver cancer modeling treated using a microwave slot antenna (Keangin et al., 2011). The mathematical model is considered coupled with electromagnetic wave propagation, heat transfer in the biological tissue, and tissue deformation. In this study, the coupled Mathematical model are solved by using axisymmetric FEM. These results presented the comparison between the model with deformation and without deformation analysis on the SAR and temperature distribution. Furthermore, some group researchers focused on the dielectric and thermal properties of biological tissue during the MWA treatment process, which can be found in the literature (Brace, 2008; Lopresto et al., 2014; Lopresto et al., 2017).

Although many previous studies of heat transfer based on the bioheat model, a few works focused on thermal ablation that has presented a completed mathematical model incorporating the coupled model of the electromagnetic wave propagation and heat transfer in the biological tissue during the MWA process. Especially, the studies considered the three dimensions (3D) of heat transfer in the biological tissue during the MWA process with the completed mathematical model was not found. However, the liver is an organ consist of many vascular systems, and it involved large vessel flow. Many studies indicated that heat transfer in biological tissue involved large blood vessels; the large blood vessels should be separately considered

(Wissler, 1971). In the field of thermal ablation studies, the 3D numerical simulation requires many resources for simulation, such as the high computer with the high performance, the long period for simulation, and high understanding for discretize 3D numerical problems. However, there are few studies that considered the 3D heat transfer in the biological tissue when using the thermal treatment. Shao et al. proposed nano-assisted radiofrequency ablation treatment (Shao et al., 2017). This study focused on the treatment area near the countercurrent vessel flow. The mathematical model was considered coupled with electric field equation, heat transfer the biological tissue, and heat transfer in large blood flow. This study could be predicted the asymmetric 3D heat transfer in the liver organ when using radiofrequency ablation treatment. Later, Nabaei et al. investigated of the effect of vessel size and distance on the cryosurgery of an adjacent tumor (Nabaei & Karimi, 2018). This study was using the 3D simulation and 3D FEM for the analysis of the 3D problem. The results showed the asymmetry heat transfer in liver cancer during cryoablation treatment. Table 2.1 summarizes previous studies of heat transfer in the biological tissue based on the simplified approach.

Although several studies developed the mathematical model with various conditions for improving predictions temperature in the biological tissue when using MWA treatment, those studies developed the mathematical model based on 2D axisymmetric assumption. This assumption has many benefits, such as a short period for computation, providing the 3D results. However, this assumption has limitations in reality implementation. In the realistic treatment, we cannot avoid treating specific areas where this assumption is available. Therefore, the study of MWA therapy in the area needs to be considered with a 3D assumption that should be developed.

Table 2.1 Summarizes studies of heat transfer in the biological tissue based on the simplified approach

References	Heat transfer model	Electromagnetic wave model	Application	Parameter	Numerical model	Model validation
Carmart et al., 1992	Bioheat eq.	SAR eq.	Design and modelization the microwave coaxial antennas array for hyperthermia system at the microwave frequency of 915 MHz.	N/A	Crank-Nicholson method for the time The residual elliptic equation is solved by the Cholesky method	N/A
Mechling et al., 1992	Bioheat eq.	SAR eq	Numerical simulation of interstitial hyperthermia microwave antenna arrays is driven at 915 and 2450 MHz in brain tissue	Insertion depths Shape of tumor	3D FEM	N/A
Skinner et al., 1998	Bioheat eq.	SAR eq.	The comparison treatment sources study between microwave ultrasound and laser in the thermal ablation process in three tissue sites: breast, brain, and liver	Heat source Geometries of tissue	2D FDM	N/A
Hirata et al., 2000	Bioheat eq.	SAR eq.	Temperature in the human eye model when exposed to the electromagnetic wave	Frequencies of electromagnetic	3D FDTD	N/A

References	Heat transfer model	Electromagnetic wave model	Application	Parameter	Numerical model	Model validation
Saito et al., 2000	Bioheat eq.	SAR eq.	Heat characteristic for composed the two coaxial-slot antennas.	Microwave antenna	3D FDTD	Temperature (experimental)
Pisa et al., 2003	Bioheat eq.	SAR eq.	The power density and temperature distribution in cancer therapy when using the sleeve-slot antennas	Array spacing	3D FDTD	Temperature increase (Alternate direction implicit solution)
Shen et al., 2005	Bioheat eq.	N/A	Numerical simulation of the thermomechanical interaction in soft tissue	N/A	3D FDM	Temperature (experimental)
Fujimoto et al., 2006	Bioheat eq.	SAR eq.	Investigated the correlation between the peak of SAR and the maximum in the head model due to a dipole antenna	Human aging	3D FDTD	N/A
Becker et al., 2007	Bioheat eq.	SAR eq.	Thermal damage in the skin electroporation and pre-cooling	Cooling period Blood vessel Electrode	3D FVM	Temperature (analytical)

References	Heat transfer model	Electromagnetic wave model	Application	Parameter	Numerical model	Model validation
Yang et al., 2007	Bioheat eq.	SAR eq.	Developed and proposed the modified bioheat for predicting the high temperature in the MWA process	Comparative mathematical model	2D FEM	Temperature (experimental)
Özen et al., 2008	Bioheat eq.	Electromagnetic wave eq.	Heat transfer analysis in the skin tissue when exposed to microwave	Mathematical model Thermal properties of skin	1D FEM	N/A
Xu et al., 2008	Bioheat eq.	N/A	Biothermomechanical behavior of skin tissue	Thermal properties of skin Mathematical model	3D FDM	Tension (experimental)
Yang et al., 2008	Bioheat eq.	N/A	Numerical model based on FEM for cryosurgery with coupled phase change and thermal stress aspects	N/A	3D FEM	Temperature (experimental) Stress (calculation)

References	Heat transfer model	Electromagnetic wave model	Application	Parameter	Numerical model	Model validation
Phasukkit et al., 2009	Bioheat eq.	SAR eq.	configured the triple antennas for hepatic ablation treatment by using numerical and experimental studies	Antenna types Antenna configuration	3D FEM	Temperature (experimental)
Wessapan et al., 2011	Bioheat eq.	Electromagnetic wave eq.	Numerical analysis the SAR distribution and temperature distribution in the human body when exposed to leakage the electromagnetic	Microwave frequencies Organs	2D FEM	SAR (numerical results)
Keangin et al., 2011	Bioheat eq.	Electromagnetic wave eq.	Investigation the heat transfer in the liver tissue during MWA treatment when using a single and double slot antenna	Number of the slot coaxial antenna	2D FEM	Temperature (experimental)
Wessapan et al., 2012	Bioheat eq.	Electromagnetic wave eq.	A numerical analysis of specific absorption rate (SAR) and temperature distributions in the realistic human head model exposed to mobile phone radiation at 900 MHz and 1800 MHz.	Electromagnetic frequencies Organs	3D FEM	SAR (numerical results)

References	Heat transfer model	Electromagnetic wave model	Application	Parameter	Numerical model	Model validation
Wang et al., 2015	Bioheat eq.	Electromagnetic wave eq.	Numerical simulation evaluation of the treatment effectiveness of a novel coaxial multi-slot antenna during MWA treatment.	Lengths of the slots Number of the slots Microwave power	2D FEM	Temperature (experimental)
Wessapan & Rattanadecho, 2016	Bioheat eq.	Electromagnetic wave eq.	The simulation of the SAR and temperature distribution in a male reproductive model exposed to an electric dipole antenna.	Microwave frequencies Types of tissue	2D FEM	SAR (numerical results)
Wu et al., 2016	Bioheat eq.	Electromagnetic wave eq.	Numerical simulation evaluates the feasibility of high frequency MWA used in cancer thermal therapy.	Microwave frequencies	2D FEM	Temperature (experimental)
Lopresto et al., 2017	Bioheat eq.	SAR eq.	Numerical simulation effects of temperature-dependent variations in the dielectric and thermal properties of the targeted tissue during MWA therapy	Thermal properties Dielectric properties	2D FDTD	Temperature (experimental)

References	Heat transfer model	Electromagnetic wave model	Application	Parameter	Numerical model	Model validation
Shao et al., 2017	Bioheat eq.	N/A	A three-dimensional finite difference analysis is employed to simulate the RFA treatment with nanoparticles.	Types of nanoparticles Concentration of nanoparticles	3D FDM	Temperature (experimental)
Nabaei & Karimi, 2018	Bioheat eq.	N/A	Numerical simulation of the effect of vessel size and distance on the cryosurgery of an adjacent tumor	Distancing of vessel nanoparticles	3D FEM	Temperature (experimental)
Wessapan & Rattanadecho, 2018	Bioheat eq.	Electromagnetic wave eq.	Numerical simulation of the SAR and temperature distribution in a human torso exposed to near-field and far-field EM radiations.	Electromagnetic frequencies Organs	2D FEM	SAR (numerical results)
Minbashi et al., 2020	Bioheat eq.	Electromagnetic wave eq.	The numerical simulation of temperature distributions in a cancerous liver tumor at its irradiation by microwaves using a dual-slot antenna with injection of nanoparticles	Types of nanoparticles	2D FEM	Temperature (experimental)

2.2 The studies of heat transfer in the biological tissue based on porous media approach

Due to the bioheat model's shortcomings, the porous media theory was used analysis the heat transfer in the biological tissue. Compared with the bioheat model, the porous media model was required few assumptions and flexible applications. In recent decades, the porous media theory has been applied in many applications, i.e., microwave heating (Rattanadecho et al., 2002; Pakdee & Rattanadecho, 2011; Cha-um et al., 2011), melting (Rattanadecho & Serttikul, 2007; Chaiyo & Rattanadecho, 2011), freezing (Serttikul et al., 2019), food (Datta, 2007; Holtz et al., 2010). Furthermore, the porous media theory has been applied to describing and predicting heat transfer in biological tissue.

Roetzel and Xuan introduced the equations to predict the transient temperature profile of the arterial and venous blood flows and the tissue within a limb (Roetzel & Xuan, 1998). The two governing equations of tissue were derived for fluid phase (blood phase) and solid phase (tissue cell), which developed based on the porous media approach. Subsequently, Khaled and Vafai and Khanafer and Vafai stress remarked that the porous media theory is most appropriate for describing the heat transfer in the biological tissue (Khaled & Vafai, 2003; Khanafer and Vafai 2006). It required few assumptions compared to the bioheat equation. Furthermore, Nakayama and Kuwahara introduced the general bioheat models based on porous media theory (Nakayama and Kuwahara, 2007). This conclusion indicated the model was established based on porous media theory required fewer assumptions than the bioheat model. Yuan proposed a thermal response of the biological tissue model during hyperthermia therapy (Yuan, 2008). This study developed a model based on local thermal non-equilibrium assumption. The results indicated the one-equation of porous media was suitable when the blood vessel diameter was less than 30 m and blood velocity lower than 0.4 cm/s. Later, Mahjoob and Vafai investigated the characterization of heat transport through biological tissue based on porous media theory when incorporating hyperthermia treatment (Mahjoob & Vafai, 2009). This result indicated the importance of utilizing the local thermal non-equilibrium model in the state of the higher metabolic heat generation. Although Mahjoob and Vafai and Yuan investigated the heat transport

in the biological tissue during hyperthermia treatment, this study was not covered the interaction of electromagnetic field and heat transport in the biological tissue.

However, there are some studies focused on the heat transfer phenomenon in the biological tissue based on porous media theory when exposed to the electromagnetic field. Wessapan and Rattanadecho presented the SAR and temperature distribution in an anatomically human eye exposed to electromagnetic field based on porous media theory (Wessapan and Rattanadecho, 2012). This study developed the human eye with multi-layers. The heating model conjugated consideration with conventional heating model and advanced bioheat model based on porous media theory. Subsequently, Keangin et al. proposed the effects of an imposed electromagnetic field on different biological media materials such as the liver, brain, bone, and skin, etc. (Keangin et al., 2013). In this study, the mathematical model was developed underlying the local thermal non-equilibrium assumption. The coupled equation of electromagnetic wave propagation and heat transfer were solved by using FEM. The results showed the effect of electromagnetic power and frequency on the temperature of solid phase and blood phase in biological materials. Later, Wessapan and Rattanadecho investigate the SAR, fluid flow and heat transfer in biological tissue due to electromagnetic near-field exposure (Wessapan & Rattanadecho, 2016). In this study, the electromagnetic wave propagation model was developed based on Maxwell's equations, and the heat transfer model was developed based on the bioheat model and porous media model.

Although some studies focused on the heat transfer phenomenon in the biological tissue based on porous media theory when exposed to the electromagnetic field, the biological tissue characteristic when using the MWA treatment process is different. Therefore, Therefore, there are few studies focused on the heat transfer phenomenon in the biological tissue when using the MWA treatment process. In 2013, the liver cancer with MWA treatment model based on the porous media approach was proposed by Rattanadecho & Keangin (Rattanadecho & Keangin, 2013). This work was the first study of heat transfer and blood flow in the two-layered porous liver during MWA process using single and double slot antenna. This study was not considered the fluid with constant velocity but considered the fluid flow with gradient temperature in the porous tissue domain. Later, Keangin and Rattanadecho investigated the transient

distribution of tissue and blood temperatures within porous liver during the MWA process using slot antenna based on the local thermal non-equilibrium model (Keangin & Rattanadecho, 2013). The mathematical model was considered coupled with the electromagnetic wave propagation model and heat transfer model, which underlying the local thermal non-equilibrium assumption. This system of equations was solved by using the axisymmetric FEM. In the simulation results, the tissue and blood temperature based on the local thermal non-equilibrium assumption were compared with the tissue temperature of the Pennes bioheat model, Klinger model, and porous model based on local thermal equilibrium assumption.

In 2018, Keangin and Rattanadecho investigated the influences of tumor diameter, tumor porosity, and input microwave power on the heat transfer and SAR distribution in the porous liver cancer model during MWA treatment process (Keangin & Rattanadecho, 2018). However, the performance of the predicted thermal models during the MWA process with systematically investigation was not found in the literatures. Therefore, the performancing comparative of the predicted heating models implemented of the liver cancer model during MWA treatment process that should be developed.

Table 2.2 Summarizes studies of heat transfer in the biological tissue based on the porous media approach

References	**Heat transfer model**	**Electromagnetic wave model**	**Application**	**Parameter**	**Numerical model**	**Model validation**
Roetzel & Xuan, 1998	Energy eq. (Two & Three eq.)	N/A	Derived the two equations predict the transient temperature profile of the arterial and venous blood flows and the tissue within a limb	Vascular types Blood flow Thermal properties	1D analytical solution	N/A
Khaled & Vafai, 2003	Energy eq. based on LTNE Energy eq. Based on LTE	N/A	Reviewed The role of porous media in modeling flow and heat transfer in biological tissues	N/A	N/A	N/A
Khanafer and Vafai 2006		N/A	This study drug delivery to develop comprehensive models based on porous media theory utilizing fewer assumptions as compared to other approaches.	Tortuosity and porosity	3D Explicit analytical	Concentration (experimental)

References	Heat transfer model	Electromagnetic wave model	Application	Parameter	Numerical model	Model validation
Nakayama and Kuwahara, 2007	Energy eq. (Two & Three eq.)	N/A	Derived mathematical model based on the volume averaging theory for bioheat transfer and blood flow	N/A	2D analytical	N/A
Yuan, 2008	Energy eq. (Two eq.)	N/A	Numerical analysis the temperature and thermal dose response of a biological tissue with blood vessel distribution undergoing hyperthermia therapy.	Vessel diameters Blood velocity Tissue porosities	3D FDM	Temperature (software FlexPDE)
Mahjoob & Vafai, 2009	Energy eq. (Two eq.)	N/A	Analytical characterization of heat transport through the porous biological tissue regulation of isothermal surfaces	Inclination angle Ratio of the effective fluid conductivity to that of the solid Upper wall shape factor	2D analytical	Temperature (simulation results)

References	Heat transfer model	Electromagnetic wave model	Application	Parameter	Numerical model	Model validation
Wessapan and Rattanadecho, 2012	Bioheat eq. Energy eq. based on LTE	Electromagnetic wave eq.	The simulation of the SAR distribution and temperature distribution in an anatomically human eye exposed to electromagnetic field based on porous media theory	Power densities	2D FEM	SAR (numerical results)
Keangin et al., 2013	Bioheat eq. based on LTNE	N/A	Numerical analysis of the porous biological tissue effects imposed electromagnetic field on different biological media.	Different biological media Electromagnetic wave power Porosity Electromagnetic wave frequencies	2D FEM	Temperature (analytical)
Wessapan & Rattanadecho, 2016	Bioheat eq.	Electromagnetic wave eq.	Numerical analysis of the SAR, fluid flow and heat transfer in the tissue during	Mathematical model	2D FEM	SAR (numerical results)

References	Heat transfer model	Electromagnetic wave model	Application	Parameter	Numerical model	Model validation
	Bioheat eq. based on LTE		exposure to a near-field EMF in different exposure conditions has been performed.	The exposure distances Various permeabilities		
Rattanadecho & Keangin, 2013	Bioheat eq. based on LTE	Electromagnetic wave eq.	Numerical study of heat transfer and blood flow coupled with electromagnetic wave propagation in two layers porous liver tissue during MWA process using a single and double slot MCA.	Single and double slots	2D FEM	Temperature (experimental)
Keangin & Rattanadecho, 2013	Bioheat eq. based on LTNE	Electromagnetic wave eq.	Numerical analysis of heat transport on local thermal non-equilibrium in porous liver during microwave ablation	Mathematical model Blood velocity Microwave power	2D FEM	Temperature (experimental)

References	Heat transfer model	Electromagnetic wave model	Application	Parameter	Numerical model	Model validation
Keangin & Rattanadecho, 2018	Bioheat eq. based on LTNE	Electromagnetic wave eq.	Numerical simulation of microwave ablation using a single-slot microwave antenna on two layers of porous liver tissue.	Porosity Microwave power Tumor diameter	2D FEM	Temperature (experimental)

CHAPTER 3
THEORIES AND MATHERMATICAL MODEL

3.1 The modeling of electromagnetic wave propagation

A microwave is a form of electromagnetic waves within a frequency range of 300 MHz to 300 GHz, mentioned in Chapter 1. In MWA treatment, microwave energy is considered to be the core of the treatment process. The microwave energy was generated at the generator and transmitted to the tumor by using the microwave antenna. The microwave energy was absorbed and converted to volumetric heating in the tumor area. The goal of this treatment is to elevate the temperature of the tumor to 52 °C, where cancer cells are destroyed (Dong et al., 1998; Goldberg et al., 2000; Whelan et al. 2005; Prakash et al., 2008; Prakash et al., 2012; Wu et al., 2013). Therefore, this treatment efficiency depends on electromagnetic wave propagation understanding during the treatment process. In the first step, the microwave can basically be described by Maxwell's equations.

$$\nabla \times \vec{E} = -\frac{\partial \vec{B}}{\partial t} \tag{3-1}$$

$$\nabla \times \vec{H} = \vec{J} + \frac{\partial \vec{D}}{\partial t} \tag{3-2}$$

$$\nabla \cdot \vec{D} = q \tag{3-3}$$

$$\nabla \cdot \vec{B} = 0 \tag{3-3}$$

where $\vec{E}$ is electric field intensity vector (V/m), $\vec{H}$ is the magnetic field intensity vector (A/m), $\vec{J}$ is the density of free currents (A/m^2), $\vec{B}$ is the magnetic flux density vector (Wb/m^2), $\vec{D}$ is the electric flux density vector (C/m^2), t is the time (s), and q is the density of free charges, respectively which can be defined in Eq. (3-5) and (3-6)

$$\vec{B} = \mu \vec{H} \tag{3-5}$$

$$\vec{D} = \varepsilon \vec{E} \tag{3-6}$$

where μ is magnetic permeability (H/m) and ε is the electrical permittivity (F/m).

The four Maxwell's equations are differential equations that are explaining the electromagnetic phenomena in the physical environment. Eq. (3-1) is the expression of Faraday's law. This equation expresses the electric field intensity in a region of time-varying magnetic flux density. Eq. (3-2) is a generalization of Ampère's circuital law. This equation expresses the magnetic field contribution generated by the displacement of current density (shown in term of $\frac{\partial \vec{D}}{\partial t}$) and density of free currents (shown in term $\vec{J}$), which comprises both the conduction current and convection current. Eq. (3-3) can be recognized as Gauss's law, in which the relation of electric flux and the electric charges in the enclosed surface. Eq. (3-4) is Gauss's law for magnetism that the divergence of the magnetic flux density through any closed surface is zero. In this research, MWA treatment involved electromagnetic wave propagation in the microwave antenna and the biological tissue. Maxwell's equations are basically fundamental for describing electromagnetic wave propagation during the treatment process.

This research focused on liver cancer treatment with the MWA process by using the single slot of microwave coaxial antenna (MCA). The slot coaxial antennas are the common antennas in MWA application of the advantages, size (small dimensions), design simplicity, low cost to manufacture, and convenient adaptation to treatment (Rattanadecho & Keangin, 2013). The propagation of the electromagnetic wave in the antenna is by a transverse electromagnetic field (TEM) (Bertram et al., 2006; Keangin et al., 2013; Wang et al., 2015) that given as:

$$\vec{E} = \vec{e}_r \frac{C}{r} e^{j(\omega t - kz)} \tag{3-7}$$

$$\vec{H} = \vec{e}_\varphi \frac{C}{rZ} e^{j(\omega t - kz)} \tag{3-8}$$

$$C = \sqrt{\frac{ZP_{in}}{\pi \cdot \ln\left(\frac{R_{outer}}{R_{inner}}\right)}} \tag{3-9}$$

$$P_{in} = \int_{r_{inner}}^{r_{outer}} Re\left(\frac{1}{2}\vec{E} \times \vec{H}^*\right) 2\pi r dr = e_z \pi \frac{C^2}{Z} \ln\left(\frac{r_{outer}}{r_{inner}}\right) \tag{3-10}$$

where *C* the arbitrary constant, ε_r is the relative permittivity of the dielectric, $Z = \frac{Z_0}{\sqrt{\varepsilon_r}}$ is the wave impedance (Ω), $Z_0 = \sqrt{\frac{\mu_0}{\varepsilon_0}}$ is the intrinsic impedance (Ω), $\varepsilon_0 = 8.8542 \times 10^{-12}$ (F/m) is permittivity of free space, $\mu_0 = 4\pi \times 10^{-7}$is the permeability of free space (H/m). P_{in} is the microwave power input (W), r_{outer} is the dielectric outer radius (m), r_{inner} is the dielectric inner radius (m), *f* is the frequency (Hz), $\omega = 2\pi f$ is the angular frequency (rad/s), *k* is the wave propagation constant (m^{-1}), which relates to the wavelength (λ) in medium: $k = \frac{2\pi}{\lambda}$. $\vec{e}$ is a unit vector of cylindrical coordinates, * is a conjugate complex number, *Re* is a real part of a complex number, and *r*,*φ*, and *z* are cylindrical coordinates centered on the axis of the coaxial cable.

Furthermore, the propagation of the electromagnetic wave in the biological tissue is by a transverse magnetic field (TM) as described by the following equation:

$$\nabla \times \left(\left(\frac{1}{\varepsilon_r} - \frac{j\sigma_{el}}{\omega \varepsilon_0}\right)^{-1} \nabla \times \vec{H}_\theta\right) - \mu_r k_0^2 \vec{H}_\theta = 0 \tag{3-11}$$

where μ_r is relative permeability (H/m), ε_r is the relative permittivity, $j = \sqrt{-1}$, $\varepsilon_0 = 8.8542 \times 10^{-12}$ (F/m), k_0 is the free space of wave number (m^{-1}), ω is the is the angular frequency (rad/s), and σ_{el} is electric conductivity (S/m).

The interaction of an electromagnetic wave with biological tissue can be defined in terms of a specific absorption rate (SAR) distribution. When the electromagnetic wave is transmitted by a microwave antenna, it passes through it and then propagates throughout the entire domain. The electromagnetic wave is absorbed and converted to the external heat source term. In this study, SAR represents the microwave power absorption deposited per unit mass in tissue (W/kg) (Rattanadecho & Keangin, 2013). The SAR is given by:

$$SAR = \frac{\sigma_{el}}{2\rho} \mid \vec{E} \mid \quad (3\text{-}12)$$

where σ_{el} is electric conductivity (S/m) and ρ is the density of material (kg/m^3).

3.2 The modeling of heat transfer in the biological tissue using simplified approach

This dissertation focused on the heat transfer in the biological tissue, specifically in the liver tissue. The thermal modeling in the biological tissue is presented as followed.

3.2.1 Pennes bioheat model

Pennes bioheat model (Pennes, 1948) is used to describe the temperature distribution in the biological tissue. In the original, it was designed for prediction temperature in human forearm, which has become well known as the Pennes bioheat equation or bioheat equation. This equation is developed based on heat diffusion. The equation that Pennes developed is expressed in its simplest form as

$$(\rho C_p)_t \frac{\partial T}{\partial t} = \nabla \cdot (k_t \nabla T) + \rho_b C_{p,b} \omega_b (T_b - T) + Q_{met} \quad (3\text{-}13)$$

where ρ is the tissue density (kg/m^3), C_p is the specific heat capacity (J/kg· ºC), T is the temperature of tissue (ºC), T_b is blood temperature (ºC), k_t is the thermal conductivity of tissue (W/m·ºC), ρ_b is the blood density (kg/m^3), ω_b is the blood perfusion rate (1/s), Q_{met} is the metabolism heat source (W/m^3). The subscription *t* and *b* represent the tissue and blood phases, respectively.

3.2.2 Wulff continuum model

The bioheat equation has been extensively applied to describe the heat transfer in the biological tissue due to the simplification. However, some researchers questioned to physical and physiological validity of the assumptions

underlying the Pennes bioheat equation. The discussion seems to have been initiated by Wulff (Wulff, 1974). In his assumption, the convection heat in the biological tissue due to the net blood flux in the biological tissue. Also, Wulff suggested the blood flow with the directional term of the from $\left(\rho C_p\right)_b \vec{u} \cdot \nabla T$ rather than the scalar perfusion term suggested by Pennes (Pennes, 1948). Thus, the governing equation for heat transfer in biological tissue should be expressed by:

$$(\rho C_p)_t \frac{\partial T}{\partial t} = \nabla \cdot (k_t \nabla T) + \left(\rho C_p\right)_b \vec{u} \cdot \nabla T + Q_{met} \tag{3-14}$$

where where ρ is the tissue density (kg/m^3), C_p is the specific heat capacity (J/kg· ºC), k_t is the thermal conductivity of tissue (W/m·ºC), $\vec{u}$ is the average blood flux density (m/s), T is the temperature (ºC), and Q_{met} is the metabolism heat source (W/m^3).

3.2.3 Klinger continuum model

Due to shortcomings of assumptions underlying the Pennes bioheat model (Pennes, 1948), Klinger pointed out the convective heat transfer in the biological tissue caused by the blood flow inside the vessels (Klinger, 1974). Klinger suggested the blood convective term that takes the form $\left(\rho C_p\right)_b \vec{V}(\bar{r}, t) \cdot \nabla T$ within the vessel rather than the scalar perfusion term suggested by Pennes. This model was developed based on vascular anatomy and considered the spatial and temporal variations of the blood velocity during the heat transfer process. Thus, the bioheat equation based on Klinger assumption can be written as:

$$(\rho C_p)_t \frac{\partial T}{\partial t} = \nabla \cdot (k_t \nabla T) + \left(\rho C_p\right)_b \vec{V}(\bar{r}, t) \cdot \nabla T + Q_{met} \tag{3-15}$$

where ρ is the tissue density (kg/m^3), C_p is the specific heat capacity (J/kg· ºC), k_t is the thermal conductivity of tissue (W/m·ºC), $\vec{V}(\bar{r}, t)$ is the blood velocity in the vessel (m/s), T is the temperature (ºC), and Q_{met} is the metabolism heat source (W/m^3).

3.2.4 The Continuum model of Chen and Holmes

Due Chen and Holmes model (Chen & Holmes, 1980) was developed based on a continuum of the tissue-blood control volume similar to Wulff (Wulff, 1974) and Klinger (Klinger, 1974). Chen and Holmes defined a differential control volume (δV) and distinguished the vascular space occupied by blood (V_b), and the space occupied by the solid tissue (δV_s). Thus, the total space of control volume (δV) can be defined as:

$$\delta V = \delta V_s + \delta V_b \tag{3-16}$$

Due to the simplified volume-averaging technique, the conservation of energy for both the solid tissue space and vascular spaces can be written as follows:

$$\left(\rho C_p\right)_{eff} \frac{\partial T_t}{\partial t} = q'_k + q'_m + q'_p \tag{3-17}$$

$$\rho_{eff} = (1 - \phi_b)\rho_s + \phi_b \rho_b \tag{3-18}$$

$$C_{p_{eff}} = \frac{1}{\rho}\Big((1 - \phi_b)\rho_s C_{p,s} + \phi_b \rho_b C_{p,b}\Big) \tag{3-19}$$

$$T_t = \frac{1}{\rho C_p}\Big((1 - \phi_b)\rho_s C_{p,s}\, T_s + \phi_b \rho_b C_{p,b}\, T_b\Big) \tag{3-20}$$

where $\phi_b = \frac{\delta V_b}{\delta V} \approx \frac{\delta V_b}{\delta V_s} \ll 1$ is the volume fraction, the ρ is the density (kg/m^3), C_p is the specific heat capacity (J/kg·ºC), T_t is local mean tissue temperature (ºC), and subscripts s, b, eff are solid tissue phase, blood phase, and effective value. The quantity q'_k denotes conductive heat gain per unit volume, q'_m is metabolic heating per unit volume, and q'_p is the perfusion energy generated per unit volume. The total conductive heat gain per unit volume (q'_k) is express by:

$$q'_k = \frac{Q_{k,s} + Q_{k,b}}{\delta V} = \nabla \cdot k_k \nabla T_t \tag{3-21}$$

where k_{eff} is the effective thermal conductivity of the combined solid tissue and vascular spaces. For $\phi_b \ll 1$, the effective thermal conductivity is approximately to the conductivity of the solid tissue.

In assumption of Chen and Holmes (Chen & Holmes, 1980), the total perfusion term due mainly to blood flow in vessels crossing the surface (δS). Consequently, the convective heat flow through δS can be written as a sum of the contribution of each vessel crossing the surface:

$$q_p' = \frac{1}{\delta V} \int \rho_b \, C_{p,b} \, Tu \cdot ds = \rho_b C_{p,b} \sum T_{bi}^0 u_i \, A_i \sin\theta_i \tag{3-22}$$

For $\phi_b \ll 1$, local mean tissue temperature (T_t) is approximately to solid tissue temperature (T_s), u was a continuous blood velocity (m/s), A_i is the flow area of the individual vessels, θ_i inclination with respect to crossing the surface, u_i and T_{bi}^0 are the mean velocity (m/s) and mean blood temperature (°C), respectively.

Furthermore, Chen and Holmes evaluated the thermal equilibration length of individual vessels with semi-quantitative. This model overcomes the limitations of the Wulff (Wulf, 1974) and Klinger (Klinger, 1974) model, which developed based on thermal equilibrium area. Under assumption the transient blood temperature is smaller than the spatial variations along a characteristic length of the individual vessel. Thus, the governing equation for the blood temperature is expressed by:

$$A_i \left(\rho C_p\right)_b u_i \frac{dT_{bi}}{dx} = U_i P_i (T_s - T_{bi}) \tag{3-23}$$

where U_i is the overall heat transfer coefficient and P_i is the circumference of the blood vessel. The length x is measured along the axis of the blood vessel, in the direction of flow. Eq. (3-23) can be written more concisely as:

$$l_{eq} \frac{dT_{bi}}{dx} = T_s - T_{bi} \tag{3-24}$$

where l_{eq} is the thermal equilibration length, imply the length over which the temperature difference will be reduced by a factor e, and defined as

$$l_{eq} = \frac{A_i(\rho C_p)_b u_i}{U_i P_i} \tag{3-25}$$

This semi-quantitative model results indicate the thermal equilibrium of the blood in the living tissue occurs not in the capillaries but occurs in the vessel diameter range of 0.2-0.5 mm. This conclusion was supported the incorrect assumption underlying the Pennes bioheat model. Chen and Holmes model the blood vessel should be separated into two categories; the first, the large vessel was separated heat transfer analysis. Second, the small size vessel should be analyzed with continuum. Furthermore, the biological tissue's heat transfer with the small vessel can be divided into three cases. The first model presented the thermal equilibration of blood temperature. In this case, the blood temperature was assumed to be the sufficiently large vessel, which enclosed the small vessel in the control volume. Hence, the heat transfer due to the blood contribution within the tissue control volume looked quite similar to the Pennes perfusion heat source and described as:

$$q'_p = \omega^* \left(\rho C_p\right)_b (T_a^* - T) \tag{3-26}$$

where ω^* is total perfusion rate in the control volume, and T_a^* is represented the temperature of blood in the largest vessel.

The second model, the heat transfer in the control volume was already thermally equilibrated vessels. The blood temperature was equal to tissue temperature everywhere in control volume, and the blood contribution assumes the form:

$$q'_p = \left(\rho C_p\right)_b \vec{u} \cdot \nabla T \tag{3-27}$$

where $\vec{u}$ is the net volume flux of blood in the control volume.

The third model is considered with nearly the equilibration of blood temperature along with the tissue temperature gradient. In this case, the heat transfer is

proportion of tissue temperature gradient based on the microvascular structure. In this case, the heat transfer is the proportion of tissue temperature gradient based on the microvascular structure. Chen and Holmes proposed the perfusion conductivity ($k_{p\beta i}$) for heat transfer in this state and expressed by:

$$q'_p = -k_{p\beta i} \cdot \nabla T \tag{3-28}$$

where $k_{p\beta i}$ is dependent on the individual vascular structure, which could be found as the extended term in the literature (Chen & Holmes, 1980)

Thus, the bioheat was developed by Chen and Holmes model can be written as:

$$(\rho C_p)_t \frac{\partial T_t}{\partial t} = \nabla \cdot \left(k_{eff} \nabla T\right) + \omega^* \left(\rho C_p\right)_b (T_a^* - T) - \left(\rho C_p\right)_b \vec{u} \cdot \nabla T + k_{p\beta i} \cdot \nabla T + Q_{met} \tag{3-29}$$

3.2.5 The Weinbaum, Jiji, and Lemons (WJL) Bioheat Model

Although Chen and Holmes's model improved the bioheat model, it is not satisfactory to implement because it required more detailed vascular structure and blood perfusion. Furthermore, Chen and Holmes's model was not considered the effect of countercurrent vessels. Weinbaum et al. proposed the three equations model for heat transfer in the biological tissue, small artery, and small vein (Weinbaum et al., 1984). This model was developed under assume the small artery and vein are parallel and blood countercurrent flow. Under the assumption neglecting axial conduction, the energy conservation equations for a heat transfer in artery and vein are written as:

$$\pi\left(\rho C_p\right)_b \cdot \frac{d\left(n r_b^2 \vec{V} \cdot T_a\right)}{ds} = -n \cdot q_a - 2\pi\left(\rho C_p\right)_b n r_b g \cdot T_a \tag{3-30}$$

$$\pi\left(\rho C_p\right)_b \cdot \frac{d\left(n r_b^2 \vec{V} \cdot T_v\right)}{ds} = -n \cdot q_v - 2\pi\left(\rho C_p\right)_b n r_b g \cdot T_v \tag{3-31}$$

where q_a is heat loss from the artery by conduction through its wall, q_v is heat gain by conduction per unit length through the vein wall into the vein, n is number of vessel density, r_b is the vessel radius, $\vec{V}$ is the mean velocity in either the artery or vein, g is defined as bleed-off, T_a and T_b are the bulk mean temperatures inside the blood vessel.

Eq. (3-29) and (3-30) can be simplified by using the mass conservation equation whereby the bleed-off accounts for transient mass flux inside the vessels. Thus, the three governing equations of the control volume were written as:

$$\left(\rho C_p\right)_b \pi r_b^2 \vec{V} \cdot \frac{d(T_a)}{ds} = - \cdot q_a \tag{3-32}$$

$$\left(\rho C_p\right)_b \pi r_b^2 \vec{V} \cdot \frac{d(T_v)}{ds} = - \cdot q_v \tag{3-33}$$

$$\rho C_p \frac{\partial T}{\partial t} = \nabla \mathrm{k} \cdot \nabla \mathrm{T} + \mathrm{ng}\left(\rho C_p\right)_b \cdot (T_a - T_v) - \mathrm{n}\pi r_b^2 \left(\rho C_p\right)_b \vec{V} \cdot \frac{d(T_a - T_v)}{ds} + Q_m \tag{3-34}$$

WJL model (Weinbaum et al., 1984) is widely criticized as conflicting with numerous experimental findings that the temperature of blood exiting the capillaries is closer to that of the tissue than to that of the vein. Moreover, the WJL model required the most detail of the anatomy of the vascular structure.

3.2.6 The Weinbaum and Jiji (WJ) Bioheat Model

The WJL model was difficult to implement in practical situations. In these shortcomings, Weinbaum and Jiji proposed a simplified model for descript the heat transfer in the biological tissue (Weinbaum & Jiji, 1985). This model was developed underlying based on the simple assumption. The average temperature in the control volume equals an average temperature of the adjacent countercurrent pair of closely spaced and nearly equilibrated vessels, which can be expressed as:

$$T \cong \frac{(T_a + T_b)}{2} \tag{3-35}$$

Moreover, Weinbaum and Jiji assumed the heat conduction through the arteries wall is conducted in through the vein wall, which can be defined as:

$$q_a \cong q_v \cong \sigma_\Delta k_t (T_a - T_b) \tag{3-36}$$

where σ_Δ is geometric shape conduction between two countercurrent vessels.

Eq. (3-35) and (3-36) was substituted in WJL model, the temperature of blood can be eliminated from the derivation. Thus, the energy equation was reduced to form simplified form:

$$\frac{\partial}{\partial x}\left(k_{eff}\frac{\partial T}{\partial x}\right) + Q_m = \rho C_p \frac{\partial T}{\partial t} \tag{3-37}$$

where

$$k_{eff} = k\left[1 + \frac{n\left\{\pi r_b^2 (\rho C_p)_b \vec{V}\cos\gamma\right\}^2}{\sigma_\Delta \cdot k^2}\right] \tag{3-38}$$

where γ is angle between the direction of a blood vessel and the local tissue temperature gradient.

However, the WJ model (Weinbaum & Jiji, 1985) was questioned to incorrectly assumption, especially the average temperature concept.

3.2.7 The Heat transfer of large vessel flow

In previous studies, the heat transfer in the large vessel should be suggested as a separate analysis. Thus, the heat transfer in a blood vessel was considered underlying the heat convection flow. The governing equations for heat transfer and flow analysis in the blood vessel can be written as:

Energy equation

$$\rho_b C_{p,b}\frac{\partial T_b}{\partial t} + \rho_b C_{p,b}\vec{V}\cdot\nabla T_b = \nabla\cdot(\mathrm{k}\nabla T)_b + Q_{ext} \tag{3-39}$$

Momentum equation

$$\rho_b \frac{\partial \vec{V}}{\partial t} + \rho_b \left(\vec{V} \cdot \nabla\right) \vec{V} = -\nabla P + \mu_b \nabla^2 \vec{V} + F \tag{3-40}$$

Continuity equation

$$\frac{\partial \rho_b}{\partial t} + \nabla \cdot \left(\rho_b \vec{V}\right) = 0 \tag{3-41}$$

where Q_{ext} is the source term (W/m^3), $\vec{V}$ is the blood velocity in the vessel (m/s), and μ_b is the blood viscosity (Pa.s), and F is the body force term (Pa).

3.3 The modeling of heat transfer in the biological tissue using porous media approach

Although the Pennes bioheat equation is considered a useful model for predicting the temperature distribution in the biological tissue due to its simplicity, it is questioned on the underlying assumptions' physical and physiological validity. In the previous section, the modified and extended bioheat models were developed to improve the bioheat's shortcoming. However, the modified and extended bioheat models required a more detailed vascular structure and less flexible to implement. In particular, the heat transfer in the biological tissue involved heat conduction combined with heat convection. The bioheat or modified bioheat models cannot capture heat convection and flow in the biological tissue during the heat transport process. In the essential of advanced medical technology, thermal ablation treatment requires effective modeling for describing thermal interaction between vascular system and tissues in the specific tissue or organs. Therefore, the advanced bioheat model incorporating thermal blood contribution, effective tissue conductivity, effective tissue capacitance, porosity variation, and a more precise representation of the heat exchange between the blood and the tissue critically should be developed. The biological tissue comprises cell and microvascular bed with the blood flow direction contains many vascular and can be

regarded as a porous media structure (Rattanadecho & Keangin, 2013). Therefore, the porous media theory is very well suited for developing a rigorous bioheat equation model.

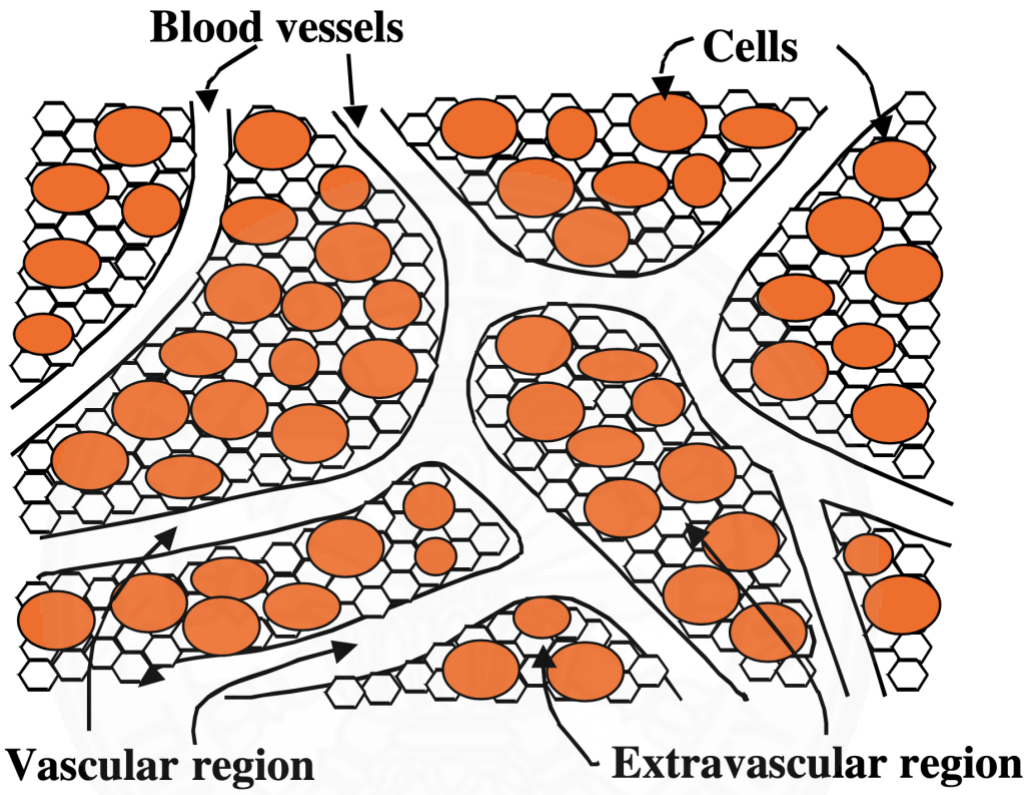

Fig. 3.1. Schematic view of biological tissue (Nakayama & Kuwahara, 2008)

The biological tissue structure comprises the dispersed solid matrix (tissue cell) and connective with the voids, which allows for the flow of nutrients, minerals, etc., to reach all cells within the tissue. Mass transfer of these substances into biological and medical applications is achieved by diffusion within the tissue. Therefore, the porous theory has been applied in the biological tissue for predicting the heat transfer, especially heat convection during heat transfer process. Therefore, the porous theory has been applied in the biological tissue to predict heat transfer, especially heat convection in the biological tissue. Compared to the simplified bioheat model, the bioheat based on the porous media approach required few assumptions and flexible in

many applications (Khaled & Vafai, 2003; Khanafer and Vafai 2006; Nakayama and Kuwahara, 2007).

In this dissertation, the bioheat model based on the porous media approach can be divided into two models: local thermal equilibrium (LTE), and local thermal non-equilibrium.

3.3.1 Local thermal equilibrium (LTE) model

The local thermal equilibrium (LTE) model is developed under the assumption of the solid phase temperature is equal to fluid phase temperature at the local position in the porous medium. This assumption occurs when heat exchange between the tissue and the blood is efficient where applied in the tissue with small vascular and slow blood velocity. This assumption that blood flowing in these small vascular would be completely equilibrated with the surrounding tissue. The governing equation for the analysis of heat transfer in the biological tissue based on the LTE assumption is given by:

$$(\rho C_p)_{eff}\frac{\partial T}{\partial t} + (\rho C_p)_b \vec{V}\cdot\nabla T = \nabla\cdot\left(k_{eff}\nabla T\right) + Q_{met} + Q_{ext} \qquad (3\text{-}42)$$

where

$$(\rho C_p)_{eff} = (1-\phi)(\rho C_p)_t + \phi(\rho C_p)_b \qquad (3\text{-}43)$$

$$k_{eff} = (1-\phi)k_t + \phi k_b \qquad (3\text{-}44)$$

where the subscript eff, t and b represent the effective value, solid phase, and blood phase, respectively. ϕ is the porosity (volume fraction of the vascular space), ρ is the tissue density (kg/m^3), C_p is the specific heat capacity (J/kg· ºC), T is the temperature of tissue (ºC), k is the thermal conductivity (W/m·ºC), ρ_b is the blood density (kg/m^3), Q_{met} is the metabolism heat source (W/m^3), and Q_{ext} is the external heat source term (W/m^3).

In the left-hand side of Eq. (3-42), the second term the blood convection in the biological tissue. Note that the perfusion term in the Pennes bioheat equation (Pennes, 1948) was derived based on the assumption of uniform blood perfusion and was equal to $\rho_b C_{p,b} \omega_b (T_b - T)$. The first term on the left-hand side represents the transient heat in the biological tissue. The first, second, and third on the right-hand side represent the conduction term, metabolic heat generated term, and external heat source term, respectively.

However, the LTE assumption model is not satisfied when applied in the high-speed flow through the porous media (Keangin et al., 2013). In this shortcoming, the bioheat model based on the local thermal non-equilibrium was introduced.

3.3.2 Local thermal non-equilibrium (LTNE) model

The local thermal non-equilibrium (LTNE) model is developed under the assumption of the solid phase temperature is not equal to fluid phase temperature at the local position in the porous medium. This model analysis the heat transfer separately considered between solid phase (tissue cells) and fluid phase (blood phase). Thus, this model can better capture the details of heat transfer phenomena, especially heat convection. The model based on the LTNE assumption is preferred to be used in many applications because there are few assumptions and few limitations (Khaled & Vafai, 2003; Khanafer and Vafai 2006; Nakayama and Kuwahara, 2007). Therefore, the model based on LTNE is used to describe the heat transfer in the biological tissue. Therefore, the two governing equations were derived that represents the heat transfer in the solid matrix phase and blood phase can be written as:

Solid matrix phase

$$(1-\phi)(\rho C_p)_t \frac{\partial T_t}{\partial t} = \nabla \cdot \left(k_{t,eff} \nabla T_t\right) - \left(\rho C_p\right)_b \omega_b (T_t - T_b) - h_{tb} a_{tb} (T_t - T_b) + (1-\phi) Q_{met} + (1-\phi) Q_{ext} \quad (3\text{-}45)$$

Blood phase

$$\phi(\rho C_p)_b \frac{\partial T_b}{\partial t} + \phi(\rho C_p)_b \vec{V} \cdot \nabla T = \nabla \cdot \left(k_{b,eff} \nabla T_b\right) + \left(\rho C_p\right)_b \omega_b (T_t - T_b) + h_{tb} a_{tb} (T_t - T_b) + \phi Q_{met} + \phi Q_{ext} \quad (3\text{-}46)$$

where T_t is the local temperature of solid matrix phase (ºC), T_b is the local temperature of blood phase (ºC), h_{tb} is the blood to tissue interfacial heat transfer coefficient (W/m^2·ºC), a_{tb} is the volumetric transfer area between the blood and the tissue (m^2/m^3), $k_{t,eff}$ is the effective thermal conductivity of the solid matrix phase (W/m·ºC), and $k_{b,eff}$ is the effective thermal conductivity of the blood phase (W/m·ºC). The effective thermal conductivity can be written as (Alazmi & Vafai, 2000; Keangin & Rattanadecho, 2013):

$$k_{t,eff} = (1 - \phi) k_t \quad (3\text{-}47)$$

$$k_{b,eff} = \phi k_b \quad (3\text{-}48)$$

where the subscript eff, t and b represent the effective value, solid phase, and blood phase, respectively.

The h_{tb} depends on the nature of the porous matrix structure and the saturating fluid and the value of this coefficient has been the subject of intense experimental interest (Rattanadecho & Keangin, 2013). High values of h_{tb} correspond to a rapid transfer of heat between the phases (LTE assumption) and small values of h_{tb} gives rise to relatively strong LTNE effects (Malashetty et al., 2008).

3.3.3 Flow convection in biological tissues

In general, the porous media model was developed based on transport equations. Under the governing equations, the heat and mass transport phenomenon are predicted in the porous media domain. Thus, mass transport is analyzed in model based on porous media approach.

Henry Darcy introduced the Darcy model based on his experimental study (Darcy, 1856). This model is considered to be the simple flow transport model in porous media. The linear proportionality between the flow velocity and the applied pressure difference. Darcy model is expressed by:

$$\nabla P = \frac{\mu}{\kappa}\vec{V} \tag{3-49}$$

where P is the pressure of fluid flow in the porous media, μ is dynamic viscosity of the pure fluid (Pa.s), $\vec{V}$ is the blood velocity in the vessel (m/s),

The Darcy model ignores the boundary effects on the flow. This assumption is not applicable when considering the boundaries of the porous medium. Therefore, the Brinkman model is usually employed.

$$\nabla P = \frac{\mu}{\kappa}\vec{V} + \tilde{\mu}\nabla^2\vec{V} \tag{3-50}$$

where $\tilde{\mu} = \frac{\mu}{\phi}\lambda^*$ is the effective viscosity of the porous medium, ϕ is the porosity of porous media, and λ^* is tortuosity.

The Brinkman model was introduced by Brinkman (Brinkman, 1947), and the Brinkman model as shown in Eq. (3-50). The first term on the left-hand side represents the gradient pressure. On the right-hand side, the first term represents the viscous term similar to the Darcy model. The second term on the right-hand side represents analogous to the momentum diffusion term in the Navier–Stokes's equation.

In the case of fluid inertia not negligible, the fluid's drag force exerted by the solid becomes significant. The generalized model for flow transport in porous media for various pertinent effects was proposed by Vafai and Tien, which developed based on the Brinkman–Forchheimer–Darcy equation (Vafai & Tien, 1982; Vafai, 1984; Khaled & Vafai, 2003). This equation is given by:

$$\frac{\rho}{\phi}\left(\frac{\partial\vec{V}}{\partial t} + \left(\vec{V}\cdot\nabla\right)\vec{V}\right) = -\nabla P + \frac{\mu}{\phi}\nabla^2\vec{V} - \frac{\mu}{\kappa}\vec{V} - \frac{\rho F\phi}{\kappa^{1/2}}\left(\vec{V}\cdot\vec{V}\right)J \tag{3-51}$$

where F is the dimensionless inertia term coefficient and J is a unit vector oriented along the velocity vector $\vec{V}$.

In the next chapters, the mentioned theory is brought to apply in the model. The liver cancer treatment with the MWA model was considered the 3D model in chapter 4 and the 2D axisymmetric model in chapter 5. In chapter 4, the mathematical model is considered couple with electromagnetic wave propagation, heat transfer in the tumor and normal liver tissue (living tissue), and the blood flow in a single vessel. Chapter 5 proposed the performancing comparative of the predicted heating models implemented of the liver cancer model by MWA. The heating models implemented were the bioheat model, the porous model with constant velocity, and the Darcy-Brinkman porous model. In this chapter, the mathematical models were developed with different governing equations for founding the performance of the different heating models.

CHAPTER 4
3D NUMERICAL ANALYSIS OF FOCUSED MICROWAVE ABLATION FOR THE TREATMENT OF PATIENTS WITH LOCALIZED LIVER CANCER EMBEDDED WITH A VERTICAL AND HORIZONTAL BLOOD VESSEL

4.1 Introduction

Microwave Ablation (MWA) is the minimally invasive and effective treatment methods for liver cancer therapy (Keangin et al., 2011; Nabaei & Karimi, 2018) This treatment is applied the microwave energy into the local cancer area or tumor area through the microwave antenna. The microwave would be absorbed and converted to the local heat generation in the tumor area (Keangin et al., 2011). The tumor temperature is increased in this treatment process. When tissue temperature rises above 52^{o}C, the cancer cell will immediately die during the MWA process (Dong et al., 1998; Goldberg et al., 2000; Whelan et al. 2005; Prakash et al., 2008; Prakash et al., 2012; Wu et al., 2013). This treatment aims to elevate the tumor temperature above 52 ^{o}C where the tumor is destroyed and without damage to the surrounding tissue (Keangin & Rattanadecho, 2013). Therefore, understanding the heat transport mechanism in the treatment area is an important factor for treatment achieved.

MWA had remarkably developed, showing the many advantages of this treatment over the surgical (Lopresto et al., 2017). The clearly advantages of MWA treatment are minimal invasiveness and rapidly treatment (Hines-Peralta et al., 2006). Although MWA was an interested and effective treatment method, the experimental and studying in the humans liver could not ordinary studied. Because it was due to humanity and the risk of unethical. Some group researchers had been experimenting with animals (Strickland et al., 2002; Hines-Peralta et al., 2006; Yang et al., 2007; Marcelin et al., 2018). However, these experimental studies had limitations compared to experimenting with a nearly realistic human liver. The numerical simulation could be applied to study the treatment. It has been the advantage of needing only a short

period, the low economic cost, humanity, and could be set up with conditions near to those of a real human liver (Keangin & Rattanadecho, 2013).

Several years ago, many researchers developed mathematical models for predicting the temperature distribution in living tissue. The most widely model was introduced by Pennes, which has become well known as the bioheat model (Pennes, 2948). The bioheat model is developed based on heat diffusion between living tissue and blood vessels. Due to the Pennes bioheat simplification, many studies have established and developed the mathematical of the extending and modifying the Pennes bioheat (Wulff, 1974; Klinger, 1974, Chen & Holmes, 1980). Moreover, some group researchers investigated the effect of the heat transfer between arteries, veins, and surrounding tissue (Keller & Seiler, 1971; Weinbaum et al, 1984; Jiji et al., 1985). The previous bioheat mathematical modeling studies were the critical foundation for developing the heat transfer in the living tissue model during the MWA process.

In 2007, Yang et al. proposed the modified bioheat for MWA treatment and comparative with their experimental (Yang et al, 2007). Yang et al. added the liver evaporation term in the bioheat equation, and their model was the suitable predicting model in the high-temperature zone. However, the modified bioheat model by Yang et al. was not accurately predicting model, which was proved by Keangin et al. (Keangin et al., 2011). Keangin et al. investigated the thermal expansion of liver cancer treatment with MWA by using numerical simulation. As a result, the deformation analysis model was highly accurate than the model without deformation analysis. Later, Wu et al. investigated the effect of multi-frequency on the liver cancer treatment model with MWA by using numerical simulation (Wu et al., 2016). Results showed the high frequencies of microwaves were significantly affected the heating pattern in the liver cancer model. Furthermore, the porous media theory was developed to be approached for heat transfer analysis in living tissue (Khaled & Vafai, 2003; Khanafer & Vafai 2006; Nakayama & Kuwahara, 2007; Wessapan & Rattanadecho, 2012; Rattanadecho & Keangin, 2013; Keangin & Rattanadecho, 2013) The advantage, the porous media approach requires fewer assumptions than the bioheat approach. However, the many porous modeling or the bioheat modeling based on the two-dimensions (2D) axisymmetric or 2D problems. The shortcoming of the 2D and 2D axisymmetric could not be applied for the diversity of treatment cases. In the realistic treatment, we could

not avoid analyzing specific cases. Therefore, the three dimensions (3D) problem has developed.

The thermal ablation studies developed mathematical modeling based on 3D heat transfer problems in the living tissue in specific cases. Especially, cases of the heat transfer in the living tissue conjugated with the blood vessels flow. In 2015, Zorbas and Samaras investigated the effect of diameter and distancing of a single vessel on the cancer treatment model with radiofrequency ablation (RFA) (Zorbas & Samaras, 2015). Shao et al. investigated the effect of nanoparticle injection on the liver cancer nearly countercurrent vessels with RFA treatment technique (Shao et al, 2017). Although the studying cancer treatment model with RFA treatment showed promising results, the treatment with the RFA technique differed from the MWA technique. Therefore, the 3D mathematical model of MWA was to be developed.

The present study presented the 3D liver cancer treatment with the MWA technique model embedded with a single blood vessel near the treatment area, as shown in Fig. 4.1. The characteristic of a vessel location between the horizontal vessel and vertical vessel was investigated. The mathematical model is considered couple with electromagnetic wave propagation, heat transfer in the tumor and normal liver tissue (living tissue), and the heat transfer in a single vessel. The mathematical models were solved by the finite element method (FEM) based on the 3D transient problem. The characteristic of the vessel location was investigated on the SAR distribution, the temperature distribution, velocity profile, and the necrotic of damaged tissue in the 3D liver cancer treatment model. The simulation results in this study can be used as a guideline for partial treatment.

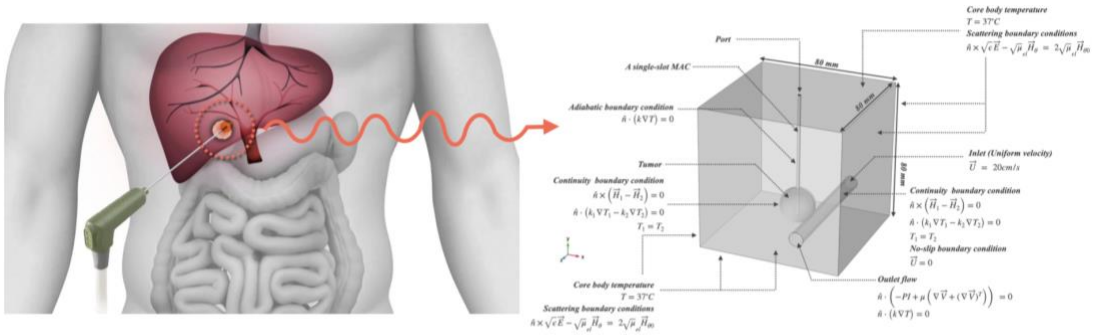

Fig. 4.1 The liver cancer with the MWA treatment concept to the 3D mathematical model.

4.2 Problem statement

This study developed the 3D numerical modeling of the liver cancer treatment with MWA by using the single slot of microwave coaxial antenna (MCA). The slot coaxial antennas are the common antennas in MWA application of the advantages, size (small dimensions), design simplicity, low cost to manufacture, and convenient adaptation to treatment (Rattanadecho & Keangin et al., 2013). The single-slot MCA has a diameter of 1.79 mm; the antenna is required as small as possible for minimally invasive (Rattanadecho & Keangin, 2013; Keangin & Rattanadecho, 2013). A wide ring-shaped slot of 1 mm is cut off the outer conductor, and the length of 5.5 mm from the short-circuited tip, that for avoiding the electric field becomes stronger near the slot (Saito et al., 2000). This antenna operated at the microwave power of 10 and frequency of 2.45 GHz. The dimension and properties of single-slot MCA are shown in Table 4.1.

Table 4.1 Dimensions and dielectric properties of single slot MCA (Keangin et al., 2011)

Material	Dimensions (mm)	Dielectric properties		
		Relative permittivity, ε_r	Electric conductivity, σ_{el} (S/m)	Relative permeability, μ_r
Inner conductor	0.135 (radial)	-	-	-
Dielectric	0.47 (radial)	2.03	0	1
Outer conductor	0.595 (radial)	-	-	-
Catheter	0.895 (radial)	2.1	0	1
Slot	1.00 (wide)	1	0	1

The 3D liver cancer treatment with the MWA technique model embedded with a single blood vessel consists of 4 domains; 1) the tumor domain was assumed spherical tumor domain and located on the center of the model, 2) normal tissue domain represented the liver domain the healthy liver tissue, where surrounded tumor domain,

3) MCA domain, and 4) a single blood vessel domain was nearly the tumor domain. This study investigated two different models, as shown in Fig. 4.2. Fig. 4.2(a) shows the liver cancer model with a single vertical vessel, and Fig. 4.2(b) shows the liver cancer model with a single horizontal vessel. This study investigated the effect of characteristic vessel location on the SAR distribution, temperature distribution, and damaged tissue area in the liver cancer model. The system of the governing equations as well as the initial condition and boundary condition were solved numerically by using FEM.

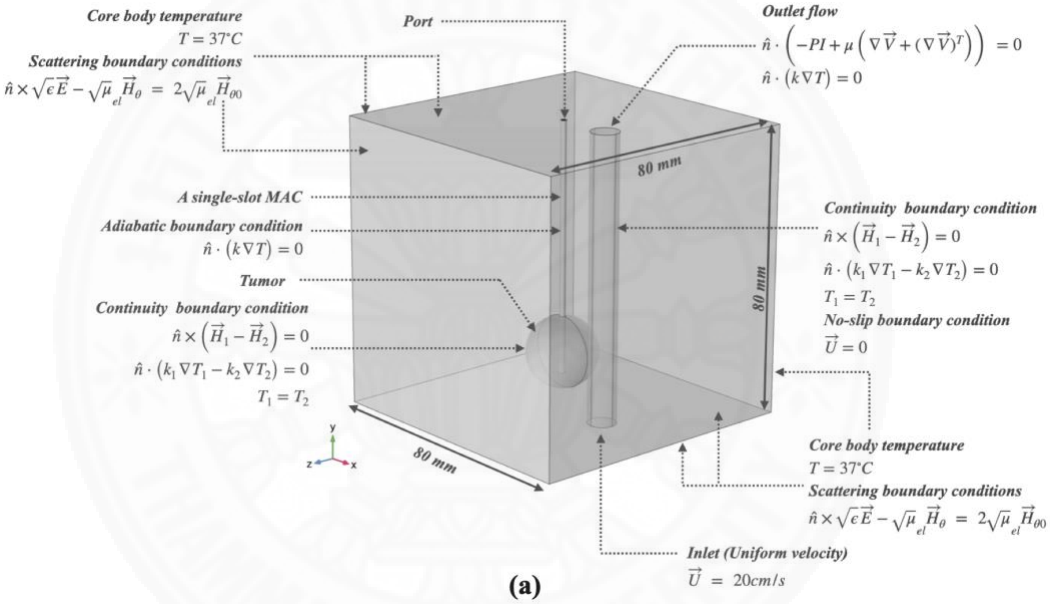

Fig. 4.2 The physical domain and boundary conditions of the liver cancer embedded with a single blood vessel model; (a) the model with a vertical vessel, (b) the model with a horizontal vessel.

4.3 The formulation and the mathematical model

This study focused on the heat transfer difference in the liver cancer tissue, where nearby a single vessel. A single slot MCA was transmitted the microwave energy into the tumor domain. The microwave power of 10 W and frequency of 2.45 GHz were operated for all cases. The two liver cancer models embedded with a single blood vessel shown in Fig. 4.2: Fig. 4.2(a) the vertical vessel model, and Fig. 4.2(b) the horizontal vessel model. The heat transfer and the damaged region between the vertical and the horizontal vessel models were comparison and investigation. The mathematical model calculated coupled with the electromagnetic wave propagation, the heat transfer in the tumor and normal liver tissue (living tissue), and the heat transfer of blood flow in a single vessel. For calculation, this 3D transient problem was solved by using FEM.

4.3.1 The Physical model

In this study, the comparison between the liver cancer treatment with the vertical and horizontal vessel was investigated. The liver cancer model with a vertical vessel was assembled with the four major parts: 1) tumor, 2) normal tissue, 3) MCA, and 4) a single blood vessel. The liver tissue was considered to be the cube ($80x80x80\ mm^3$). The MCA was inserted on the top of the domain into the spherical tumor and parallel with the Y-axis. The center of the tumor and the slot were set to the insertion depth of 64 mm (Y-axis = 16 mm). The spherical tumor of 20 mm diameter was located on the center of the X and Z planes. A vertical blood vessel of 8 mm diameter was located parallel with the MCA and away from the MCA of 12 mm. The dimensions of the physical domain were based on literature (Rattanadecho & Keangin et al., 2013; Shao et al, 2017).

The liver cancer model with a horizontal vessel was assembled with four parts, as same as the model with a vertical vessel. The dimension of liver cancer with a horizontal vessel model was equally set to the vertical model, except for the

vessel location. The center of a horizontal vessel was set at the same level as the center of tumor. A horizontal blood vessel was placed along the X-axis and away from the MCA of 12 mm, as same as the model with the vertical vessel. The physical properties of MCA, liver tissue, tumor, and blood are shown in Table 4.2

4.3.2 The electromagnetic wave propagation analysis

The electromagnetic wave propagation affected the performance of the MWA treatment. The governing equations and conditions of electromagnetic wave propagation are considered to all domains. To reduce the complexity of the problem, the following assumptions are made:

1. The electromagnetic wave propagation is propagated in three dimensions (3D) analysis.
2. The electromagnetic wave propagation in the MCA is characterized by transverse electromagnetic fields (TEM) (Bertram et al., 2006; Keangin et al., 2011).
3. The electromagnetic wave propagation in the living tissue is characterized by transverse magnetic fields (TM) (Bertram et al., 2006; Keangin et al., 2011).
4. The model assumes that the dielectric properties of the liver are uniform and constant.

The propagation of the electromagnetic wave propagation in the antenna is by a transverse electromagnetic field (TEM) (Bertram et al., 2006; Keangin et al., 2011; Rattanadecho & Keangin, 2013), that given as:

Electric field ($\vec{E}$) $$\vec{E} = \vec{e}_r \frac{C}{r} e^{j(\omega t - kz)} \quad (4\text{-}1)$$

Magnetic field ($\vec{H}$) $$\vec{H} = \vec{e}_\varphi \frac{C}{rZ} e^{j(\omega t - kz)} \quad (4\text{-}2)$$

where $C = \sqrt{\frac{ZP_{in}}{\pi \cdot \ln(r_{outer}/r_{inner})}}$ is the arbitrary constant, Z is the wave impedance (Ω), Pin is the microwave power input (W), r_{outer} is the dielectric outer radius (m), r_{inner} is the dielectric inner radius (m), f is the frequency (Hz), $\omega = 2\pi f$ is the angular frequency

(rad/s), k is the wave propagation constant (m^{-1}), which relates to the wavelength (λ) in medium: $k = \frac{2\pi}{\lambda}$.

The propagation of the electromagnetic wave in the living tissue is by a transverse magnetic field (TM) as described by the following equation:

$$\nabla \times \left(\left(\frac{1}{\varepsilon_r} - \frac{j\sigma_{el}}{\omega \varepsilon_0} \right)^{-1} \nabla \times \vec{H}_\theta \right) - \mu_r k_0^2 \vec{H}_\theta = 0 \qquad (4\text{-}3)$$

where $\vec{H}_\theta$ is magnetic field intensity (A/m), μ_r is relative permeability, ε_r is relative permittivity, $\varepsilon_0 = 8.8542 \times 10^{-12}$ F/m is permittivity of free space, σ_{el} is electric conductivity (S/m), k_0 is the free space wavenumber (m^{-1}), and $\omega = 2\pi f$ is the angular frequency (rad/s).

The interaction of an electromagnetic wave with living tissue could be defined in terms of an SAR distribution. When the single-slot MCA transmits the electromagnetic wave, it passes through it and then propagates throughout the entire domain. The electromagnetic wave is absorbed and converted to the heat generation in liver tissue. In this study, SAR represents the microwave power absorption deposited per unit mass in tissue (W/kg) (Rattanadecho & Keangin, 2013). The SAR is given by:

$$\mathrm{SAR} = \frac{\sigma_{el}}{2\rho} \left| \vec{E} \right| \qquad (4\text{-}4)$$

where σ_{el} is the electrical conductivity (S/m), ρ is the tissue density (kg/m^3), and $\vec{E}$ is the electric field intensity (V/m). The SAR was converted to the heat generated in the living tissue, which is defined as:

$$Q_{ext} = \frac{\sigma_{el} |\vec{E}|^2}{2} = \rho \cdot \mathrm{SAR} \qquad (4\text{-}5)$$

The boundary conditions of electromagnetic wave propagation are applied for all models. The electromagnetic wave boundary conditions of the model shown in Fig. 4.2, and the following conditions are made:

1. The outside of the computation domain is considered as a scattering boundary condition to eliminate the reflections:

$$\hat{\mathrm{n}} \times \sqrt{\varepsilon}\vec{E} - \sqrt{\mu_{\mathrm{el}}}\vec{H}_{\theta} = 2\sqrt{\mu_{\mathrm{el}}}\vec{H}_{\theta 0} \quad (4\text{-}6)$$

2. The interfaces between different mediums are considered as a continuity boundary condition:

$$\hat{\mathrm{n}} \times \left(\vec{H}_1 - \vec{H}_2\right) = 0 \quad (4\text{-}7)$$

3. The boundary conditions of the inner and outer conductor of MCA as the perfect electric conductor (PEC) boundary conditions:

$$\hat{\mathrm{n}} \times \vec{E} = 0 \quad (4\text{-}8)$$

4. The port boundary condition is applied at the inlet of MCA with the microwave power set of 10 W.

Table 4.2 The dielectric and thermal properties of the tissue (Keangin & Rattanadecho, 2013; Koksungnoen et al., 2018)

properties	Normal Tissue	Tumor	Blood
Relative permittivity, ε_r	43	48.16	58.3
Electric conductivity, σ_{el} (S/m)	1.69	2.096	2.54
Density, ρ (kg/m^3)	1030	1040	1058
Thermal conductivity, k_{th}(W/m·ºC)	0.497	0.57	0.45
Specific heat capacity C_p (J/kg· ºC)	3,600	3,960	3,960

4.3.3 The heat transfer in the living tissue analysis

The heat transfer of living tissue analysis is applied in the tumor and liver demains based on the bioheat equation. For the reduced the complexity of the problem, the heat transfer in the living tissue follows the assumptions are made:

1. The heat transfer of the living tissue based on the bioheat approach is considered in three dimensions (3D) analysis.
2. The heat transfer of living tissue analysis is considered only in the tumor and liver tissue domains.
3. The chemical reaction and phase change in the living tissue are ignored.
4. The heat transfer of the single-slot MCA is ignored.
5. The liver tissue and tumor tissue are assumed the homogeneous and thermally isotropic.
6. The thermal properties of the living tissue are uniform.

The heat transfer analysis of the living tissue can be described by the Pennes bioheat equation (Pennes, 1948), which can be written as follows:

$$\rho_t C_{p,t} \frac{\partial T}{\partial t} = \nabla \cdot k_{th,t} \nabla T + \rho_b C_{p,b} \omega_b (T_b - T) + Q_{met} + Q_{ext} \quad (4\text{-}9)$$

where ρ_t is the density of living tissue (kg/m^3), $C_{p,t}$ is the specific heat capacity of tissue (J/kg.ºC), T is temperature of living tissue (ºC), $k_{th,t}$ is the thermal conductivity of tissue (W/m.ºC), ρ_b is the destiny of blood (kg/m^3), $C_{p,b}$ is the specific heat capacity of blood (J/kg.ºC), ω_b is blood perfusion rate (s^{-1}), Q_{met} is the the metabolism heat source (W/m^3) and Q_{ext} is the external heat source term (W/m^3). This theory can be recalled in the previous chapter.

In the literature that concluded, the blood perfusion rate of tumors lower than that in normal liver tissue. The blood perfusion rate of the normal liver tissue and the tumor is $6.4 \times 10^{-3} s^{-1}$ and $2.12 \times 10^{-3} s^{-1}$, respectively (Jain, 1988; Shao et al., 2017). Furthermore, the blood perfusion rate varies and is sensitive to the degree of damage tissue. Therefore, for accuracy of calculation will be considered the blood perfusion rate to the function of degrees of damage tissue, that given as:

$$\omega_b(t) = \omega_{b0} \qquad \text{for } \Omega(t) \leq 0 \qquad (4\text{-}10a)$$

$$\omega_b(t) = \omega_{b0}[1 + 25\Omega(t) - 260\Omega(t)^2] \qquad \text{for } 0 < \Omega(t) \leq 0.1 \qquad (4\text{-}10b)$$

$$\omega_b(t) = \omega_{b0}\exp[-\Omega(t)] \qquad \text{for } \Omega(t) \geq 0.1 \qquad (4\text{-}10c)$$

where, ω_b is the blood perfusion rate of living tissue. The ω_{b0} is the constant blood perfusion rate of living tissue, and $\Omega(t)$ is the degree of tissue injury. As show in Eq. (4-22). The thermal conductivity of the living tissue is also considered as temperature dependent parameter, approximate as piecewise function (Trujillo & Berjano, 2013).

$$k_{th,t}(T) = k_{ref} + 0.0013 \times (T - T_{ref}) \qquad T \leq 100^{\circ}C \qquad (4\text{-}11a)$$

$$k_{th,t}(T) = k(100) \qquad T > 100^{\circ}C \qquad 4\text{-}11b)$$

In the specific heat (C_p) of the living tissue is considered piecewise function of temperature to liver cancer model. This function is giving constant value of C_p when the temperature below 63.5 ºC, but temperature upper 63.5 ºC, this function is giving linear increasing function for C_p (Dos Santos, 2009).

$$C_p(T) = C_0 \qquad T \leq 63.5^{\circ}C \qquad (4\text{-}12a)$$

$$C_p(T) = C_0 + C_1 \times (T - 63.5) \qquad T > 63.5^{\circ}C \qquad (4\text{-}12b)$$

The boundary conditions of heat transfer are applied in the living domain. The heat transfer boundary conditions of the model shown in Fig. 4.2 and the following conditions are made:

1. The interfaces between the living tissue and the MCA are considered as the thermally insulated boundary condition:

$$\hat{n} \cdot (k\nabla T) = 0 \quad (4\text{-}13)$$

2. The interfaces between the normal liver tissue and the tumor are considered as the thermal continuity boundary conditions:

$$\hat{n} \cdot (k_1\nabla T_1 - k_2\nabla T_2) = 0 \quad (4\text{-}14a)$$

$$T_1 = T_2 \quad (4\text{-}14b)$$

3. The surrounding of the normal liver tissue domain is assumed to be constant the core body temperature:

$$T = 37°C \quad (4\text{-}15)$$

4.3.4 The heat Transfer and blood flow analysis of blood vessel

The heat convection analysis is only applied in a single blood vessel. The governing equation and the boundary conditions are applied in the two models with the same condition. For the reduced the complexity of the problem, the heat transfer of the blood vessel embedded in living tissue follow the assumptions are made:

1. The heat convection of the countercurrent blood vessels is considered in three dimensions (3D) analysis.
2. The blood flow in the single vessel considered is the transient convection and steady flow.
3. The blood is an incompressible and Newtonian fluid.
4. Chemical reaction of the countercurrent blood vessels is ignored.
5. The buoyancy effects of blood flow are neglected.
6. Fluid properties of blood vessel are uniform and constant.

The heat convection can describe the heat convection of blood flow based on the energy equation, the equation of continuity, and the momentum equation, which can be written as follows:

Energy equation

$$\rho_b C_{p,b} \frac{\partial T_b}{\partial t} = \nabla \cdot k_b \nabla T_b + Q_{met} - \rho_b C_{p,b} \vec{V} \cdot \nabla T_b \quad (4\text{-}16)$$

Momentum equation

$$\rho_b (\vec{V} \cdot \nabla)\vec{V} = -\nabla P + \mu_b \nabla^2 \vec{V} \quad (4\text{-}17)$$

Continuity equation

$$\nabla \cdot (\rho_b \vec{V}) = 0 \quad (4\text{-}18)$$

where $\vec{V}$ is the velocity vector (m/s), ∇P is the pressure gradient vector (Pa) and μ_b is the blood viscosity (Pa.s). This theory can be recalled in the previous chapter, as shown in Eq. 3-39 to 3-41.

The boundary conditions of heat convection are applied for a blood vessel and shown in Fig. 4.2, and the following conditions are made:

1. The inlet of a single blood vessel is assumed to be uniform velocity (Lee et al., 2012; Shao et al., 2017) and constant the core body temperature:

$$\vec{V} = 20 \text{cm/s} \quad (4\text{-}19a)$$

$$T = 37°C \quad (4\text{-}19b)$$

2. The outlet of a single blood vessel is assumed to be outflow boundary condition:

$$\hat{n} \cdot \left(-PI + \mu(\nabla \vec{V} + (\nabla \vec{V})^{\tau})\right) = 0 \quad (4\text{-}20a)$$

$$\hat{n} \cdot (k \nabla T) = 0 \quad (4\text{-}20b)$$

3. The wall of a single blood vessel is considered as the thermal continuity boundary condition, and no-slip boundary conditions:

$$\hat{n} \cdot (k_1 \nabla T_1 - k_2 \nabla T_2) = 0 \quad (4\text{-}21a)$$

$$T_1 = T_2 \quad (4\text{-}21b)$$

$$\vec{V} = 0 \quad (4\text{-}21c)$$

4.3.5 The thermal damaged tissue analysis

The thermal damaged tissue analysis is applied in the normal tissue and tumor domains. For the reduced the complexity of the problem, the thermal damaged tissue analysis follows the assumptions are made:

1. The thermal damaged of the living tissue is considered in three dimensions (3D) analysis.
2. The tissue damaged analysis is caused by thermal treatment.

Thermal damage is the thermal injury of living tissue, for which the injury model proposed by Henriques & Moritz is used, namely the Arrhenius damage model (Moritz & Henriques, 1947). The thermal damage tissue can be defined as denaturation of the proteins in living tissue, as follows:

$$\Omega(t) = A\int_0^t \exp\left(\frac{-E_a}{RT}\right) dt \quad (4\text{-}22)$$

where $\Omega(t)$ is the cumulative tissue damage, A is the frequency factor (s^{-1}), E_a is the activation energy (J/mol), and R is the universal gas constant (J/mol·K). The fraction of necrotic tissue (θ_d) can be expressed as:

$$\theta_d = 1 - \exp(-\Omega(t)) \quad (4\text{-}23)$$

4.3.6 Initial condition

The initial electromagnetic field of the model was a set of 0 V/m. The initial temperature was set of the core temperature, which of 37 ºC. The initial velocity was set of 0 m/s and 0 mm, respectively. The microwave frequency was operating of 2.45 GHz and microwave power of 10 W for all cases.

4.4 Calculation procedure

In this study, the numerical procedure analyzes the liver cancer treatment with the MWA process embedded with a single blood vessel on the 3D transient problem. The computation model is coupled with the electromagnetic wave propagation, heat transfer in the living tissue, heat transfer in a single blood flow. The computation model is solved with FEM by using COMSOL™ Multiphysics, to demonstrate the effect of a vessel location on heat transfer phenomenon during the treatment process. The 3D model is discretized using triangular elements with Lagrange quadratic shape functions, and the elements are adaptive in sensitive areas. The initial time-steps and the maximum time-steps to solve the transient problem are $1x10^{-4}$ s and 0.1 s, respectively. The mesh independence test for the liver cancer treatment model is shown in Fig. 4.3, which represented the temperature at a sensitive point. The density of elements, approximately 1,963,012 elements, meshes independently. Increasing the number of elements past this point did not lead to significantly different computational results.

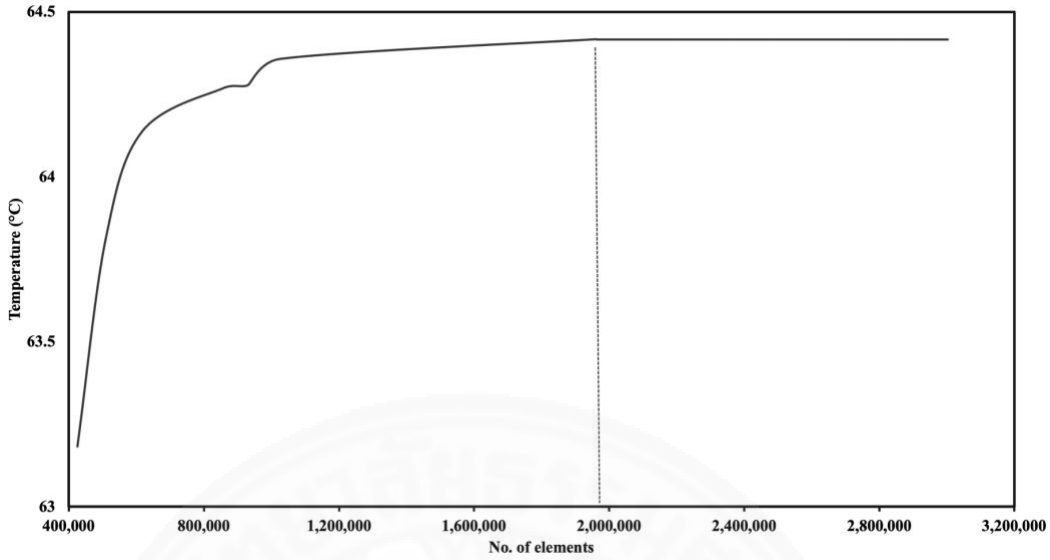

Fig. 4.3 Grid independence test

4.5 Results and discussion

This work focused on different vessels located between the horizontal and vertical vessels on the SAR distribution, temperature distribution, blood flow, and damaged tissue in the liver cancer during the MWA treatment process. The coupled model of electromagnetic wave propagation, heat transfer in the biological tissue, and blood convection equations are solved numerically.

4.5.1 Verification of the model

In order to verify the model accuracy, the present numerical study was validated against the experimental results obtained by Yang et al. (Yang et al., 2007) under the same testing conditions. In the validation model, the MWA process operated with the microwave power input of 75 W with a frequency of 2.45 GHz, and the initial temperature was set at 8°C. The MWA using single slot MCA had a radius of 1.25 mm. The MCA was inserted 20 mm deep into the living tissue and the heating time was 50 s. The verification results show the transient temperature of two points, which is 4.5 and 9.5 mm away from the MCA, as shown in Fig. 4.4. Verification results

were clearly in good agreement with the experimental results and gave confidence in the accuracy of the presented numerical models.

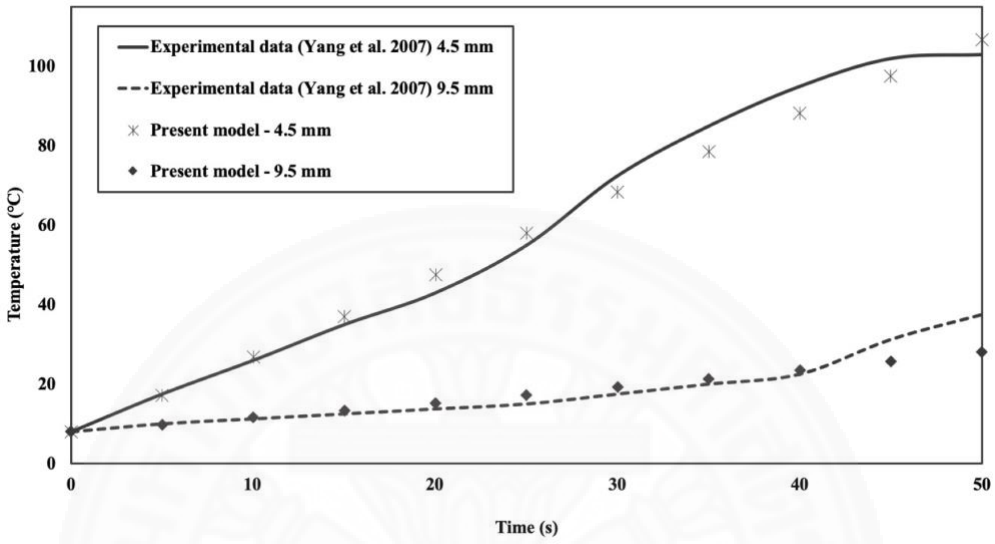

Fig. 4.4 The validation results of the calculated tissue temperature to the tissue temperature obtained by Yang et al. (Yang et al., 2007)

4.5.2 The electromagnetic wave propagation analysis

The basic principle of MWA treatment process is to apply the microwave energy into the tumor area. The microwave energy was transmitted by using MCA. The microwave energy was absorbed and converted to the internal heat generation in the tumor. This treatment aimed to create damage in the tumor by using thermal energy from the microwave source. The SAR distribution is one of the most important factors affecting the effectiveness of the treatment (Rattanadecho & Keangin, 2013). The liver cancer model with a single blood vessel is used single-slot MCA for treatment. The MCA operated on the microwave frequency of 2.45 GHz and microwave power of 10 W for all cases. The electromagnetic wave propagation between the model with the vertical and horizontal vessels was compared and represented on the SAR distribution on the cross-section plane, as shown in Fig. 4.5. The cross-section plane was set on the center of model that through the center of tumor and center of a single vessel.

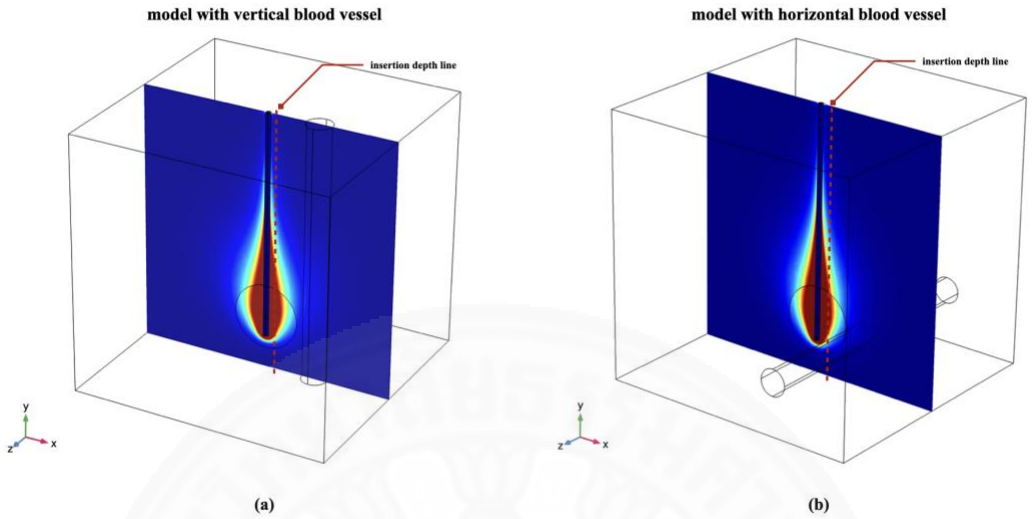

Fig. 4.5 The SAR distribution at the cross-section plane with microwave power of 10 W, and frequency of 2.45 GHz; (a) the model with a vertical vessel, (b) the model with a horizontal vessel.

Fig 4.5 shows the SAR intensity distribution exhibit similar to the water of the droplet. The highest value of SAR appealed to the slot area and decreased with the distance away from the slot. In the area of the tumor, the SAR distribution is higher than the area of the normal tissue. Fig. 4.6 shows the SAR profile with the insertion depth line between model with vertical and horizontal vessel at the heating of 10 min. The insertion depth line is parallel to the MCA and away from the MCA centerline of 2.5 mm. The maximum of SAR appeared in the slot area and decreased with distance away from the slot, which corresponded with the 2D SAR distribution. The value of SAR between the model with a vertical vessel and the horizontal vessel were similarly distributed. This is because the two models used an MCA and the dielectric properties of materials with the same treatment conditions. Furthermore, the location of a single vessel was far away from the SAR distribution intensive area. Therefore, the location characteristic of a single vessel has not affected the SAR distribution between the models with the vertical and horizontal vessel.

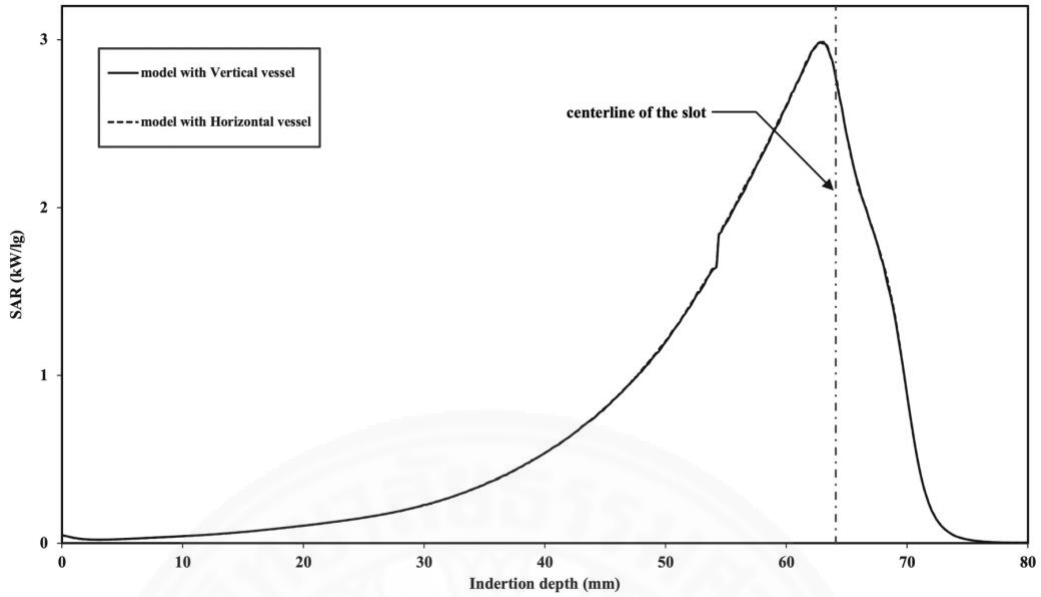

Fig. 4.6 SAR profile at the insertion depth line between the model embedded with a vertical and horizontal vessel with microwave power of 10 W, and frequency of 2.45 GHz.

4.5.3 The heat transfer analysis

The characteristic of temperature distribution in the liver cancer model during the MWA treatment process is related to the effective performance of this treatment. In this study, the volumetric heating effect on the living tissue is induced by microwave energy. The microwave energy is transmitted by the MCA into the tumor area. The microwave energy is absorbed and converted to volumetric heating in the living tissue domain. In order to study the heat transfer in the model, the coupled effects of the electromagnetic wave propagation, heat transfer in the living tissue, and heat transfer in a single blood vessel flow. Fig. 4.7 shows the 2D-plot temperature and blood velocity on the cross-section plane of the 3D liver cancer model during the MWA process at the heating time of 10 min, Fig. 4.7(a) shows 2D-plot temperature and blood velocity in the model with a vertical vessel, and Fig. 4.7(b) shows 2D-plot temperature and blood velocity in the model with a horizontal vessel. The temperature intensity occurred in the slot area and decreased with distance away from the slot. This result corresponded with the SAR distribution (as shown in Fig. 4.5) because SAR in the

living tissue owned the energy absorption. After that, the microwave energy absorption is converted to thermal energy, lead to increased temperature in the living tissue.

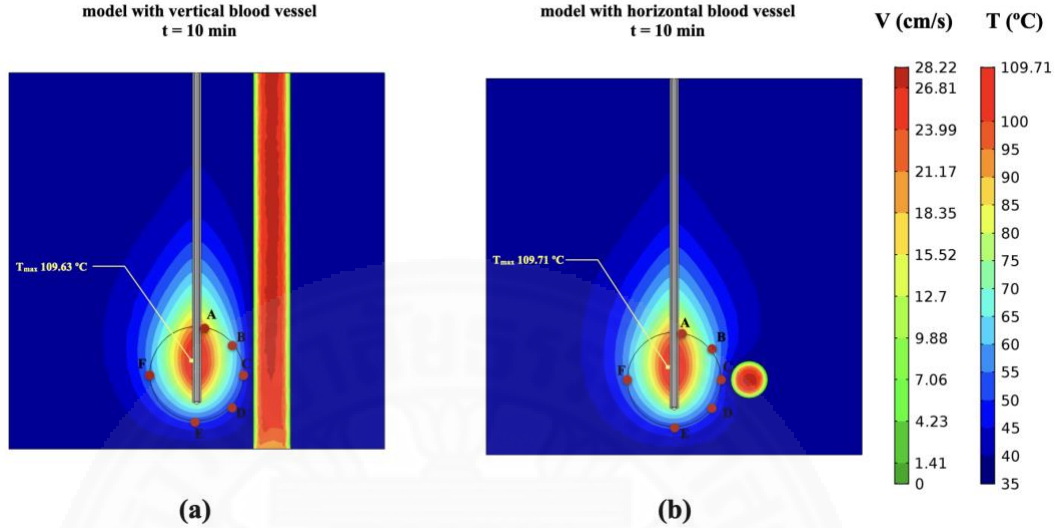

Fig. 4.7 Temperature and velocity fields at the cross-section plane with microwave power of 10 W, frequency of 2.45 GHz, and heating time of 10 min; (a) the model with a vertical vessel, (b) the model with a horizontal vessel.

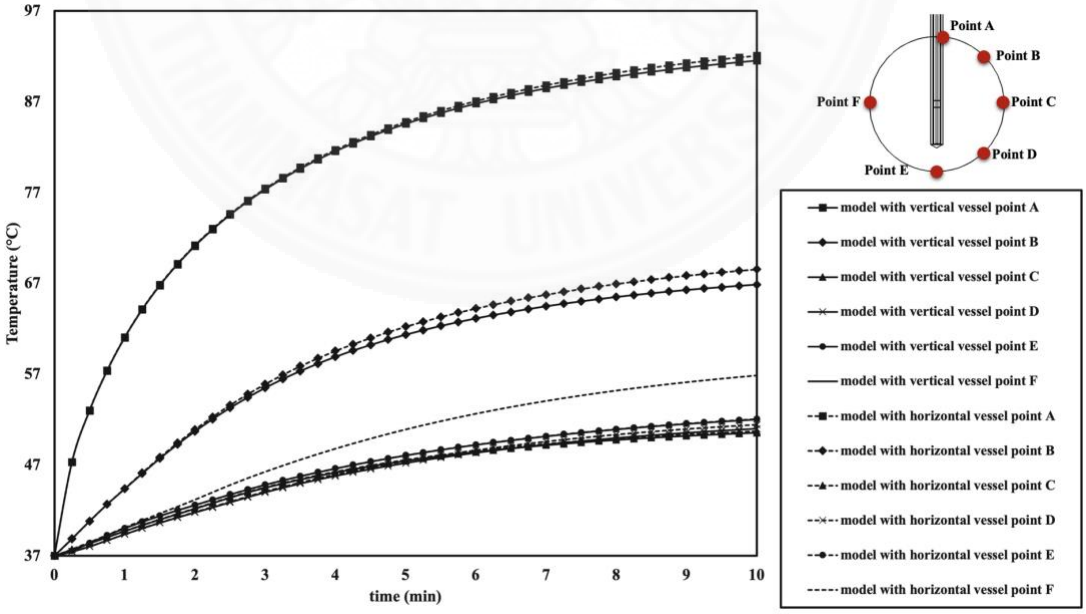

Fig 4.8 The comparison of the transient temperature at the selected points between model with a vertical and horizontal vessel with microwave power of 10 W, frequency of 2.45 GHz

The intensity temperature distribution exhibit similar to the water of the droplet, corresponding to the SAR distribution. However, the temperature distribution around the area of blood vessel flow is different. The different points between the model with a vertical and horizontal vessel can be observed on the low-temperature contour at the area close to a single blood vessel. In this area, the heat transfer phenomenon plays the role of blood convection by a single vessel. The maximum temperature on the cross-section plane of the model with a vertical and horizontal vessel is 109.63 ºC and 109.71 ºC, respectively. Although a vertical and horizontal blood vessel was equally uniform inlet velocity and vessel length, the temperature distributions differed. The characteristic of temperature distribution induced the heat transfer by a vertical blood vessel was higher than a horizontal blood vessel.

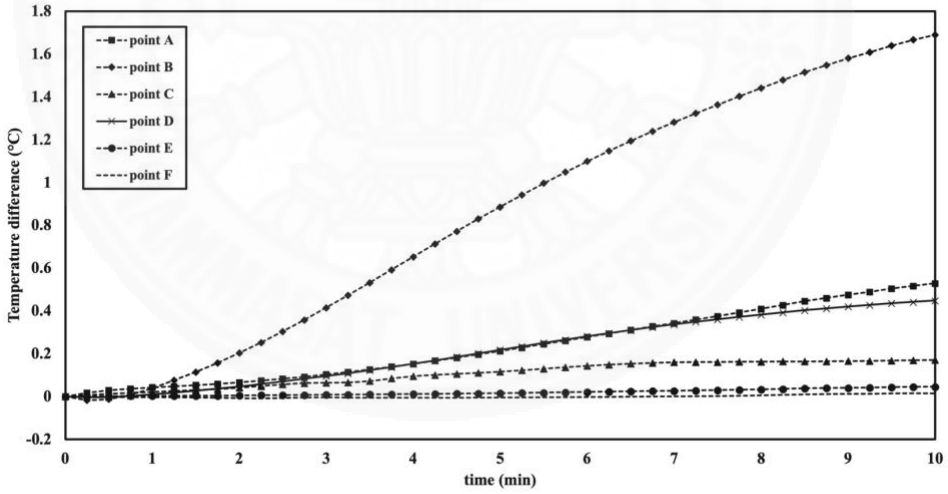

Fig. 4.9 The transient temperature difference of the selected points between model with a horizontal and vertical vessel with microwave power of 10 W, and frequency of 2.45 GHz

Fig. 4.8 shows the transient temperature of the model with a vertical and horizontal vessel on the selected points. The selected points were located around the tumor boundaries (as shown in Fig. 4.7-4.8). For all points, the temperature increases with the heating time. The temperature of point A was highest increased and following with the point B, F, E, D, and C, respectively. The temperature difference between the two models can be clearly observed at the point B. Fig. 4.9 shows the transient temperature difference of point A to F between the model with a horizontal vessel and a vertical vessel. The temperature difference of point B was the highest value and following by point A, D, C, E, and F, respectively. The transient temperature of point A was to the highest increasing, but the temperature difference between the two models was not the highest value. At point C that closest to a single vessel, the temperature difference was not the highest value. The highest temperature difference is shown on point B, in which the area is not the highest temperature increasing and not closest to a blood vessel. This result was affected by the temperature distribution, which induced the heat transfer by a vertical blood vessel was higher than the heat transfer by a horizontal blood vessel.

The microwave energy was transmitted by a single slot MCA into the tumor and normal liver tissue. The microwave energy is absorbed and converted to heat by dielectric heating. The microwave energy absorbed was intensely distributed on the slot area and decreased with the distance away from the slot. The temperature distribution was similarly distributed to the SAR distribution. Because the energy absorbed by the microwave was converted to thermal energy, leading to increased temperature in this living tissue. A single vertical and horizontal vessel was embedded in the area closed to the treatment area. The heat transfer in this area was conjugated between heat conduction and heat convection. However, the vertical blood vessel was transferred heat energy than the horizontal vessel. The characteristic heat pattern in this model induced the surface area of the vertical blood vessel close to the hot spot area than the horizontal blood vessel.

4.5.4 The damaged tissue analysis

This treatment aimed to create the fully damaged only tumor area and without damage to the normal tissue area. In this study, the tissue damage was only

affected by thermal energy and considered only the living domain. The thermal damage model was investigated based on the Arrhenius damage model. The fraction of damaged tissue increases with the degree of thermal denaturation (percentage of denatured collagen), where $\theta_d = 0$ indicates no damage in the liver tissue. In contrast, $\theta_d = 1$ indicates a fully damaged liver tissue. Fig. 4.10 shows the fraction of the damaged tissue distribution and blood velocity vector on the cross-section plane of the 3D liver cancer model during the MWA process at the heating time of 10 min; Fig. 4.10(a) shows the fraction of the damaged tissue distribution and blood velocity vector in the model with a vertical vessel, and Fig. 4.10(b) shows the fraction of the damaged tissue distribution and blood velocity vector in the model with a horizontal vessel. The fully damaged tissue occurred in the tumor area and upper of the tumor. The shape of the damaged tissue was similar to the water of the droplet, which corresponded with SAR and temperature distribution.

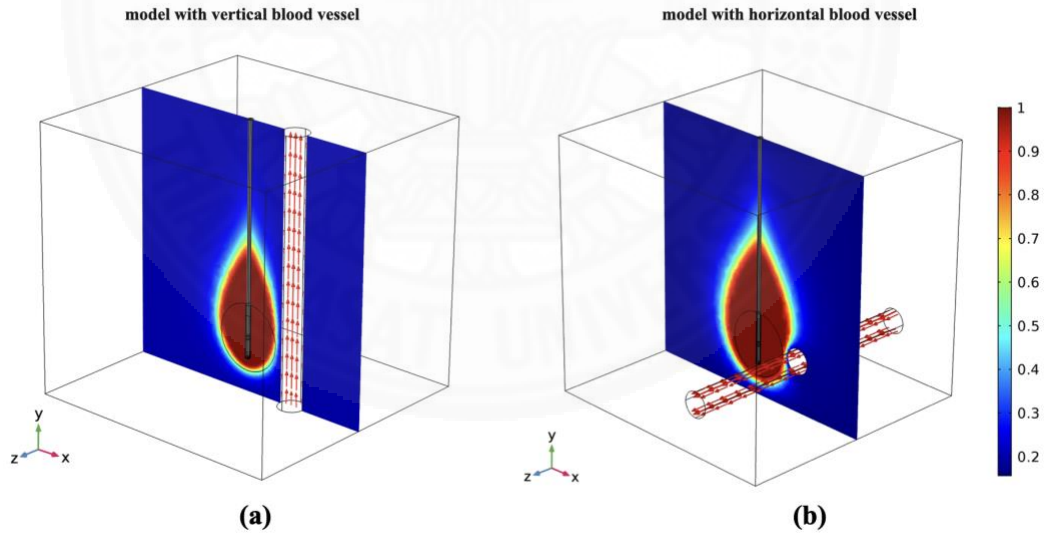

Fig. 4.10 The fraction of damaged tissue distribution and velocity arrow at the cross-section plane with microwave power of 10 W, frequency of 2.45 GHz, and heating time of 10 min; (a) the model with a vertical vessel, (b) the model with a horizontal vessel.

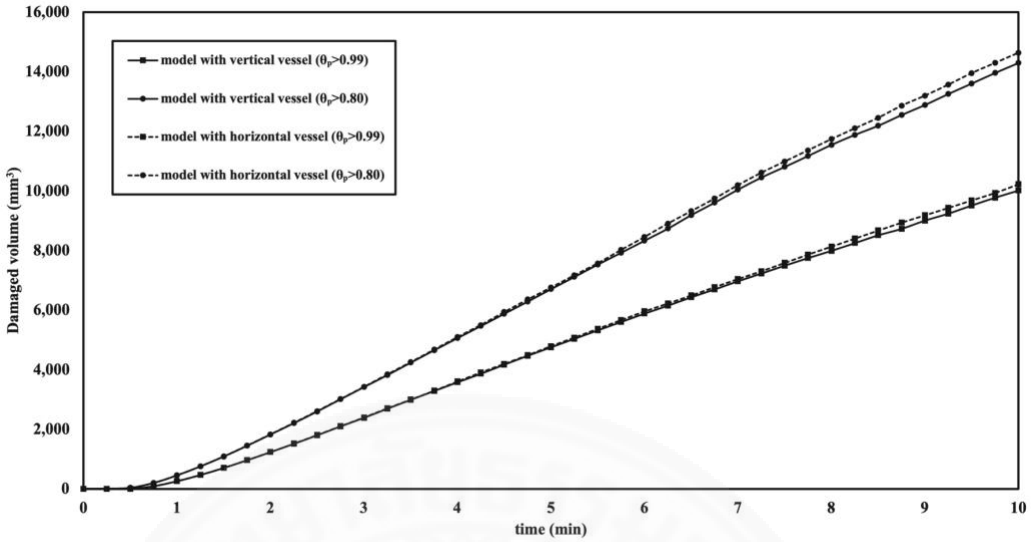

Fig. 4.11 The comparison volumetric of damaged tissue between the model with a vertical and horizontal vessel, with microwave power of 10 W, frequency of 2.45 GHz

Fig. 4.11 shows the transient volumetric of damaged tissue between the model with a vertical and horizontal vessel. The fraction values of damaged tissue were the value of fully damaged tissue ($\theta_d > 0.99$) and the value of high damaged tissue ($\theta_d > 0.80$). The volumetric of damaged tissue increased with the heating time. The volumetric damaged tissue faction above 0.80 was higher than the volumetric of fully damaged tissue faction. That because the volumetric damaged tissue faction above 0.80 was including the volumetric of fully damaged tissue together. The volumetric of fully damaged between the model with vertical and horizontal was slightly different. That because the full of damaged tissue was occurring in the hot spot area, which was slightly affected by the characteristic of a blood vessel located. However, the volumetric damaged tissue faction above 0.80 shows a clear difference between the two models. This volumetric included the volume of living tissue wider than the boundaries tumor, which included the area close to a single blood vessel located. Therefore, the effect of a blood vessel located clearly occurred. Finally, the damaged tissue analysis on this living tissue depended on the temperature distribution, which was owed the microwave power absorbed.

4.6 Conclusion

The 3D numerical analysis of the SAR, temperature, and damaged tissue in liver cancer model embedded with a single vessel during MWA treatment in different vessel located has been performed. The effect of a vertical blood vessel and a horizontal blood vessel on the heat transfer was systematically investigated. The SAR, temperature, and damaged tissue in the liver cancer model embedded with a single vessel during MWA treatment were obtained by numerical simulation of the electromagnetic wave propagation, heat transfer, blood flow, and damaged tissue equations. The electromagnetic wave propagation was expressed mathematically by Maxwell's equations. The heat transfer model was developed based on the bioheat equation in the living tissue domain and energy conservation equation of the fluid (blood) flow. Furthermore, the blood flow analysis was expressed mathematically by the momentum and continuity equations. The damaged tissue model was developed based on the the Arrhenius damage model.

As a result, the SAR distribution between the model with a vertical blood vessel and a horizontal blood vessel were similarly distributed. The blood vessel was located far away from the slot area, which SAR distributed intensively. However, the temperature distribution between the model with a vertical blood vessel and a horizontal blood vessel was clearly different in the area near a single blood vessel. The effect of a blood vessel located on the heat transfer was occurred on the transient temperature points at the boundary of tumor. The model with a horizontal blood vessel shows the transient temperature points increased than the model with a vertical blood vessel. That because of the heat pattern induced to heat transfer by a vertical vessel higher than a horizontal vessel. The result of damaged tissue corresponds with the temperature distribution.

The microwave power absorbed in the liver cancer was owning to the energy absorption. Later, the energy absorption was converted to thermal energy, leading to increased living tissue temperature and damaged tissue volumetric. A blood vessel flows nearby the treatment area affected the heat transfer in the treatment area, which related to the effective performance of the treatment process. Therefore, this study presented the effect of the blood vessel location near the treatment area with the

symmetrical investigation. The simulation results in this study can be used as a guideline concerning the effect of blood vessel location, which nearby the treatment area during the MWA process.

CHAPTER 5
THE COMPARATIVE OF THE PERFORMANCE FOR PREDICTED THERMAL MODELS DURING MICROWAVE ABLATION PROCESS USING A SLOT ANTENNA

5.1 Introduction

Microwave ablation (MWA) is a new technology for focused cancer treatment. This treatment is an alternative treatment for liver cancer (Martin et al., 2010; Keangin et al., 2011; Correa-Gallego et al., 2014), which one of the cancers that have a low survival rate (Poston et al., 2011). The MWA has applied the microwave power to the target tissue (tumor) by microwave antenna. The microwave is absorbed and converted to the heat generation in the tumor. The tissue temperature rises to 52 ºC for a heating time of 1 min, or the instantaneous tissue temperature exceeds 54 ºC, the cell will be killed immediately (Dong et al., 1998; Goldberg et al., 2000; Whelan et al. 2005; Prakash et al., 2008; Prakash et al., 2012; Wu et al., 2013). The goal of this treat tissue by the microwave heating and without damaging it to the surrounding tissue. Furthermore, MWA has many advantages and powerful treatment techniques compared with conventional treatment for localized liver cancer treatment. However, MWA has dangerous when used incorrect conditions during treatment, such as the heat spread over the boundaries of the tumor area. When the heat spread over the boundaries of the tumor, the temperature of healthy tissue is rising. The increase of the healthy tissue temperature is resulting in the protein denaturation process, which is dangerous on the healthy tissue. Therefore, the studies of correct conditions are necessary.

MWA is a popular treatment technique for primary and metastatic liver tumors (Liu et al., 2010; Xu et al., 2010; Ren et al., 2011), and has advantages over the other thermal ablation (such as radiofrequency ablation (RFA)) (Carrafiello et al., 2008; Brace, 2009; Li et al., 2011;). It could not apply to human liver beings due to be unethical. Many researchers have been experimenting with animals (Strickland et al., 2002; Hines-Peralta et al., 2006; Wu et al., 2013; Saccomandi et al., 2015; Lopresto et al., 2017; Marcelin et al., 2018;). However, these experimental studies had limitations

compared to experimenting with a nearly realistic human liver. The numerical simulation could be applied to study the treatment. It has been the advantage of needing only a short period, the low economic cost, humanity, and could be set up with conditions near to those of a real human liver. Most simulation studies of liver cancer treatment with thermal therapy used the Pennes bioheat model, introduced by Pennes (Pennes, 1948).

The Pennes bioheat model has been widely applied in many studies about heat transfer in biological tissue, in particular, this has applied in the thermal ablation models (Okajima et al., 2009; Phasukkit et al., 2009; Liangruksa et al., 2011). Although the Pennes bioheat model is widespread and has been applied in several studies, this model requires many assumptions and may limit their application (Keangin & Rattanadecho, 2013). Therefore, researchers proposed the new model, the modified bioheat model, or the couple bioheat with other models for reduced the many assumptions and highly accurate in the specific situations.

Wulff and Klinger proposed the new bioheat equation, pointing out the shortcomings of the Pennes bioheat model, because of not considering the moving blood through the biological tissue heat convection in any direction (Klinger, 1974; Wulff, 1974). In 2007, Yang et al. developed a modified bioheat model for prediction temperature profiles during MWA in a high temperature state (Yang et al., 2007). After that, Keangin et al. developed the numerical model of liver cancer treatment with MWA, which included thermal deformation analysis during the treatment process (Keangin et al., 2011). In 2016, Wu et al. proposed the model of MWA in liver tissue with the multi-frequency (Wu et al., 2016).

Although the bioheat model could be modified to improve accuracy and efficiency, the bioheat models have some limitations. This model cannot handle several physical effects, in particular, the directional of blood flow and convective heat transfer mechanism. Some researchers proposed the porous media model applied in the biological tissue for improved model accuracy and efficiency. The realistic, the biological tissue includes the cell, blood vessel, and interstitial space, which can be defined as the solid phase and fluid phase in the biological domain (Mahjoob & Vafai, 2009). Therefore, the biological tissue could assume a porous structure (Roetzel & Xuan, 1998; Nakayama & Kuwahara, 2008). Thus, the porous media theory can be

applied in biological tissue (Rattanadecho & Keangin, 2013). In 2009, Mahjoob and Vafai proposed the hyperthermia treatment in the two biological models, based on the local thermal non-equilibrium (LTNE) model in porous media theory (Mahjoob & Vafai, 2009). The advantages of utilizing a porous media model in biological tissue has few assumptions as compared to different established bioheat transfer models (Mahjoob & Vafai, 2009).

In 2013, the liver cancer with MWA treatment model based on the porous media approach was proposed by Rattanadecho & Keangin (Rattanadecho & Keangin, 2013). This work was the first study of heat transfer and blood flow in the two-layered porous liver during MWA process using single and double slot antenna. This study was considered the fluid with constant velocity but considered the fluid with fluid flow equations in the porous tissue domain. Keangin et al. presented the mathematical model of biological materials based on porous theory. This model imposed the electromagnetic field on biological materials such as the liver, brain, bone, and skin, etc. The results showed the effect of electromagnetic power and frequency on the temperature of solid phase and blood phase in biological materials (Keangin et al., 2013). After that, Keangin and Rattanadecho developed the porous liver cancer model during MWA treatment. The mathematical model based on LTNE approach and the equations of the model considered couple with electromagnetic wave propagation and heat transfer analysis. The simulation results showed the effect of the model approach, porosity, and microwave power during MWA treatment (Keangin & Rattanadecho, 2013).

Although the performancing comparative of the predicted thermal models during the MWA process, there are a few studies. In particular, the systematical studies of the performancing comparative heat modeling implemented in the biological tissue. Therefore, the porous model was applied in the biological tissue coupled with the blood flow model with the heat transfer model, which is necessary and exciting. The comparative of the thermal models during the MWA process on the heat transfer affects the accuracy and effectiveness of the liver cancer model. Furthermore, the systematic study of the different heating models in the early stage of heating time to the long stage of heating time has not appeared. Therefore, the fundamental of the different heating

implemented could be selected as the suitable heat models for the right condition and situation.

This study proposed the performancing comparative of the predicted heating models implemented of the liver cancer model by MWA with microwave power of 10 W and frequency of 2.45 GHz. The heating models implemented were the bioheat model, the porous model with constant velocity, and the Darcy-Brinkman porous model. The porous models (the porous model with constant velocity and the Darcy-Brinkman porous model) were based on the local thermal equilibrium (LTE) approach. The mathematics of all models considered coupled with the electromagnetic wave propagation and heat transfer in the liver tissue. In the specific Darcy-Brinkman porous model deemed to be fully combined with the electromagnetic wave propagation, heat transfer, and flow analysis in the liver cancer model. The effect of the bioheat model, the porous model with constant velocity, and the Darcy-Brinkman porous model on the temperature distribution was systematically comparison. For accuracy, the numerical model was validated with experimental results by Yang et al. (Yang et al., 2007). In finally, this study presented suitable models for prediction temperature profiles during MWA treatment for various conditions. The fundamental understanding of models could be a guideline for effective treatment.

5.2 Modeling and formulation

The anatomic structure of the model consists of the liver tissue domain and the microwave antenna domain. The liver tissue domain (tumor and healthy tissue) as porous media materials consist of solid and fluid phases (blood phase), in which domains considered with electromagnetic wave propagation, heat transfer, blood flow analysis (Brinkman model extended Darcy). The microwave antenna domain is less affected by heat transfer, therefore considered with electromagnetic wave propagation only. This study developed the numerical of liver cancer model with MWA based on the LTE porous model. Furthermore, this study investigated the performancing comparative of the heating models implemented of the liver cancer treatment with MWA on the heat transfer.

5.2.1 Problem description

MWA is a type of thermal ablation. This technique is using the microwave frequency induced external heat in a specific area. The microwave frequency is transmitted by using a microwave antenna, in which the microwave coaxial antenna (MCA) is used extensively (Rattanadecho & Keangin, 2013). This study was developed the numerical model of liver cancer treatment with MWA by using a single-slot MCA transmitting the microwave power into a specific area (tumor domain). The single-slot MCA has a diameter of 1.79 mm, the antenna is required as small as a possible for minimally invasive (Keangin & Rattanadecho, 2013). A wide of the ring-shaped slot of 1 mm is cut off the outer conductor, and the length of 5.5 mm from the short-circuited tip, that for avoiding the electric field becomes stronger near the slot (Saito et al., 2000). The microwave antenna operated at the power of 10 W and frequency of 2.45 GHz, which is used for MWA treatment. The dimension and properties of single-slot MCA are shown in Table 5.1. The goal of this treatment treated liver by microwave heating and without damaged to the surrounding tissue.

Table 5.1 Dimensions and dielectric properties of single slot MCA (Keangin et al., 2011)

Material	Dimensions (mm)	Dielectric properties		
		Relative permittivity, ε_r	Electric conductivity, σ_{el} (S/m)	Relative permeability, μ_r
Inner conductor	0.135 (radial)	-	-	-
Dielectric	0.47 (radial)	2.03	0	1
Outer conductor	0.595 (radial)	-	-	-
Catheter	0.895 (radial)	2.1	0	1
Slot	1.00 (wide)	1	0	1

In this study, the liver cancer domain based on the porous media model. The porous liver cancer consists of 2 domains, the porous tumor, and the porous healthy tissue. The center of the tumor sets on the center slot and tumor radius of 10

mm. All domains are considered as an axisymmetric model, which the geometry of porous liver cancer, as shown in Fig. 5.1(a). The porous tissue domains (tumor and healthy tissue domain) are based on LTE in the porous media theory. The geometry of the model based on Bioheat was adapted to the geometry of the porous liver. In this study, the liver cancer model with MWA by using single-slot MCA for all cases. The mathematical of the porous model is considered to couple with the electromagnetic wave propagation, heat transfer, and fluid (blood) flow based on LTE assumption. The dielectric and thermal properties of the model are selected from the literature (Keangin et al., 2011; Keangin & Rattanadecho, 2013; Shao et al., 2017, Koksungnoen et al., 2018), as shown in Table 5.2.

Table 5.2 The dielectric and thermal properties of the tissue (Keangin & Rattanadecho, 2013; Koksungnoen et al., 2018)

properties	Normal Tissue	Tumor	Blood
Relative permittivity, ε_r	43	48.16	58.3
Electric conductivity, σ_{el} (S/m)	1.69	2.096	2.54
Density, ρ (kg/m^3)	1030	1040	1058
Thermal conductivity, k_{th}(W/m·ºC)	0.497	0.57	0.45
Specific heat capacity C_p (J/kg· ºC)	3,600	3,960	3,960

5.2.2 Equations of electromagnetic wave propagation analysis

The electromagnetic wave propagation was considered in all domains. The governing equations and boundary conditions of electromagnetic wave propagation were applied for all models.

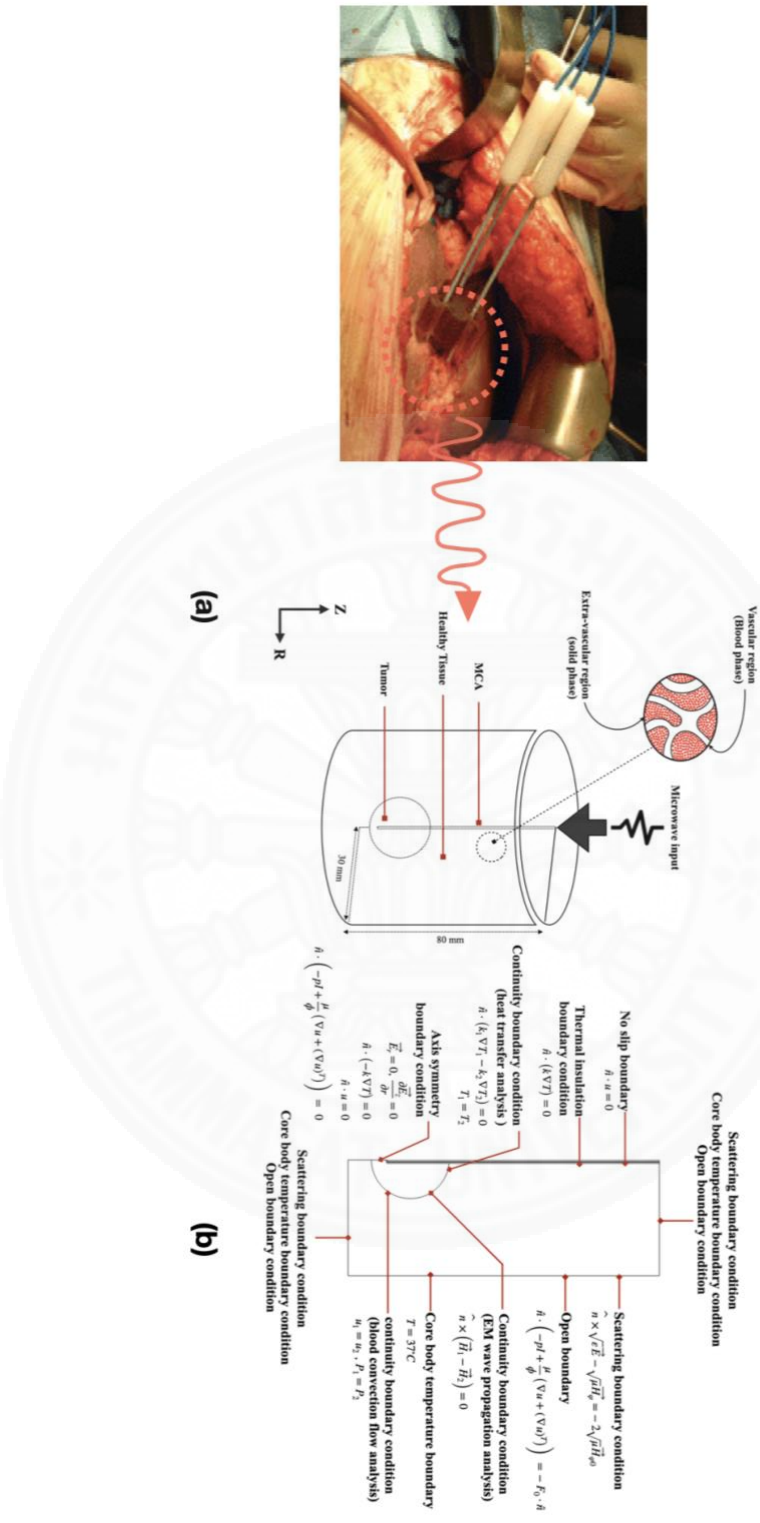

Fig. 5.1 The physical domain and boundary conditions of porous liver cancer model with MWA; (a) The physical domain, (b) The boundary conditions

5.2.2.1 Governing equation and assumptions of electromagnetic wave propagation analysis

The electromagnetic wave propagation is considered in all domains. To reduce the complexity of the problem, the following assumptions are made.

1. The electromagnetic wave propagation considered in the 2-D axisymmetric model on r-z coordinates.
2. The electromagnetic wave propagation in the MCA is characterized by transverse electromagnetic fields (TEM) (Bertram et al., 2006)
3. The electromagnetic wave propagation is characterized by transverse magnetic fields (TM). (Bertram et al., 2006)
4. The model assumes that the dielectric properties of the liver are uniform.

The propagation of the electromagnetic wave in the antenna is by a transverse electromagnetic field (TEM) (Keangin et al., 2011) that given as:

Electric field ($\vec{E}$) $$\vec{E} = \vec{e}_r \frac{C}{r} e^{j(\omega t - kz)} \quad (5\text{-}1)$$

Magnetic field ($\vec{H}$) $$\vec{H} = \vec{e}_\varphi \frac{C}{rZ} e^{j(\omega t - kz)} \quad (5\text{-}2)$$

where $\vec{E}$ is the electric field intensity (V/m), $\vec{H}$ is the magnetic field in intensity (A/m), r,φ, and z are cylindrical coordinates centered on the axis of the coaxial cable. $C = \sqrt{\frac{ZP_{in}}{\pi \cdot \ln(r_{outer}/r_{inner})}}$ is the arbitrary constant, Z is the wave impedance (Ω), Pin is the microwave power input (W), r_{outer} is the dielectric outer radius (m), r_{inner} is the dielectric inner radius (m), f is the frequency (Hz), $\omega = 2\pi f$ is the angular frequency (rad/s), k is the wave propagation constant (m^{-1}), which relates to the wavelength (λ) in medium: $k = \frac{2\pi}{\lambda}$.

Furthermore, the propagation of the electromagnetic wave in the biological tissue is by a transverse magnetic field (TM) as described by the following equation:

$$\nabla \times \left(\left(\frac{1}{\varepsilon_r} - \frac{j\sigma_{el}}{\omega \varepsilon_0} \right)^{-1} \nabla \times \vec{H}_\theta \right) - \mu_r k_0^2 \vec{H}_\theta = 0 \quad (5\text{-}3)$$

where $\vec{H}_\theta$ is magnetic field intensity (A/m), μ_r is relative permeability, ε_r is relative permittivity, $\varepsilon_0 = 8.8542 \times 10^{-12}$ F/m is permittivity of free space, σ_{el} is electric conductivity (S/m), k_0 is the free space wavenumber (m^{-1}), and $\omega = 2\pi f$ is the angular frequency (rad/s).

The interaction of an electromagnetic wave with biological tissue can be defined in terms of the specific absorption rate (SAR) distribution. When the electromagnetic wave is transmitted by an MCA, it passes through it and then propagates throughout the entire domain. The electromagnetic wave is absorbed and converted to the external heat source term. In this study, SAR represents the microwave power absorption deposited per unit mass in tissue (W/kg) (Rattanadecho & Keangin, 2013). The SAR is given by:

$$\text{SAR} = \frac{\sigma_{el}}{2\rho} \mid \vec{E} \mid \quad (5\text{-}4)$$

where σ_{el} is the electrical conductivity (S/m), ρ is the tissue density (kg/m^3), and $\vec{E}$ is the electric field intensity (V/m).

5.2.2.2 Boundary conditions of electromagnetic wave propagation analysis

The boundary conditions of electromagnetic wave propagation were adapted for all cases. The EM boundary conditions of the porous liver show in Fig. 5.1(b), and the following conditions are made:

1. The outside of the computation domain is considered as a scattering boundary condition to eliminate the reflections:

$$\hat{n} \times \sqrt{\epsilon}\vec{E} - \sqrt{\mu}_{el}\vec{H}_\theta = 2\sqrt{\mu}_{el}\vec{H}_{\theta 0} \quad (5\text{-}5)$$

2. The interfaces between different mediums are considered as a continuity boundary condition:

$$\hat{\mathrm{n}} \times \left(\vec{H}_1 - \vec{H}_2\right) = 0 \tag{5-6}$$

3. The boundary conditions of the inner and outer conductor of MCA as the perfect electric conductor (PEC) boundary conditions:

$$\hat{\mathrm{n}} \times \vec{E} = 0 \tag{5-7}$$

4. The port boundary condition is applied at the inlet of MCA with the microwave power level set to 10 W.
5. The electrical symmetry boundary condition is applied at r =0:

$$\vec{E}_r = 0 \tag{5-8a}$$

$$\frac{\partial \vec{E}_z}{\partial r} = 0 \tag{5-8b}$$

5.2.3 Equations of heat transfer and blood flow analysis

In this study, the liver cancer model during MWA treatment was compared and applied by three heating models: the bioheat model, the porous model with constant velocity, and the Darcy-Brinkman porous model.

5.2.3.1 Governing equation and assumptions of heat transfer and blood flow analysis

The heat transfer and blood flow are considered in the tissue domains only, i.e., healthy tissue and tumor domain. For reduce the complexity of the problem, the assumptions of the Darcy-Brinkman porous model have been offered into the analysis:

1. Heat transfer, as well as heat convection, are considered in the 2-D axisymmetric model on r-z coordinates.

2. The liver tissue domains (healthy tissue and tumor) of the porous liver model are considered the homogeneous porous media materials, thermally isotropic, and saturated with blood.
3. The LTE heat transfer between solid and blood phases is considered.
4. The blood perfusion rate term is assumed to be constant for all cases.
5. The blood in the porous liver is incompressible and Newtonian.
6. The Boussinesq approximation is applied to the buoyancy term of the flow analysis.
7. The chemical reactions and phase changes are ignored.
8. The porosities and thermal properties of the porous liver are assumed to be constant and uniformed.
9. The analysis of heat transfer and flow in the MCA are ignored.

The heat transfer analysis of the porous liver model was considered the transient problem, and couples with electromagnetic wave propagation. The heat transfer in the liver tissue is obtained by solving the energy equation, which based on the LTE approach in porous media theory. The equations are given as follows:

$$(\rho C_p)_{eff}\frac{\partial T}{\partial t} + \rho_b C_{p,b} u \cdot \nabla T = k_{th,eff}\nabla^2 T + \rho_b C_{p,b}\omega_b(T_b - T) + Q_{met} + Q_{ext} \quad \text{(5-9a)}$$

$$(\rho C_p)_{eff} = (1-\phi)(\rho C_p)_s + \phi(\rho C_p)_b \quad \text{(5-9b)}$$

$$k_{th,eff} = (1-\phi)k_{th,s} + \phi k_{th,b} \quad \text{(5-9c)}$$

where, the subscription eff, s, th and b represent the effective value, solid phase, thermal and blood phase, respectively. ϕ is the porosity (volume fraction of the vascular space), ρ is the tissue density (healthy liver tissue or tumor) (kg/m^3) , C_p is the specific heat capacity (J/kg· ºC), T is the temperature of tissue (ºC), k_{th} is the thermal conductivity (W/m·ºC), ρ_b is the blood density (kg/m^3), ω_b is the blood perfusion rate

(1/s), Q_{met} is the metabolism heat source ($Q_{met} = 33{,}800$ W/m^3) (Rabin & Shitzer, 1998) and Q_{ext} is the external heat source term (W/m^3). The external heat source term is converted from SAR distribution, which is defined as:

$$\mathrm{Q_{ext}} = \frac{\sigma_{\mathrm{el}}|\vec{E}|^2}{2} = \rho \cdot \mathrm{SAR} \tag{5-10}$$

where, the parameters are corresponding with Eq. (5-4). It well-known, the blood perfusion rate of the large tumor slower than that in the healthy tissue. For the healthy tissue, the blood perfusion rate is 6.4 x 10^{-3} 1/s, while the blood perfusion rate of tumor is 2.12 x 10^{-3} 1/s (Shao et al., 2017; Jain & Ward-Hartley, 1984). The blood perfusion rate was applied to a constant value in all cases.

The flow analysis was applied only, i.e., the Darcy-Brinkman porous model. The Brinkman equation extended Darcy equation was first developed by Brinkman (Brinkman, 1949), and used for investigating the blood flow in the Darcy-Brinkman porous model. The governing equations describing the flow phenomenon in the Darcy-Brinkman porous model are given as follows (Rattanadecho & Keangin, 2013):

Continuity equation

$$\rho\nabla \cdot (\vec{V}) = 0 \tag{5-11}$$

Momentum equation

$$\rho_b \frac{\partial \vec{V}}{\partial t} = \left(-PI + \frac{\mu}{\phi}\left(\nabla\vec{V} + (\nabla\vec{V})^{\tau}\right)\right) - \frac{\mu\vec{V}}{\kappa} + F \tag{5-12}$$

where $\vec{V}$ is the blood velocity vector (m/s), P is the pressure in porous liver (Pa), $\mu = 0.003$ Pa/s is the viscosity of blood (Nabaei & Karimi, 2018), $F = g\beta(T - T_i)$ is the body force that applied the buoyancy term, $\beta = 1 \times 10^{-4}$ 1/K is the coefficient of thermal expansion, T_i is the reference temperature (°C), which is considered as the initial temperature of model, and κ is the permeability (m^2), which can be expressed by the following (Nield & Bejan, 2006; Vafai, 1984):

$$\kappa = \frac{\phi^3 d_p^2}{175(1-\phi)^2} \tag{5-13}$$

where $d_p = 1 \times 10^{-4}$ m^2 is the diameter of tissue cells. The inertial effect of blood flow was relatively low, which was neglected (Rattanadecho & Keangin, 2013).

In order to implement the porous model with constant velocity in the porous liver model, the governing equation is Eq. (5-9) but ignore the Eq. (5-11)-(5-12) (Keangin & Rattanadech, 2013). Also, the heat transfer for the bioheat model was considered the transient problem, and couples with electromagnetic wave propagation. The heat transfer in the liver tissue is obtained by solving only the bioheat equation (Wessapan & Rattanadecho, 2018, Wongchadakul et al., 2018). The equation is given by:

$$\rho_s C_{p,s} \frac{\partial T}{\partial t} = k_{th,s} \nabla^2 T + \rho_b C_{p,b} \omega_b (T_b - T) + Q_{met} + Q_{ext} \tag{5-14}$$

This theory can be recalled in the chapter 3.

5.2.3.2 Boundary conditions of heat transfer and flow analysis

The boundary conditions of heat transfer and flow were applied for the porous liver models and the only boundary conditions of heat transfer was applied the bioheat liver model. The boundary conditions of porous liver model were shown in Fig. 5.1(b), and to following conditions are made:

1. The top, right, and bottom sides of the liver domain is assumed to be constant the core body temperature for the bioheat and porous models, as shown in Eq. (5-15a). Furthermore, the top, right, and bottom sides of the porous models are assumed to be open boundary conditions, as shown in Eq. (5-15b).

$$T = 37°\mathrm{C} \tag{15a}$$

$$\widehat{n} \cdot \left(-PI + \frac{\mu}{\phi}\left(\nabla\vec{V} + (\nabla\vec{V})^{\tau}\right)\right) = -F_0 \cdot \hat{n} \tag{15b}$$

2. The interfaces between the healthy tissue and the tumor are considered as the thermal and flow continuity boundary conditions for the porous models, as shown in Eq. (5-16a) - (5-16d). The interfaces between the healthy tissue and the tumor are considered as only the thermal continuity boundary conditions for the bioheat model, as shown in Eq. (5-16a) - (5-16b).

$$\widehat{n} \cdot (k_1 \nabla T_1 - k_2 \nabla T_2) = 0 \tag{5-16a}$$

$$T_1 = T_2 \tag{5-16b}$$

$$\vec{V}_1 = \vec{V}_2 \tag{5-16c}$$

$$P_1 = P_2 \tag{5-16d}$$

3. The interfaces of healthy tissue and tumors with MCA are considered thermally insulated for all models and no-slip boundary conditions for the only porous models.

$$\widehat{n} \cdot (k\nabla T) = 0 \tag{5-17a}$$

$$\widehat{n} \cdot \vec{V} = 0 \tag{5-17b}$$

$$\widehat{n} \cdot \left(-PI + \frac{\mu}{\phi} \left(\nabla \vec{V} + (\nabla \vec{V})^{\tau} \right) \right) = 0 \tag{5-17c}$$

4. The thermal symmetry boundary conditions are applied r=0 for all models and including the symmetry of flow boundary conditions for only the porous models.

$$\hat{n} \cdot (k\nabla T) = 0 \tag{5-18a}$$

$$\widehat{n} \cdot \vec{V} = 0 \tag{5-18b}$$

$$\widehat{n} \cdot \left(-PI + \frac{\mu}{\phi} \left(\nabla \vec{V} + (\nabla \vec{V})^{\tau} \right) \right) = 0 \tag{5-18c}$$

5.2.4 Initial condition

The initial electromagnetic fields of the models are set to 0 V/m, the initial temperature of the models is set to the core temperature, which of 37 ºC, while the initial velocity is set of 0 m/s.

5.3 Calculation procedure

This study developed the numerical of liver cancer model with MWA based on the LTE porous media model. The numerical models are solved by the FEM to analyze a 2D axisymmetric transient problem. The electromagnetic wave propagation analysis was applied in all domains. The heat transfer and blood flow were applied only tissue domains (healthy tissue and tumor domain). The performancing comparative of predicted thermal models during MWA: the bioheat model, the porous model with constant velocity, and the Darcy-Brinkman porous model were investigated on the heat transfer in the identical condition. The numerical models were discretized using triangular elements with Lagrange quadratic shape functions, and the elements were adaptive in sensitive areas. The initial time-steps and the maximum time-steps to solve the transient problem were $1x10^{-4}$ s and 0.1 s, respectively. The convergence test for the liver cancer model is showing the relation with the temperature at the sensitive point. The density of elements, approximately 41,720 elements, was mesh independent. Increasing the number of elements past this point did not lead to significantly different computational results, as shown in Fig. 5.2. All simulations are computed with 2D symmetry FEM analysis by using COMSOL^{TM} Multiphysics.

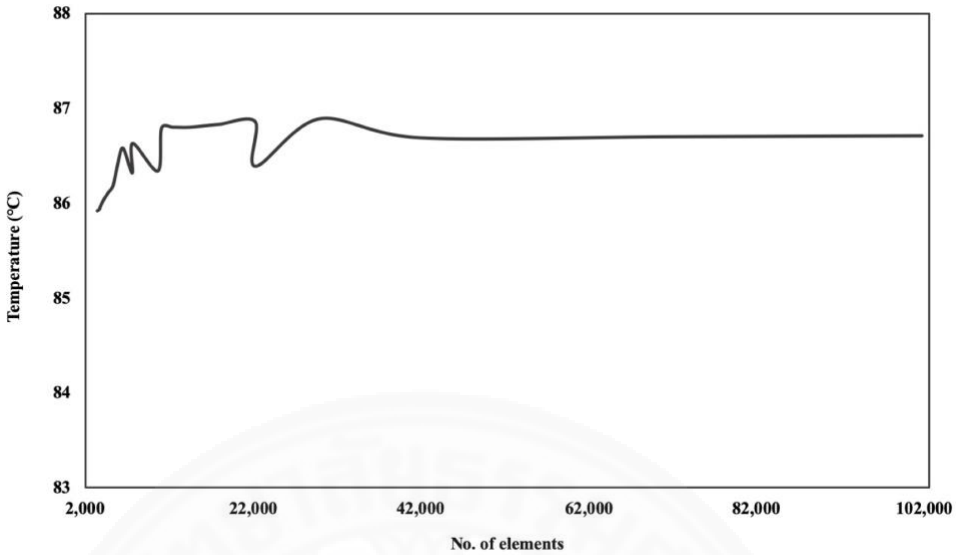

Fig. 5.2 Grid independence test

5.4 Results and Discussion

5.4.1 Verification of model

In order to verify the accuracy of the present numerical study, the present numerical model was validated against the experimental results obtained by Yang et al. (Yang et al., 2007) for the MWA of the bovine liver under the same testing conditions. In the validation model, the microwave power input was 75 W with a frequency of 2.45 GHz, and the initial temperature of the liver domain was set to 8 °C. The MCA was inserted 20 mm deep into the liver tissue, and the duration for a heating time was 180 s. The simulation results against the experimental results received by literature (Yang et al., 2007) are shown in Fig. 5.3, which shows the temperature of two points 4.5 and 9.5 mm away from the MCA, in dependence on the heating time. The error between the presented model and Yang et al.'s experiment results shows in table 5.3. The simulation results are clearly in good agreement with the experimental results. This gives confidence in the accuracy of the presented numerical models.

Table 5.3 Comparisons of RMSE of the liver tissue temperature between the presented model and Yang et al. (Yang et al., 2007; Keangin et al., 2011)

Position (mm)	Comparisons of RMSE with experiment from Yang et al., (ºC)	
	Presented study (Brinkman)	Yang et al. (simulation model)
4.5	3.95	11.03 (Keangin et al., 2011)
9.5	3.50	5.57 (Keangin et al., 2011)

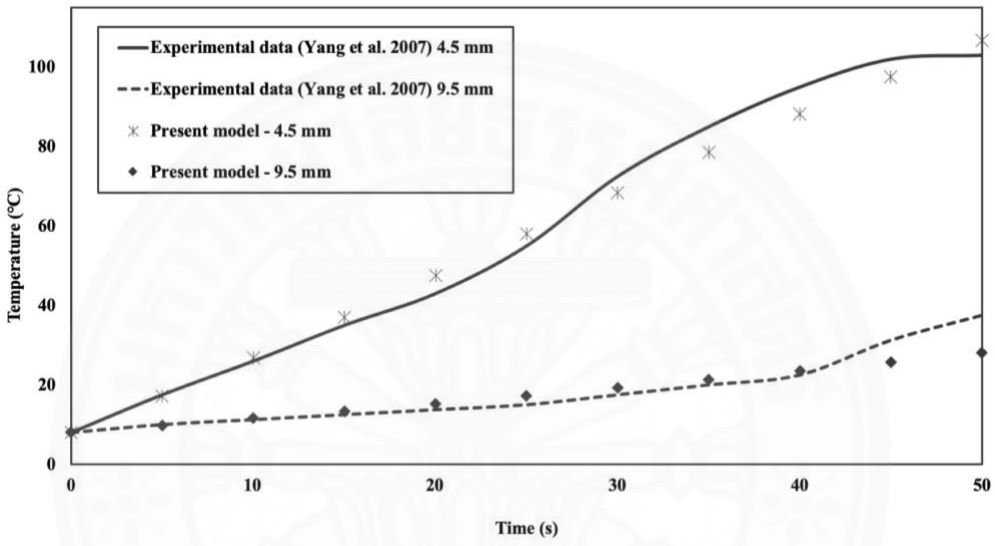

Fig. 5.3 The validation results of the calculated tissue temperature to the tissue temperature obtained by Yang et al. (Yang et al., 2007).

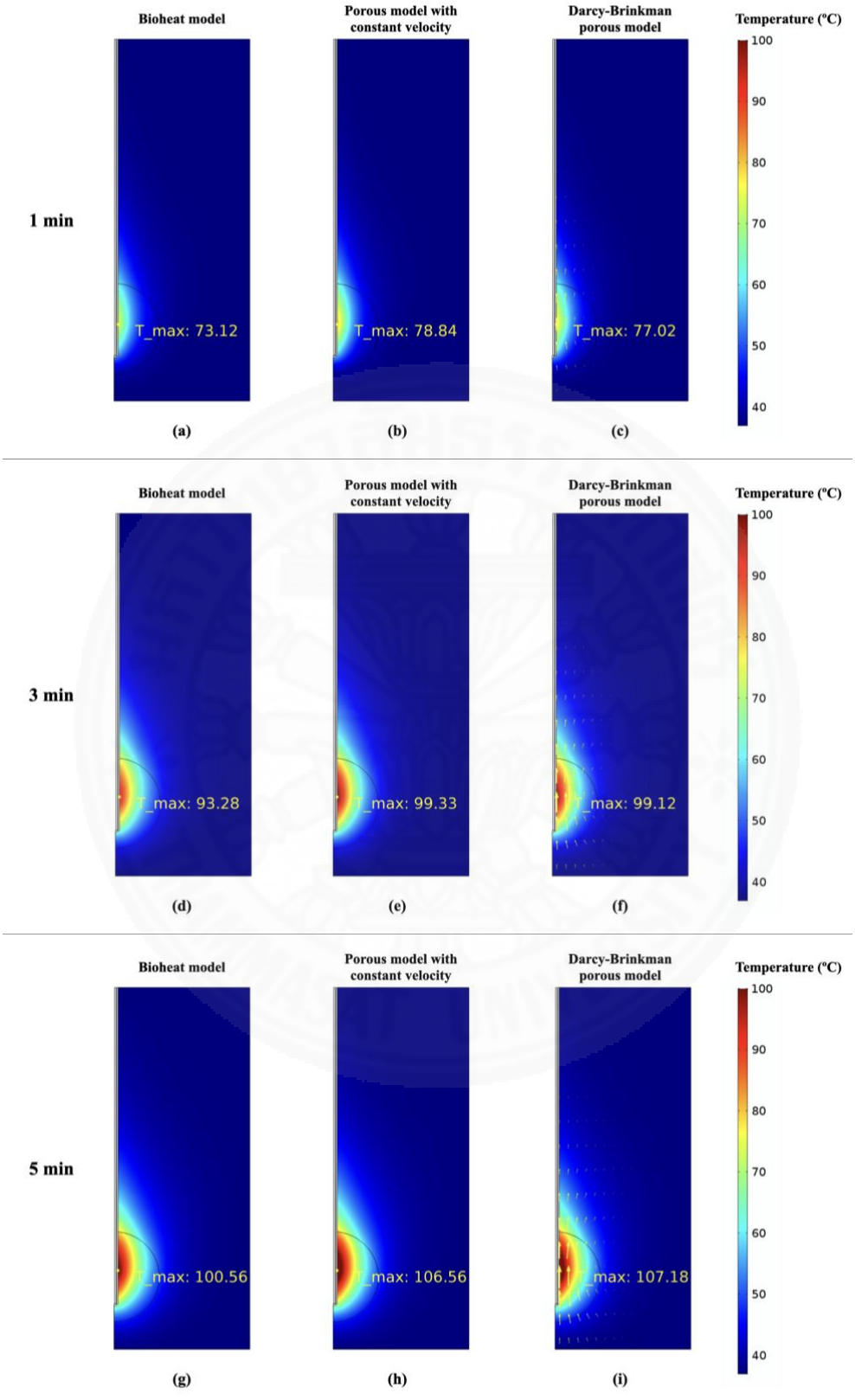

Fig. 5.4 The temperature distribution and velocity vector of the difference liver cancer models with MWA for a heating time of 1, 3, and 5 min, the microwave power of 10 W, and microwave frequency of 2.45 GHz.

5.4.2 The comparative of the performance of thermal models

In this section, the MWA technique is used to treat in the liver cancer with microwave power of 10 W, a frequency of 2.45 GHz, and a heating time period of 5 min for all cases. The mathematical models considered couple with the electromagnetic wave propagation, heat transfer, and flow analysis. The three liver cancer models were applied the bioheat model, the porous model with constant velocity, and the Darcy-Brinkman porous model. The electromagnetic wave propagation analysis based on the same governing equations and conditions. Thus, the electromagnetic wave propagation with the bioheat model, the porous model with constant velocity, and the Darcy-Brinkman porous model was identical. Fig. 5.4 shows the 2D-plot temperature and blood velocity vector of the bioheat model, the porous model with constant velocity, and the Darcy-Brinkman porous model for a heating time of 1, 3, and 5 min. The high temperature zone or the hot spot area of the liver cancer model has appeared around the slot area and decrease with distance from the slot. The hot spot area in the liver cancer model was similar to the water of droplet. The temperature was distributed in the direction of antenna insertion (z-axis) more than the radius side (r-axis). Besides, the temperature profiles of the bioheat model, the porous model with constant velocity, and the Darcy-Brinkman porous model were similarly distributed.

However, Fig. 5.4 shows the maximum temperature of the three heating models, and they were different. The maximum temperature of the bioheat model was 73.12 ºC, 93.28 ºC, and 100.56 ºC for the heating time of 1 min, 3 min, and 5 min, respectively (shown in Figs. 5.4(a), 5.4(d), and 5.4(g)). The maximum temperature of the porous model with constant velocity was 78.84 ºC, 99.33 ºC, and 106.56 ºC (shown in Figs. 5.4(b), 5.4(e), and 5.4(h)). The maximum temperature of the Darcy-Brinkman porous model was 77.02 ºC, 99.12 ºC, and 107.18 ºC (shown in Figs. 5.4(c), 5.4(f), and 5.4(i)). In all the figures henceforth, the arrows represent the direction and the magnitude of blood velocity in the liver domain. The maximum temperature of the three models increased with the heating time. The maximum temperature of the porous model with constant velocity shows the highest temperature, followed by the Darcy-Brinkman porous model and the bioheat model, respectively. The maximum

temperature of the porous model with constant velocity and the Darcy-Brinkman porous model was similar trend when the heating time increased. This because in the early state, the heat transfer of the Darcy-Brinkman porous model plays the role of conduction. After that, the heat convection of the Darcy-Brinkman porous model increased and forcefully when the heating time increased. Furthermore, the heat transfer of the Darcy-Brinkman porous model is strongly convection with the heating time increased. The blood convection flow is driven by the effect of the buoyancy term, which is increased by the gradient temperature in the model. These comparative results show the porous models' maximum temperatures (with the constant velocity and the Darcy-Brinkman) similarly when the heating time increased.

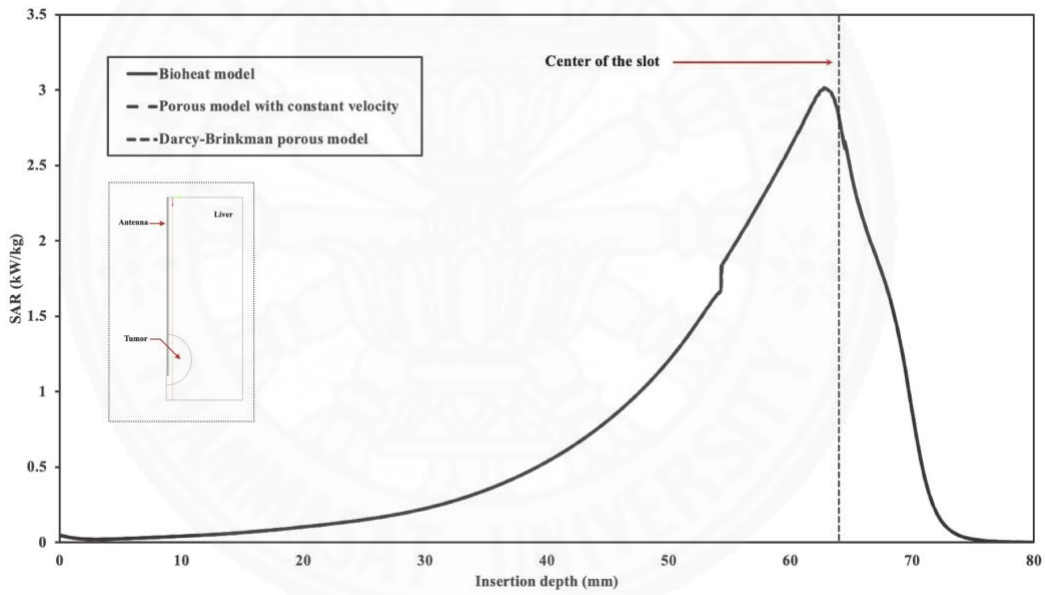

Fig. 5.5 The SAR distribution of the difference liver cancer models at the insertion depth line with microwave power of 10 W, and frequency of 2.45 GHz.

In this study, the microwave propagation in the liver tissue (i.e., healthy tissue and tumor) is considered axisymmetric propagation and the characterization with TM mode. When the microwave penetration in the tissue, the microwave is contributed to the heat generation in liver tissue by using the dipole rotation mechanism. The goal of this treatment is to destroy the target tissue by without damaged in the surrounding healthy tissue. The electromagnetic wave propagation is

the first mechanism for this treatment. Therefore, electromagnetic wave propagation has to investigate. Fig. 5.5 shows the SAR distribution of the liver cancer models at the insertion depth line. The SAR distribution is strongly distributed near a slot of the antenna and decreased with distance from a slot. In this simulation results, the SAR of all models is similarly profiles. That because electric field intensity and the dielectric properties of all models are nearly the same. The temperature distribution in Fig. 5.6 is a similar trend with the SAR distribution, but the temperature between each models is different, especially in the hot spot zone.

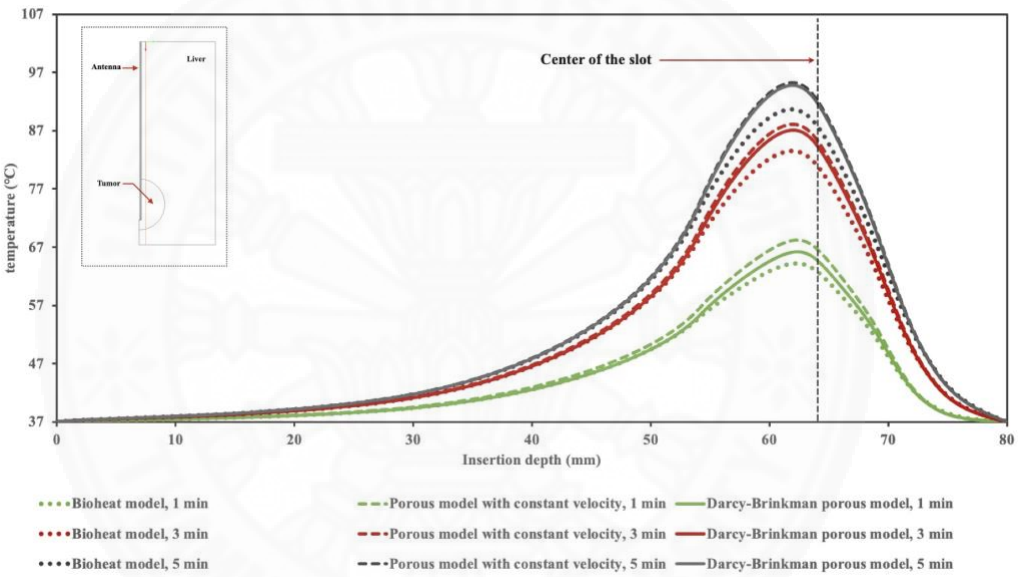

Fig. 5.6 The temperature distribution of the difference liver cancer models at the insertion depth line with microwave power of 10 W, and frequency of 2.45 GHz.

The insertion line in the liver cancer model was the line to parallel with MCA and away from MCA of 2.5 mm (r = 2.5 mm), as shown in Fig. 5.6. Fig. 5.6 shows the temperature distribution of the liver cancer models along with the insertion depth line for a heating time of 1, 3, and 5 min. The maximum temperature of all models appeared around the slot area and decreased with distance away from the slot. The temperature distribution increases with heating time. In the hot spot zone, the temperature of the liver cancer model with the different models is clearly the difference. In the early stage of heating, the temperature distribution between models is slightly

different. When treatment time increases, the temperature distribution between the bioheat model and the porous models were clearly different. Furthermore, the temperature distribution of the porous model with constant velocity and the Darcy-Brinkman porous model was seemed to be the trend. This because the effect of heat convection was increasing when the gradient temperature was increasing. Moreover, the temperature difference between the porous model with constant velocity and the Darcy-Brinkman porous model was decreasing with heating time, corresponding with the result from Fig. 5.4.

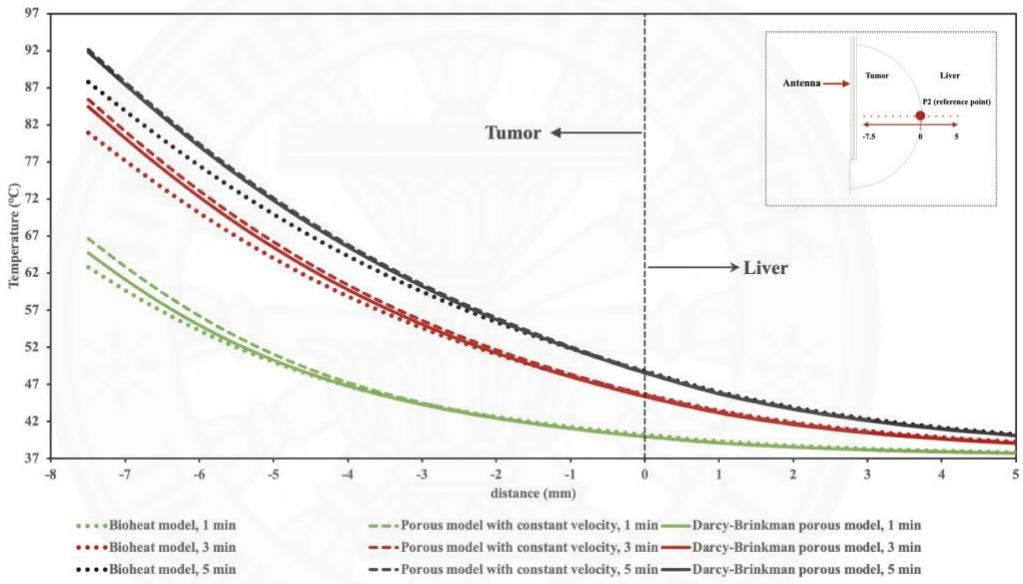

Fig. 5.7 The temperature distribution of the difference liver cancer models along at the monitoring points for a heating time of 1, 3, 5 min with the microwave power of 10 W, and frequency of 2.45 GHz.

The position of the temperature monitoring points at the center of the slot line, which P2 position is a point at the boundary of the tumor and along with the center of the slot line, as shown in Fig. 5.7. Left hand side of P2, these points are monitoring the temperature in the tumor domain. Right hand side, the points on the right side of the P2 monitoring the temperature in the healthy liver domain. Fig. 5.7 shows the temperature distribution of the liver cancer model at the monitoring points with a heating time of 1, 3, 5 min. The temperature of the left-hand side was higher than

the right-hand side. The temperature distribution of the porous model with constant velocity was most quickly increasing, followed by the Darcy-Brinkman porous model and bioheat model, respectively. In the hot spot zone (left side), the temperature distribution of the liver cancer with different thermal models implemented have clearly seen the difference. In case of porous model, the stronger heat convection clearly observed in the high temperature area, because in this area, the blood convection is strongly dependent with gradient temperature. However, the distance away from the slot could not observe the effect of the different thermal models on the temperature distribution. Furthermore, the temperature distribution of the porous model with constant velocity and the Darcy-Brinkman porous model is a similar trend, when the heating time increases, corresponding with Fig. 5.4-5.6.

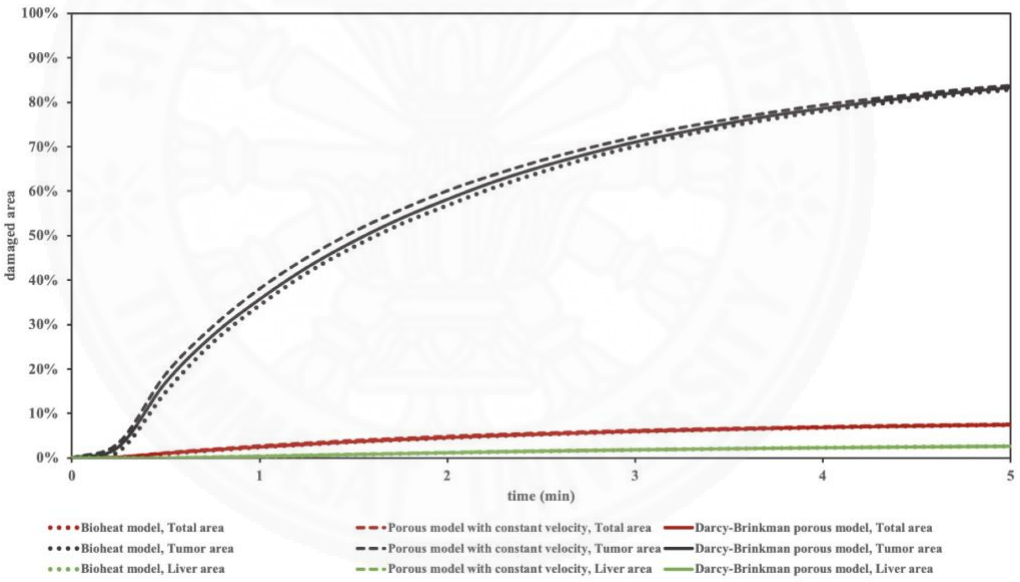

Fig. 5.8 The percentage of the damaged area in the difference liver cancer models with the microwave power of 10 W and the microwave frequency of 2.45 GHz.

Fig. 5.8 shows the percentage of the damaged area of the models. The damaged area of the liver cancer model with the MWA was calculated by integrating the area, in which the temperature of the area increases over 52 ºC. This integrating area was divided by the total area. This section represented the area as the specific tumor area, the specific healthy liver area, and the total area. The total area was a combination

of the area of the tumor and healthy liver. The damaged area increases with the heating time. The most percentage of damage has occurred in the tumor area, followed by the total area (tumor area, including healthy liver) and the healthy liver, respectively. The effect of the thermal models implemented on the percentage of the damaged area could be seen in the only tumor, as the hot spot area has appeared in the tumor area. The damaged area of the thermal models was corresponding with the temperature distribution. For the heating time of 5 min, the tumor damage of 82.75%, 83.75%, and 83.30% for the bioheat model, the porous model with constant velocity, the Darcy-Brinkman porous model, respectively. Simultaneously, the healthy liver damage of 2.54%, 2.59%, and 2.59% for the bioheat model, the porous model with constant velocity, and the Darcy-Brinkman porous model, respectively. Although this treatment was damaged on the healthy liver, nevertheless, it is only a small amount of destruction (less than 3% also all models).

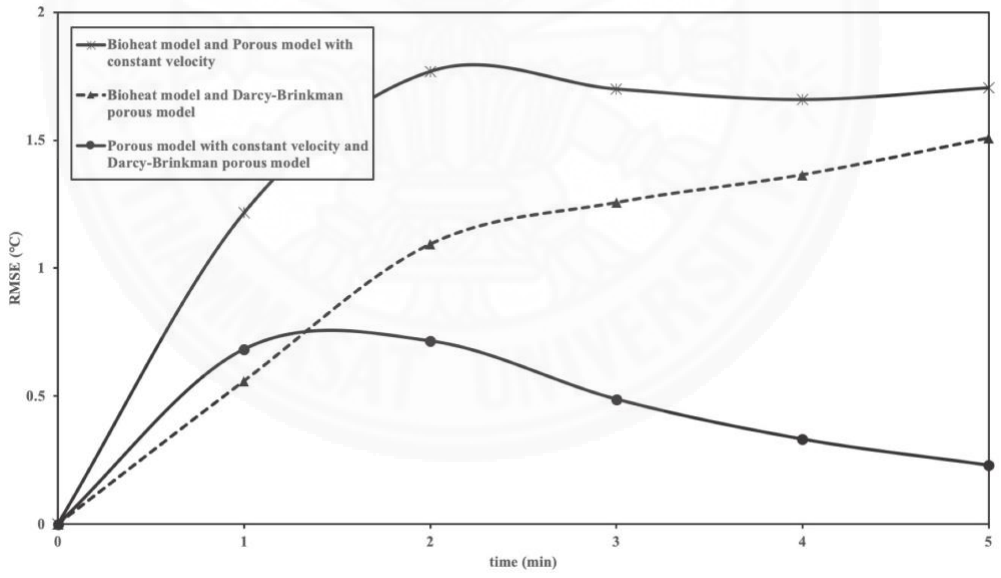

Fig. 5.9 The RMSE of the comparative temperatures with the different thermal models implemented in the liver cancer model with MWA for the microwave power of 10 W and the microwave frequency of 2.45 GHz

The Root Mean Square Error (RMSE) of the temperature difference between the bioheat model, the porous model with constant velocity, and the Darcy-

Brinkman porous model shows in Fig. 5.9 The RMSE of the porous models (the porous model with constant velocity and the Darcy-Brinkman porous model) decreases with the heating time. On the other hand, the RMSE of the porous models and the bioheat model increases with the heating time. The RMSE of the porous model with constant velocity and the bioheat model more than the Darcy-Brinkman porous model and the bioheat model. In the initial heating time, the heat transfer of Darcy-Brinkman porous model plays in the role of conduction mode. However, when the heating time increased, the heat transfer of the Darcy-Brinkman porous model plays in the role of convection combined with conduction modes. These results were shown on the temperature profiles difference between the Darcy-Brinkman porous model, the Bioheat, and the porous model with velocity constant.

In the early stage of the heating time, the effect of the thermal models implemented on the temperature distribution was not different. Because of the heat transfer of the early state was influenced by the heat conduction. After that, the temperature distribution of the thermal models implemented could be differently increased. In particular, the hot spot zones could clearly see the temperature differences. When increasing the heating time, the heat convection of the Darcy-Brinkman porous model has become stronger. It was seen to be the temperature of the Darcy-Brinkman porous model has similarly distributed the temperature of the porous model with constant velocity. Thus, the heat transfer of this state was driven by the heat convection more than the heat conduction. Furthermore, in the initial stage of heating time, the bioheat model could be implemented for the prediction temperature in the liver cancer model at an area far away from the hot spot. However, in the area of high temperature have to use the Darcy-Brinkman porous model for the prediction temperature in liver cancer model.

5.5 Conclusion

This work presents the numerical study of the heat transfer as well as the heat convection coupled with the electromagnetic wave propagation in the porous liver cancer model. The performancing comparative of the predicted thermal models during the MWA process using a slot antenna with microwave power of 10 W and frequency

of 2.45 GHz was systematically investigated. The bioheat model, the porous model with constant velocity, and the Darcy-Brinkman porous model were implemented in the liver cancer model. The simulation of the porous model was in good agreement with the experimental results obtained by Yang et al. (Yang et al., 2007), as shown in Fig. 5.2. Key findings that occurred from this study:

1. The heating models have affected on temperature prediction in liver cancer model with MWA. Especially, in the area of the high temperature. In this area, The Darcy-Brinkman porous model has a flexible used than the porous model with constant velocity and the bioheat model. However, in the area far away from the hot spot, the three heating models have not different.
2. The effect of the different heating models on the heat transfer had clearly appeared in the hot spot area and similarly distributed in the area far away from the hot spot.
3. In the early stage of heating time, the heat transfer of the Darcy-Brinkman porous model and the bioheat model were roughly similar. When the heating time increased, the heat transfer of the Darcy-Brinkman porous model and the porous model with constant velocity were seemed to be the trend.
4. In the early stage of heating time, the effect of the thermal models implemented on the temperature distribution was not different. After that, the temperature distribution of the thermal models implemented could be differently increased. Because of the heat convection is strongly dependent with gradient temperature.

The four key findings could be concluded the effect of the thermal models on the heat transfer was necessary for consideration in the liver cancer treatment, especially in the high temperature area. The Darcy-Brinkman porous model was effective in various situations, such as the role of conduction or the role of convection, or combination heat transfer. Therefore, the Darcy-Brinkman porous model was suggested for the heat transfer prediction in liver cancer model with the MWA technique, especially in the high temperature areas and the highest microwave power.

The difference point between the porous model and the bioheat can be expressed in the difference in the equations. The equation of the bioheat model based on heat diffusion. This equation added blood perfusion term in the heat conduction equation. The heat transfer mechanism of the bioheat model plays in the role of

conduction. On the other hand, the equation of the porous media based on heat convection. In the early state of heating, heat transfer plays in the role of conduction. Therefore, the temperature distribution is slightly different between porous models and bioheat model. After that, the heat transfer of the porous models plays in the role of convection. Nevertheless, the heat transfer of the bioheat still plays in the role of conduction. It is not a suggestion for the medium and extended state of heating time, in which heat transfer of the bioheat and porous models occurs differently.

In the next step of this research, we will develop the numerical modeling for approaching realistic liver tissue will be performed with the deformation analysis in the porous liver. The study will also consider the local non-thermal equilibrium (LNTE) heat transfer model in analyzing biological tissues subjected to microwave energy.

CHAPTER 6
OVERALL CONCLUSIONS AND RECOMMENDATIONS FOR FUTURE WORK

Nowadays, cancer is a threat to humans. According to facts, cancer is the human cause of death more than any crime and any pandemics. Besides, approximately 70% of human deaths from cancer occur in low- and middle-income countries, and Thailand is one of those countries. In dealing with cancer, It is urgent and cannot wait. Preventing cancer risk and including early detection of cancer is necessary for the healthcare system. However, cancer treatment is the most important factor for dealing with cancer. Surgery, surgery, chemotherapy, and radiation are conventional treatments, which the first options for cancer treatment. These treatments are limited and side effects on specific patients. Therefore, alternative treatment is introduced, and nowadays, the microwave ablation (MWA) treatment is one of the treatments that is extensively gaining attention.

Microwave ablation (MWA) is a minimally invasive cancer treatment method that induces thermal injury into the tumor by using microwave energy. The microwave energy is created at the generator and transmitted by the microwave antenna to the local cancer area or tumor. The microwave would be absorbed and converted to the local heat generation in this area that causes of local temperature is increased. When the tissue temperature exceeded the lethal temperature, the cancer cell will be destroyed. The benefits of MWA are rapid treatment, effective treatment in a specific area, a short recovery period, less postoperative pain, and fewer complications. Although MWA has an effective treatment method and many advantages compared with conventional treatment for localized liver cancer, MWA has dangerous when used incorrect conditions during treatment, such as the heat spread over the boundaries of the tumor area. Therefore, the studies of correct conditions and pre-treatment simulation are necessary.

Although MWA was an interesting and effective treatment method, the experimental and study in the humans liver could not be studied because it was due to humanity and the risk of unethical. Some group researchers have been experimenting

with animals, but not enough. The phenomenon of heat and electromagnetic wave dissipation in animal organs cannot imply to realistic human organs. It has been the advantage of needing only a short period, the low economic cost, humanity, and could be set up with conditions near to those of a real human liver. The MWA studies are focused on the heat transfer and SAR distribution in the biological tissue, The MWA studies focus on the heat transfer and SAR distribution phenomenon in the biological tissue during treatment because it indicates treatment effectiveness. Although there are some studies investigated the heat transfer and SAR distribution phenomenon in the biological tissue during MWA treatment process,

Although MWA was an interesting and effective treatment method, the experimental and study in the humans liver could not be studied because it was due to humanity and the risk of unethical. Some group researchers have been experimenting with animals, but not enough. The phenomenon of heat and electromagnetic wave dissipation in animal organs cannot imply to realistic human organs. The numerical modeling was developed for this shortcoming. The MWA studies focused on the heat transfer and SAR distribution phenomenon in the biological tissue during treatment because it indicated treatment effectiveness. Although some studies investigated the heat transfer and SAR distribution phenomenon in the biological tissue during the MWA treatment process with systematic investigations, these studies were considered based on the two-dimensional (2D) assumptions that do not cover specific situations. The treatment area near the large vessel is one of the various situations that cannot apply the 2D assumption. Furthermore, comparative studies of the predicted heating models implemented to liver cancer during the MWA process with the systematic investigation were not demonstrated.

This dissertation presented the numerical analysis of specific absorption rate and heat transfer in liver cancer during the MWA treatment process using the coaxial slot antenna. This dissertation focused on the treatment area near the large blood vessel, which area has to consider with the three-dimensional (3D) assumption. Besides, the effect of the locality of the large blood vessel on specific absorption rate and heat transfer is investigated systematically. Moreover, the comparison of the predicted heating models implemented to liver cancer during MWA was investigated on the heat transfer and specific absorption rate distribution. For the numerical

simulation accuracy, the simulation results were validated with the experimental results of the literature. Furthermore, the damaged tissue by thermal injury was presented in this study.

Moreover, the detailed study in this dissertation can separate into two major categories as follows:

1. 3D numerical analysis of focused microwave ablation for the treatment of patients with localized liver cancer embedded with a vertical and horizontal blood vessel (Chapter 4)
2. The comparative of the performance for predicted thermal models during the microwave ablation process using a slot antenna (Chapter 5)

The overall conclusions of electromagnetic wave propagation and heat transfer in liver cancer during the MWA treatment process can be summarized as follows:

1) SAR distribution in liver cancer during the MWA treatment process is not annoyed by a large blood vessel near the treatment area. The intensity of SAR dissipates in the area around the slot and decreases with distance away from the slot. The SAR of the model with the vertical vessel and the horizontal vessel is similarly distributed. Thus, the large blood vessel near the treatment area cannot affect SAR distribution in liver cancer during the MWA treatment process, especially SAR distribution in the tumor area.

2) Temperature distribution in liver cancer during the MWA treatment process is affected by a large blood vessel near the treatment area. The maximum temperature is found at the area close to the slot. The hot spot zone appears at the slot area, and the temperature decreased with distance away from the slot. The SAR intensity and high temperature were similar to the water of the droplet. However, the temperature of liver cancer near a large blood vessel during the MWA process is not symmetrical distribution. This result indicates the shortcomings of the 2D assumption for describing the heat transfer in liver cancer near a large vessel during the MWA treatment process. Furthermore, the temperature distribution in the model with the horizontal vessel is higher than the model with the vertical vessel because of SAR and temperature distributions when treatment with slot coaxial antenna.

3) The damaged tissue distribution in liver cancer during the MWA treatment process is affected by a large blood vessel near the treatment area and correspondence with the temperature distribution. The lethally damaged tissue fraction appears at the slot area, damaged tissue decrease with distance away from the slot. The damaged tissue distribution is asymmetrically distributed, corresponding with the temperature distribution in the same case. To determine the amount of damaged tissue, we found that the damaged tissue of the model with a horizontal vessel was higher than the model with a vertical vessel. However, the damaged tissue in this study is affected by only thermal injury consideration.

4) The comparative heat transfer in liver cancer during the MWA treatment process with three heating models is investigated. The heating models have affected to temperature prediction in liver cancer during the MWA treatment process, especially in the area of high temperature. In this area, The Darcy-Brinkman porous model has a flexible use than the porous model with constant velocity and the bioheat model. However, in the area far away from the hot spot, the three heating models have not different. However, the effect of the different heating models on the heat transfer had clearly appeared in the hot spot area and similarly distributed in the area far away from the hot spot.

5) The liver cancer based on the Darcy-Brinkman porous model during the MWA process demonstrates that the difference in heat transfer mechanism in liver cancer varies with treatment duration. In the early state of the MWA process, heat transfer was influenced by heat conduction. After that, the heat convection of the Darcy-Brinkman porous model has become stronger. The heat transfer after the initial state is combined between heat conduction and heat convection. Thus, the heat transfer phenomenon in liver cancer during MWA treatment should be considered by the heating model to take into account blood direction such as a bioheat model based on the porous media approach.

This dissertation suggested the Darcy-Brinkman porous media model for predicting the temperature distribution in liver cancer during the MWA process. This model has a flexible use than the porous model with constant velocity and the bioheat model. Furthermore, the treatment area nearby the large blood vessel flow should avoid the vertical blood vessel than the horizontal blood because the vertical blood vessel

affected the temperature distribution in the treatment area than the horizontal blood vessel.

Finally, this dissertation study presented the numerical study of the SAR, heat transfer, and damaged tissue distribution in liver cancer during the MWA treatment process with a coaxial slot antenna. It is shown that the mathematical model of liver cancer with MWA treatment is presented, and the model can use to successfully explain the transport phenomena within liver cancer in specific conditions. Furthermore, the obtained values represent the accurate phenomena to determine the liver tissue's temperature distribution due to microwave energy from the MWA treatment and the effect of the large blood vessel near the treatment area. The presence of SAR and heat transfer phenomena during MWA treatment in a specific area may benefit and guidelines for practice treatment with MWA.

This study concluded the effect of blood locality on the heat transfer in liver cancer during MWA treatment based on 3D assumption. However, during MWA treatment near the large vessel, liver cancer was not considered the distancing of blood vessel location. Furthermore, the dielectric properties are not indicated as a function of frequency and temperature, which may affect the simulation results' accuracy. Thus, many ideas for additional study in cancer treatment with MWA in the biological tissue and medical applications of electromagnetic energy are suggested in future work.

REFERENCES

Ahmed, M., & Goldberg, S. N. (2011). Basic science research in thermal ablation. Surgical Oncology Clinics, 20(2), 237-258.

Alazmi, B., & Vafai, K. (2000). Analysis of variants within the porous media transport models. J. Heat Transfer, 122(2), 303-326.

Ananthakrishnan, A., Gogineni, V., & Saeian, K. (2006, March). Epidemiology of primary and secondary liver cancers. In Seminars in interventional radiology (Vol. 23, No. 1, p. 47). Thieme Medical Publishers.

Ansari, D., & Andersson, R. (2012). Radiofrequency ablation or percutaneous ethanol injection for the treatment of liver tumors. World journal of gastroenterology: WJG, 18(10), 1003.

Arkin, H., Xu, L. X., & Holmes, K. R. (1994). Recent developments in modeling heat transfer in blood perfused tissues. IEEE Transactions on Biomedical Engineering, 41(2), 97-107.

Baird, D., Hughes, R. I., & Nordmann, A. (Eds.). (2013). Heinrich Hertz: classical physicist, modern philosopher (Vol. 198). Springer Science & Business Media.

Baust, J., Gage, A. A., Ma, H., & Zhang, C. M. (1997). Minimally invasive cryosurgery—technological advances. Cryobiology, 34(4), 373-384.

Becker, S. M., & Kuznetsov, A. V. (2007). Thermal damage reduction associated with in vivo skin electroporation: A numerical investigation justifying aggressive pre-cooling. International Journal of Heat and Mass Transfer, 50(1-2), 105-116.

Bertram, J. M., Yang, D., Converse, M. C., Webster, J. G., & Mahvi, D. M. (2006). Antenna design for microwave hepatic ablation using an axisymmetric electromagnetic model. Biomedical engineering online, 5(1), 15.

Bosman, F. T., Carneiro, F., Hruban, R. H., & Theise, N. D. (2010). WHO classification of tumours of the digestive system(No. Ed. 4). World Health Organization.

Brace, C. L. (2008, August). Temperature-dependent dielectric properties of liver tissue measured during thermal ablation: Toward an improved numerical model. In 2008 30th Annual International Conference of the IEEE Engineering in Medicine and Biology Society (pp. 230-233). IEEE.

Brace, C. L. (2009). Microwave ablation technology: what every user should know. Current problems in diagnostic radiology, 38(2), 61-67.

Brace, C. L. (2009). Radiofrequency and microwave ablation of the liver, lung, kidney, and bone: what are the differences?. Current problems in diagnostic radiology, 38(3), 135-143.

Bridgewater, J., Galle, P.R., Khan, S.A Llovet, J.M., Park, J.W., Patel, T., Pawlik, T.M., & Gores, G.J. (2014). Guidelines for the diagnosis and management of intrahepatic cholangiocarcinoma, Journal of Hepatology, 60(6), 1268-1289

Brinkman, H. C. (1949). On the permeability of media consisting of closely packed porous particles. Flow, Turbulence and Combustion, 1(1), 81.

Bruix, J. (2005). sherman M. Management of hepatocellular carcinoma. Hepatology, 42, 1208-36.

Bruix, J., Boix, L., Sala, M., & Llovet, J. (2004). BCLC Group Liver Unit. Focus on hepatocellular carcinoma. Cancer Cell, 5, 215-219.

Bruix, J., Sherman, M., Llovet, J. M., Beaugrand, M., Lencioni, R., Burroughs, A. K., ... & Rodés, J. (2001). Clinical management of hepatocellular carcinoma. Conclusions of the Barcelona-2000 EASL conference. Journal of hepatology, 35(3), 421-430.

Camart, J. C., Fabre, J. J., Prevost, B., Pribetich, J., & Chive, M. (1992). Coaxial antenna array for 915 MHz interstitial hyperthermia: design and modelization-power deposition and heating pattern-phased array. IEEE transactions on microwave theory and techniques, 40(12), 2243-2250.

Carrafiello, G., Laganà, D., Mangini, M., Fontana, F., Dionigi, G., Boni, L., ... & Fugazzola, C. (2008). Microwave tumors ablation: principles, clinical applications and review of preliminary experiences. International Journal of Surgery, 6, S65-S69.

Cha-um, W., Rattanadecho, P., & Pakdee, W. (2011). Experimental and numerical analysis of microwave heating of water and oil using a rectangular wave guide: influence of sample sizes, positions, and microwave power. Food and Bioprocess Technology, 4(4), 544-558.

Chaiyo, K., & Rattanadecho, P. (2011). Numerical analysis of microwave melting of ice-saturated porous medium filled in a rectangular waveguide with resonator using a combined transfinite interpolation and PDE methods. International journal of heat and mass transfer, 54(9-10), 2043-2055.

Charny, C. K., Weinbaum, S., & Levin, R. L. (1990). An evaluation of the Weinbaum-Jiji bioheat equation for normal and hyperthermic conditions.

Chato, J. C. (1980). Heat transfer to blood vessels. Journal of biomechanical engineering, 102(2), 110-118.

Chatterjee, S., Basak, T., & Das, S. K. (2007). Microwave driven convection in a rotating cylindrical cavity: A numerical study. Journal of Food Engineering, 79(4), 1269-1279.

Chen, M. M., & Holmes, K. R. (1980). Microvascular contributions in tissue heat transfer. Annals of the New York Academy of Sciences, 335(1), 137-150.

Correa-Gallego, C., Fong, Y., Gonen, M., D'Angelica, M. I., Allen, P. J., DeMatteo, R. P., ... & Kingham, T. P. (2014). A retrospective comparison of microwave ablation vs. radiofrequency ablation for colorectal cancer hepatic metastases. Annals of surgical oncology, 21(13), 4278-4283.

Correa-Gallego, C., Fong, Y., Gonen, M., D'Angelica, M. I., Allen, P. J., DeMatteo, R. P., ... & Kingham, T. P. (2014). A retrospective comparison of microwave ablation vs.

radiofrequency ablation for colorectal cancer hepatic metastases. Annals of surgical oncology, 21(13), 4278-4283.

Curley, S. A., Izzo, F., Ellis, L. M., Vauthey, J. N., & Vallone, P. (2000). Radiofrequency ablation of hepatocellular cancer in 110 patients with cirrhosis. Annals of surgery, 232(3), 381.

Datta, A. K. (2001). Handbook of microwave technology for food application. CRC Press.

Datta, A. K. (2007). Porous media approaches to studying simultaneous heat and mass transfer in food processes. I: Problem formulations. Journal of food engineering, 80(1), 80-95.

Di, D. R., He, Z. Z., Sun, Z. Q., & Liu, J. (2012). A new nano-cryosurgical modality for tumor treatment using biodegradable MgO nanoparticles. Nanomedicine: Nanotechnology, Biology and Medicine, 8(8), 1233-1241.

Dong, B. W., Liang, P., Yu, X. L., Zeng, X. Q., Wang, P. J., Su, L., ... & Li, S. O. N. G. (1998). Sonographically guided microwave coagulation treatment of liver cancer: an experimental and clinical study. AJR. American journal of roentgenology, 171(2), 449-454.

Ebara, M., Okabe, S., Kita, K., Sugiura, N., Fukuda, H., Yoshikawa, M., ... & Saisho, H. (2005). Percutaneous ethanol injection for small hepatocellular carcinoma: therapeutic efficacy based on 20-year observation. Journal of hepatology, 43(3), 458-464.

Fujimoto, M., Hirata, A., Wang, J., Fujiwara, O., & Shiozawa, T. (2006). FDTD-derived correlation of maximum temperature increase and peak SAR in child and adult head models due to dipole antenna. IEEE transactions on electromagnetic compatibility, 48(1), 240-247.

Goldberg, S. N., Gazelle, G. S., & Mueller, P. R. (2000). Thermal ablation therapy for focal malignancy: a unified approach to underlying principles, techniques, and diagnostic imaging guidance. American journal of roentgenology, 174(2), 323-331.

Hines-Peralta, A. U., Pirani, N., Clegg, P., Cronin, N., Ryan, T. P., Liu, Z., & Goldberg, S. N. (2006). Microwave ablation: results with a 2.45-GHz applicator in ex vivo bovine and in vivo porcine liver. Radiology, 239(1), 94-102.

Hirata, A., Matsuyama, S. I., & Shiozawa, T. (2000). Temperature rises in the human eye exposed to EM waves in the frequency range 0.6-6 GHz. IEEE Transactions on Electromagnetic Compatibility, 42(4), 386-393.

Holtz, E., Ahrné, L., Rittenauer, M., & Rasmuson, A. (2010). Influence of dielectric and sorption properties on drying behaviour and energy efficiency during microwave convective drying of selected food and non-food inorganic materials. Journal of Food Engineering, 97(2), 144-153.

Izzo, F., Granata, V., Grassi, R., Fusco, R., Palaia, R., Delrio, P., ... & Curley, S. A. (2019). Radiofrequency ablation and microwave ablation in liver tumors: an update. The oncologist, 24(10), e990.

Jain, R. K., & Ward-Hartley, K. I. M. B. E. R. L. Y. (1984). Tumor blood flow-characterization, modifications, and role in hyperthermia. IEEE Transactions on sonics and ultrasonics, 31(5), 504-525.

Jiji, L. M., Weinbaum, S., & Lemons, D. E. (1984). Theory and experiment for the effect of vascular microstructure on surface tissue heat transfer—part II: model formulation and solution.

Keangin, P., & Rattanadecho, P. (2013). Analysis of heat transport on local thermal non-equilibrium in porous liver during microwave ablation. International Journal of Heat and Mass Transfer, 67, 46-60.

Keangin, P., & Rattanadecho, P. (2018). A numerical investigation of microwave ablation on porous liver tissue. Advances in Mechanical Engineering, 10(8), 1687814017734133.

Keangin, P., Rattanadecho, P., & Wessapan, T. (2011). An analysis of heat transfer in liver tissue during microwave ablation using single and double slot antenna. International Communications in Heat and Mass Transfer, 38(6), 757-766.

Keangin, P., Vafai, K., & Rattanadecho, P. (2013). Electromagnetic field effects on biological materials. International Journal of Heat and Mass Transfer, 65, 389-399.

Keangin, P., Wessapan, T., & Rattanadecho, P. (2011). Analysis of heat transfer in deformed liver cancer modeling treated using a microwave coaxial antenna. Applied Thermal Engineering, 31(16), 3243-3254.

Khaled, A. R., & Vafai, K. (2003). The role of porous media in modeling flow and heat transfer in biological tissues. International Journal of Heat and Mass Transfer, 46(26), 4989-5003.

Khanafer, K., & Vafai, K. (2006). The role of porous media in biomedical engineering as related to magnetic resonance imaging and drug delivery. Heat and mass transfer, 42(10), 939-953.

Klinbun, W., & Rattanadecho, P. (2017). An investigation of the dielectric and thermal properties of frozen foods over a temperature from–18 to 80° C. International Journal of Food Properties, 20(2), 455-464.

Klinger, H. G. (1974). Heat transfer in perfused biological tissue—I: General theory. Bulletin of Mathematical Biology, 36, 403-415.

Klinger, H. G. (1978). Heat transfer in perfused biological tissue—II. The “macroscopic” temperature distribution in tissue. Bulletin of mathematical biology, 40(2), 183-199.

Koksungnoen, S., Rattanadecho, P., & Wongchadakul, P. (2018). 3D numerical model of blood flow in the coronary artery bypass graft during no pulse and pulse situations:

Effects of an anastomotic angle and characteristics of fluid. Journal of Mechanical Science and Technology, 32(9), 4545-4552.

Lencioni, R., & Crocetti, L. (2007). Radiofrequency ablation of liver cancer. Techniques in vascular and interventional radiology, 10(1), 38-46.

Li, X., Zhang, L., Fan, W., Zhao, M., Wang, L., Tang, T., ... & Liu, Y. (2011). Comparison of microwave ablation and multipolar radiofrequency ablation, both using a pair of internally cooled interstitial applicators: results in ex vivo porcine livers. International Journal of Hyperthermia, 27(3), 240-248.

Liang, P., & Wang, Y. (2007). Microwave ablation of hepatocellular carcinoma. Oncology, 72(Suppl. 1), 124-131.

Liangruksa, M., Ganguly, R., & Puri, I. K. (2011). Parametric investigation of heating due to magnetic fluid hyperthermia in a tumor with blood perfusion. Journal of Magnetism and Magnetic Materials, 323(6), 708-716.

Liu, F. Y., Yu, X. L., Liang, P., Wang, Y., Zhou, P., & Yu, J. (2010). Comparison of percutaneous 915 MHz microwave ablation and 2450 MHz microwave ablation in large hepatocellular carcinoma. International Journal of Hyperthermia, 26(5), 448-455.

Llovet, J.M., Zucman-Rossi, J., Pikarsky, E., Sangro, B., Schwartz, M., Sherman, M. & Gores G. (2016). Hepatocellular carcinoma. Nature reviews Disease primers 2, 16018

Lopresto, V., Pinto, R., & Cavagnaro, M. (2014). Experimental characterisation of the thermal lesion induced by microwave ablation. International Journal of Hyperthermia, 30(2), 110-118.

Lopresto, V., Pinto, R., Farina, L., & Cavagnaro, M. (2017). Microwave thermal ablation: effects of tissue properties variations on predictive models for treatment planning. Medical engineering & physics, 46, 63-70.

Lounsberry, W. (1995). The early histologic changes following electrocoagulation. Gastrointest Endosc, 41, 68-70.

Lozano, R., Naghavi, M., Foreman, K., Lim, S., Shibuya, K., Aboyans, V., ... & Remuzzi, G. (2012). Global and regional mortality from 235 causes of death for 20 age groups in 1990 and 2010: a systematic analysis for the Global Burden of Disease Study 2010. The lancet, 380(9859), 2095-2128.

Lubner, M. G., Brace, C. L., Hinshaw, J. L., & Lee Jr, F. T. (2010). Microwave tumor ablation: mechanism of action, clinical results, and devices. Journal of Vascular and Interventional Radiology, 21(8), S192-S203.

Mahjoob, S., & Vafai, K. (2009). Analytical characterization of heat transport through biological media incorporating hyperthermia treatment. International Journal of Heat and Mass Transfer, 52(5-6), 1608-1618.

Malashetty, M. S., Swamy, M., & Heera, R. (2008). Double diffusive convection in a porous layer using a thermal non-equilibrium model. International journal of thermal sciences, 47(9), 1131-1147.

Marcelin, C., Leiner, J., Nasri, S., Petitpierre, F., Le Bras, Y., Yacoub, M., ... & Cornelis, F. (2018). In vivo percutaneous microwave ablation in kidneys: Correlation with ex vivo data and ablation work. Diagnostic and interventional imaging, 99(1), 3-8.

Martin, R. C., Scoggins, C. R., & McMasters, K. M. (2010). Safety and efficacy of microwave ablation of hepatic tumors: a prospective review of a 5-year experience. Annals of surgical oncology, 17(1), 171-178.

Maxwell, J. C. (1890). A dynamical theory of the electromagnetic field (1865). The Scientific Papers of James Clerk Maxwell, 2.

McGahan, J. P., & Dodd III, G. D. (2001). Radiofrequency ablation of the liver: current status. American Journal of Roentgenology, 176(1), 3-16.

McGahan, J. P., BROWNING, P. D., BROCK, J. M., & TESLUK, H. (1990). Hepatic ablation using radiofrequency electrocautery. Investigative radiology, 25(3), 267-270.

Mechling, J. A., & Strohbehn, J. W. (1992). Three-dimensional theoretical SAR and temperature distributions created in brain tissue by 915 and 2450 MHz dipole antenna arrays with varying insertion depths. International journal of Hyperthermia, 8(4), 529-542.

Meredith, K., Lee, F., Henry, M. B., Warner, T., & Mahvi, D. (2005). Microwave ablation of hepatic tumors using dual-loop probes: results of a phase I clinical trial. Journal of gastrointestinal surgery, 9(9), 1354-1360.

Minbashi, M., Kordbacheh, A. A., Ghobadi, A., & Tuchin, V. V. (2020). Optimization of power used in liver cancer microwave therapy by injection of Magnetic Nanoparticles (MNPs). Computers in Biology and Medicine, 120, 103741.

Nabaei, M., & Karimi, M. (2018). Numerical investigation of the effect of vessel size and distance on the cryosurgery of an adjacent tumor. Journal of thermal biology, 77, 45-54.

Nakayama, A., & Kuwahara, F. (2008). A general bioheat transfer model based on the theory of porous media. International Journal of Heat and Mass Transfer, 51(11-12), 3190-3199.

Nield, D. A., & Bejan, A. (2006). Convection in porous media (Vol. 3). New York: springer.

Okajima, J., Maruyama, S., Takeda, H., & Komiya, A. (2009). Dimensionless solutions and general characteristics of bioheat transfer during thermal therapy. Journal of Thermal Biology, 34(8), 377-384.

Oshima, F., Yamakado, K., Nakatsuka, A., Takaki, H., Makita, M., & Takeda, K. (2008). Simultaneous microwave ablation using multiple antennas in explanted bovine livers: relationship between ablative zone and antenna. Radiation medicine, 26(7), 408-414.

Özen, Ş., Helhel, S., & Cerezci, O. (2008). Heat analysis of biological tissue exposed to microwave by using thermal wave model of bio-heat transfer (TWMBT). Burns, 34(1), 45-49.

Pakdee, W., & Rattanadecho, P. (2011). Natural convection in a saturated variable-porosity medium due to microwave heating. Journal of heat transfer, 133(6).

Parkin, D. M., Bray, F., Ferlay, J., & Pisani, P. (2005). Global cancer statistics, 2002. CA: a cancer journal for clinicians, 55(2), 74-108.

Pennes, H. H. (1948). Analysis of tissue and arterial blood temperatures in the resting human forearm. Journal of applied physiology, 1(2), 93-122.

Phasukkit, P., Tungjitkusolmun, S., & Sangworasil, M. (2009). Finite-element analysis and in vitro experiments of placement configurations using triple antennas in microwave hepatic ablation. IEEE Transactions on Biomedical Engineering, 56(11), 2564-2572.

Phasukkit, P., Tungjitkusolmun, S., & Sangworasil, M. (2009). Finite-element analysis and in vitro experiments of placement configurations using triple antennas in microwave hepatic ablation. IEEE Transactions on Biomedical Engineering, 56(11), 2564-2572.

Pisa, S., Cavagnaro, M., Piuzzi, E., Bernardi, P., & Lin, J. C. (2003). Power density and temperature distributions produced by interstitial arrays of sleeved-slot antennas for hyperthermic cancer therapy. IEEE transactions on microwave theory and techniques, 51(12), 2418-2426.

Poston, G. J., Tait, D., O'Connell, S., Bennett, A., & Berendse, S. (2011). Diagnosis and management of colorectal cancer: summary of NICE guidance. Bmj, 343, d6751.

Poulou, L. S., Botsa, E., Thanou, I., Ziakas, P. D., & Thanos, L. (2015). Percutaneous microwave ablation vs radiofrequency ablation in the treatment of hepatocellular carcinoma. World journal of hepatology, 7(8), 1054.

Prakash, P., Deng, G., Converse, M. C., Webster, J. G., Mahvi, D. M., & Ferris, M. C. (2008). Design optimization of a robust sleeve antenna for hepatic microwave ablation. Physics in Medicine & Biology, 53(4), 1057.

Prakash, P., Salgaonkar, V. A., Clif Burdette, E., & Diederich, C. J. (2012). Multiple applicator hepatic ablation with interstitial ultrasound devices: Theoretical and experimental investigation. Medical physics, 39(12), 7338-7349.

Rabin, Y., & Shitzer, A. (1998). Numerical solution of the multidimensional freezing problem during cryosurgery.

Ratanadecho, P., Aoki, K., & Akahori, M. (2001). Experimental and numerical study of microwave drying in unsaturated porous material. International Communications in Heat and Mass Transfer, 28(5), 605-616.

Rattanadecho, P., & Keangin, P. (2013). Numerical study of heat transfer and blood flow in two-layered porous liver tissue during microwave ablation process using single and double slot antenna. International Journal of Heat and Mass Transfer, 58(1-2), 457-470.

Rattanadecho, P., & Klinbun, W. (2011). Theoretical analysis of microwave heating of dielectric materials filled in a rectangular waveguide with various resonator distances. Journal of heat transfer, 133(3).

Rattanadecho, P., & Serttikul, C. (2007). Simulation of melting of ice under a constant temperature heat source using a combined transfinite interpolation and partial differential equation methods. Journal of Porous Media, 10(7).

Rattanadecho, P., Aoki and, K., & Akahori, M. (2002). Experimental validation of a combined electromagnetic and thermal model for a microwave heating of multi-layered materials using a rectangular wave guide. J. Heat Transfer, 124(5), 992-996.

Rattanadecho, P., Suwannapum, N., Watanasungsuit, A., & Duangduen, A. (2007). Drying of dielectric materials using microwave-continuous belt furnace. ASME Journal of Manufacturing Sciences and Engineering, 129(1), 157-163.

Ren, H., Liang, P., Yu, X., Wang, Y., Lu, T., & Li, X. (2011). Treatment of liver tumours adjacent to hepatic hilum with percutaneous microwave ablation combined with ethanol injection: a pilot study. International Journal of Hyperthermia, 27(3), 249-254.

Roetzel, W., & Xuan, Y. (1998). Transient response of the human limb to an external stimulust. International journal of heat and mass transfer, 41(1), 229-239.

Rossi, S., Fornati, F., Pathies, C., & Buscarini, L. (1990). Thermal lesions induced by 480 KHz localized current field in guinea pig and pig liver. Tumori Journal, 76(1), 54-57.

Sabiston, D. C., Townsend, C. M., Beauchamp, R. D., Evers, B. M., & Mattox, K. L. (2001). Sabiston textbook of surgery: the biological basis of modern surgical practice. Wb Saunders.

Saccomandi, P., Schena, E., Massaroni, C., Fong, Y., Grasso, R. F., Giurazza, F., ... & Cazzato, R. L. (2015). Temperature monitoring during microwave ablation in ex vivo porcine livers. European Journal of Surgical Oncology (EJSO), 41(12), 1699-1705.

Saito, K., Hayashi, Y., Yoshimura, H., & Ito, K. (2000). Heating characteristics of array applicator composed of two coaxial-slot antennas for microwave coagulation therapy. IEEE Transactions on Microwave Theory and Techniques, 48(11), 1800-1806.

Sanchez, R., Van Sonnenberg, E., D'agostino, H., Goodacre, B., & Esch, O. (1993). Percutaneous tissue ablation by radiofrequency thermal energy as a prelim to tumour ablation. Minimally Invasive Therapy, 2(6), 299-305.

Serttikul, C., Datta, A. K., & Rattanadecho, P. (2019). Effect of layer arrangement on 2-D numerical analysis of freezing process in double layer porous packed bed. Journal homepage: http://iieta. org/Journals/IJHT, 37(1), 273-284.

Shao, Y. L., Arjun, B., Leo, H. L., & Chua, K. J. (2017). Nano-assisted radiofrequency ablation of clinically extracted irregularly-shaped liver tumors. Journal of thermal biology, 66, 101-113.

Shao, Y. L., Arjun, B., Leo, H. L., & Chua, K. J. (2017). Nano-assisted radiofrequency ablation of clinically extracted irregularly-shaped liver tumors. Journal of thermal biology, 66, 101-113.

Shao, Y. L., Leo, H. L., & Chua, K. J. (2018). Studying of the thermal performance of a hybrid cryo-RFA treatment of a solid tumor. International Journal of Heat and Mass Transfer, 122, 410-420.

Shen, W., Zhang, J., & Yang, F. (2005). Modeling and numerical simulation of bioheat transfer and biomechanics in soft tissue. Mathematical and Computer Modelling, 41(11-12), 1251-1265.

Shock, S. A., Meredith, K., Warner, T. F., Sampson, L. A., Wright, A. S., Winter III, T. C., ... & Lee Jr, F. T. (2004). Microwave ablation with loop antenna: in vivo porcine liver model. Radiology, 231(1), 143-149.

Sia, D., Villanueva, A., Friedman, S. L., & Llovet, J. M. (2017). Liver cancer cell of origin, molecular class, and effects on patient prognosis. Gastroenterology, 152(4), 745-761.

Skinner, M. G., Iizuka, M. N., Kolios, M. C., & Sherar, M. D. (1998). A theoretical comparison of energy sources-microwave, ultrasound and laser-for interstitial thermal therapy. Physics in Medicine & Biology, 43(12), 3535.

Strickland, A. D., Clegg, P. J., Cronin, N. J., Swift, B., Festing, M., West, K. P., ... & Lloyd, D. M. (2002). Experimental study of large-volume microwave ablation in the liver. British Journal of Surgery, 89(8), 1003-1007.

Torre, L. A., Bray, F., Siegel, R. L., Ferlay, J., Lortet-Tieulent, J., & Jemal, A. (2015). Global cancer statistics, 2012. CA: a cancer journal for clinicians, 65(2), 87-108.

Tzou, D. Y. (1995). Experimental support for the lagging behavior in heat propagation. Journal of thermophysics and heat transfer, 9(4), 686-693.

Vafai, K. (1984). Convective flow and heat transfer in variable-porosity media. Journal of Fluid Mechanics, 147, 233-259.

Vafai, K., & Tien, C. L. (1982). Boundary and inertia effects on convective mass transfer in porous media. International Journal of Heat and Mass Transfer, 25(8), 1183-1190.

Voizard, N., Cerny, M., Assad, A., Billiard, J. S., Olivié, D., Perreault, P., ... & Tang, A. (2019). Assessment of hepatocellular carcinoma treatment response with LI-RADS: a pictorial review. Insights into imaging, 10(1), 1-22.

Wang, T., Zhao, G., & Qiu, B. (2015). Theoretical evaluation of the treatment effectiveness of a novel coaxial multi-slot antenna for conformal microwave ablation of tumors. International Journal of Heat and Mass Transfer, 90, 81-91.

Weinbaum, S. J. L. M., Jiji, L. M., & Lemons, D. E. (1984). Theory and experiment for the effect of vascular microstructure on surface tissue heat transfer—Part I: Anatomical foundation and model conceptualization.

Weinbaum, S., & Jiji, L. M. (1985). A new simplified bioheat equation for the effect of blood flow on local average tissue temperature.

Wessapan, T., & Rattanadecho, P. (2012). Specific absorption rate and temperature increase in human eye subjected to electromagnetic fields at 900 MHz. Journal of heat transfer, 134(9).

Wessapan, T., & Rattanadecho, P. (2016). Flow and heat transfer in biological tissue due to electromagnetic near-field exposure effects. International Journal of Heat and Mass Transfer, 97, 174-184.

Wessapan, T., & Rattanadecho, P. (2016). Temperature induced in the testicular and related tissues due to electromagnetic fields exposure at 900 MHz and 1800 MHz. International Journal of Heat and Mass Transfer, 102, 1130-1140.

Wessapan, T., & Rattanadecho, P. (2018). Temperature induced in human organs due to near-field and far-field electromagnetic exposure effects. International journal of heat and mass transfer, 119, 65-76.

Wessapan, T., Srisawatdhisukul, S., & Rattanadecho, P. (2011). Numerical analysis of specific absorption rate and heat transfer in the human body exposed to leakage electromagnetic field at 915 MHz and 2450 MHz. Journal of Heat Transfer, 133(5).

Wessapan, T., Srisawatdhisukul, S., & Rattanadecho, P. (2012). Specific absorption rate and temperature distributions in human head subjected to mobile phone radiation at different frequencies. International Journal of Heat and Mass Transfer, 55(1-3), 347-359.

Whelan, W. M., Davidson, S. R. H., Chin, L. C. L., & Vitkin, I. A. (2005). A novel strategy for monitoring laser thermal therapy based on changes in optothermal properties of heated tissues. International Journal of Thermophysics, 26(1), 233-241.

Wissler, E. H. (1971). Comparison of computed results obtained from two mathematical models: a simple 14-node model and a complex 250-node model. Journal de physiologie, 63(3), 455-458.

Wissler, E. H. (1987). Comments on the new bioheat equation proposed by Weinbaum and Jiji.

Wolf, F. J., Grand, D. J., Machan, J. T., Dipetrillo, T. A., Mayo-Smith, W. W., & Dupuy, D. E. (2008). Microwave ablation of lung malignancies: effectiveness, CT findings, and safety in 50 patients. Radiology, 247(3), 871-879.

Wongchadakul, P., Rattanadecho, P., & Wessapan, T. (2018). Implementation of a thermomechanical model to simulate laser heating in shrinkage tissue (effects of wavelength, laser irradiation intensity, and irradiation beam area). International Journal of Thermal Sciences, 134, 321-336.

Wright, A. S., Sampson, L. A., Warner, T. F., Mahvi, D. M., & Lee, Jr, F. T. (2005). Radiofrequency versus microwave ablation in a hepatic porcine model. Radiology, 236(1), 132-139.

Wu, S., Hou, J., Ding, Y., Wu, F., Hu, Y., Jiang, Q., ... & Yang, Y. (2015). Cryoablation versus radiofrequency ablation for hepatic malignancies: a systematic review and literature-based analysis. Medicine, 94(49).

Wu, T., Li, P., Shao, Q., Hong, J., Yang, L., & Wu, S. (2013). A simulation-experiment method to characterize the heat transfer in ex-vivo porcine hepatic tissue with a realistic microwave ablation system. Numerical Heat Transfer, Part A: Applications, 64(9), 729-743.

Wu, X., Liu, B., & Xu, B. (2016). Theoretical evaluation of high frequency microwave ablation applied in cancer therapy. Applied Thermal Engineering, 107, 501-507.

Wulff, W. (1974). The energy conservation equation for living tissue. IEEE transactions on biomedical engineering, (6), 494-495.

Xu, F., Lu, T. J., & Seffen, K. A. (2008). Biothermomechanical behavior of skin tissue. Acta Mechanica Sinica, 24(1), 1-23.

Xu, J., Jia, Z. Z., Song, Z. J., Yang, X. D., Chen, K., & Liang, P. (2010). Three-dimensional ultrasound image-guided robotic system for accurate microwave coagulation of malignant liver tumours. The International Journal of Medical Robotics and Computer Assisted Surgery, 6(3), 256-268.

Xu, Y., Moser, M. A., Zhang, E., Zhang, W., & Zhang, B. (2019). Large and round ablation zones with microwave ablation: A preliminary study of an optimal aperiodic tri-slot coaxial antenna with the π-matching network section. International Journal of Thermal Sciences, 140, 539-548.

Yang, B., Wan, R. G., Muldrew, K. B., & Donnelly, B. J. (2008). A finite element model for cryosurgery with coupled phase change and thermal stress aspects. finite elements in analysis and design, 44(5), 288-297.

Yang, D., Converse, M. C., Mahvi, D. M., & Webster, J. G. (2007). Expanding the bioheat equation to include tissue internal water evaporation during heating. IEEE Transactions on Biomedical Engineering, 54(8), 1382-1388.

Yiu, W. K., Basco, M. T., Aruny, J. E., Cheng, S. W., & Sumpio, B. E. (2007). Cryosurgery: a review. The International journal of angiology: official publication of the International College of Angiology, Inc, 16(1), 1.

Yu, N. C., Lu, D. S., Raman, S. S., Dupuy, D. E., Simon, C. J., Lassman, C., ... & Busuttil, R. W. (2006). Hepatocellular carcinoma: microwave ablation with multiple straight and loop antenna clusters—pilot comparison with pathologic findings. Radiology, 239(1), 269-275.

Yuan, P. (2008). Numerical analysis of temperature and thermal dose response of biological tissues to thermal non-equilibrium during hyperthermia therapy. Medical engineering & physics, 30(2), 135-143.

APPENDIX A
ADDITIONAL SIMULATION RESULTS FOR OF FOCUSED MiCROWAVE ABLATION FOR THE TREATMENT OF PATIENTS WITH LOCALIZED LIVER CANCER EMBEDDED WITH A VERTICAL AND HORIZONTAL BLOOD VESSEL

The SAR distribution on the cross-section planes between model with vertical vessel and horizontal vessel, (a) the model with vertical vessel, (b) the model with horizontal vessel.

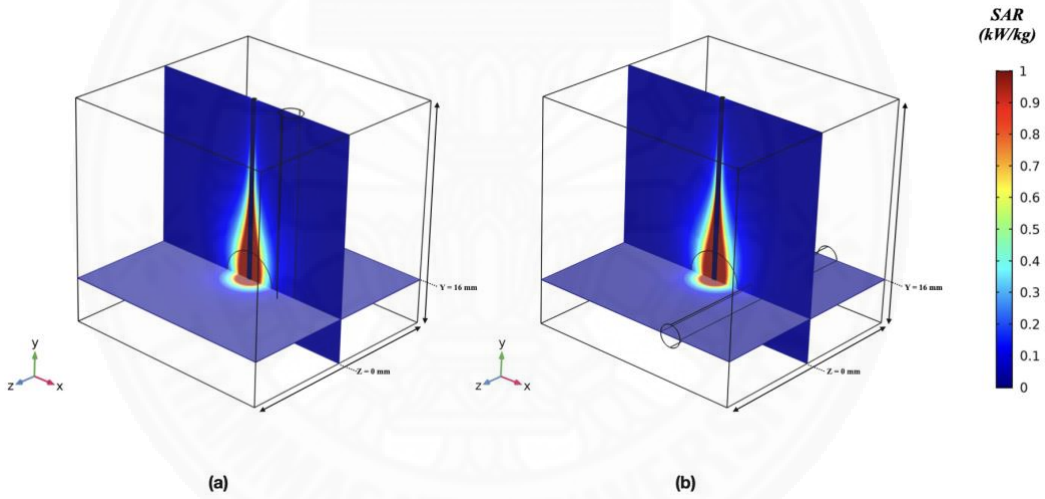

The SAR distribution on the XY plane of the model with vertical vessel, (a) the plane at Z of 10 mm, (b) the plane at Z of 0 mm, (c) the plane at Z of -10 mm.

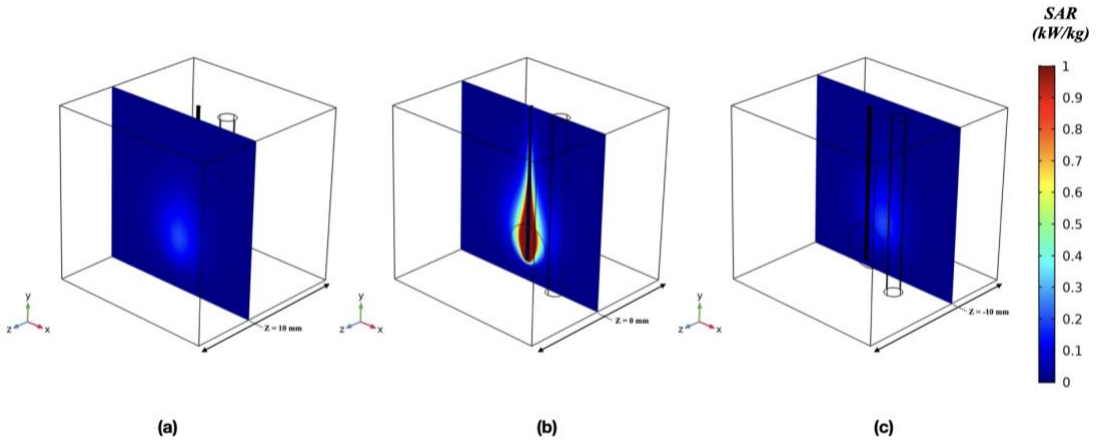

The SAR distribution on the XY plane of the model with horizontal vessel, (a) the plane at Z of 10 mm, (b) the plane at Z of 0 mm, (c) the plane at Z of -10 mm.

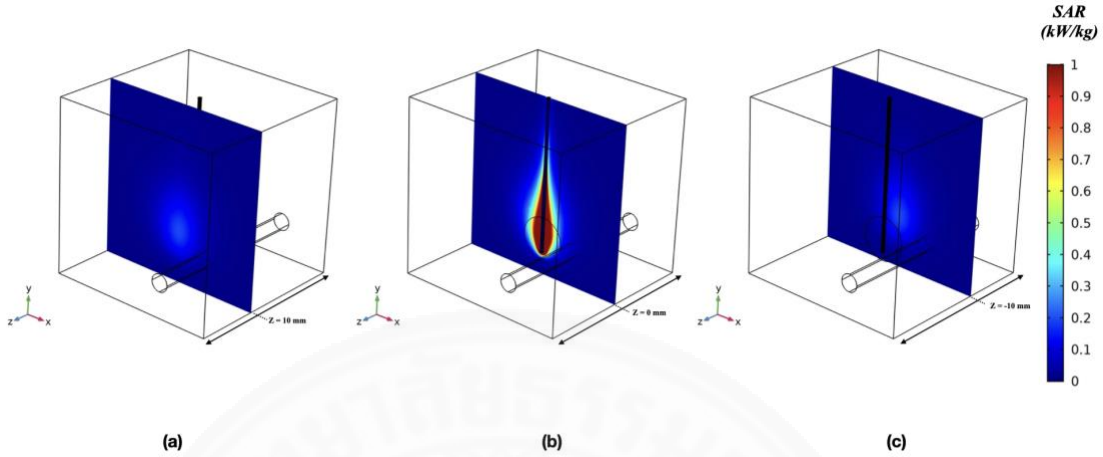

The SAR distribution on the XZ plane of the model with vertical vessel, (a) the plane at Z of 10 mm, (b) the plane at Z of 0 mm, (c) the plane at Z of -10 mm.

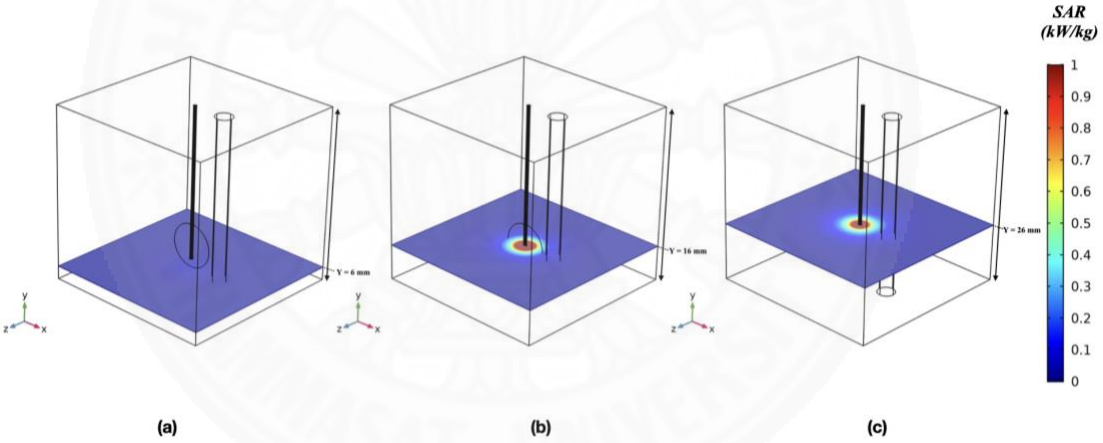

The SAR distribution on the XZ plane of the model with horizontal vessel, (a) the plane at Z of 10 mm, (b) the plane at Z of 0 mm, (c) the plane at Z of -10 mm.

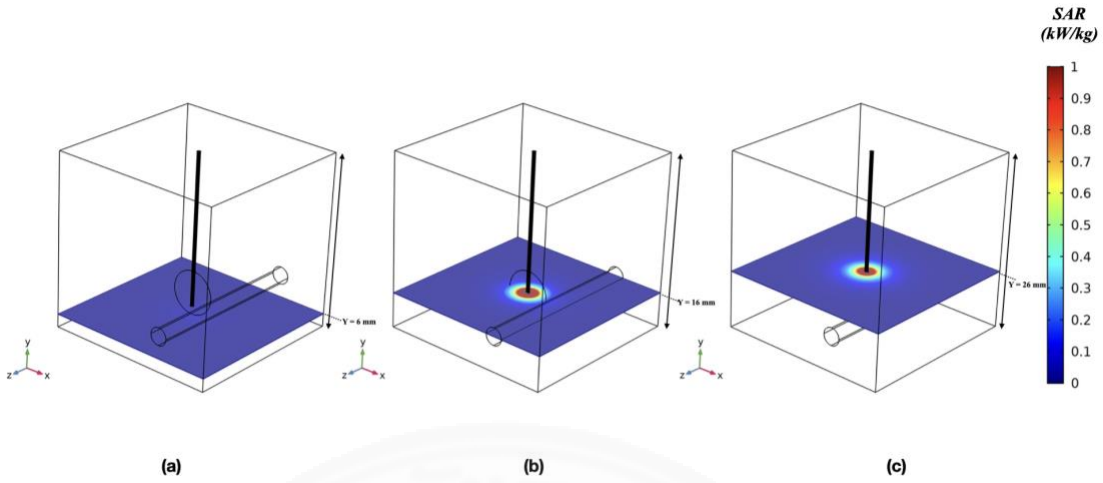

The temperature distribution on the cross-section planes between model with vertical vessel and horizontal vessel, (a) the model with vertical vessel, (b) the model with horizontal vessel.

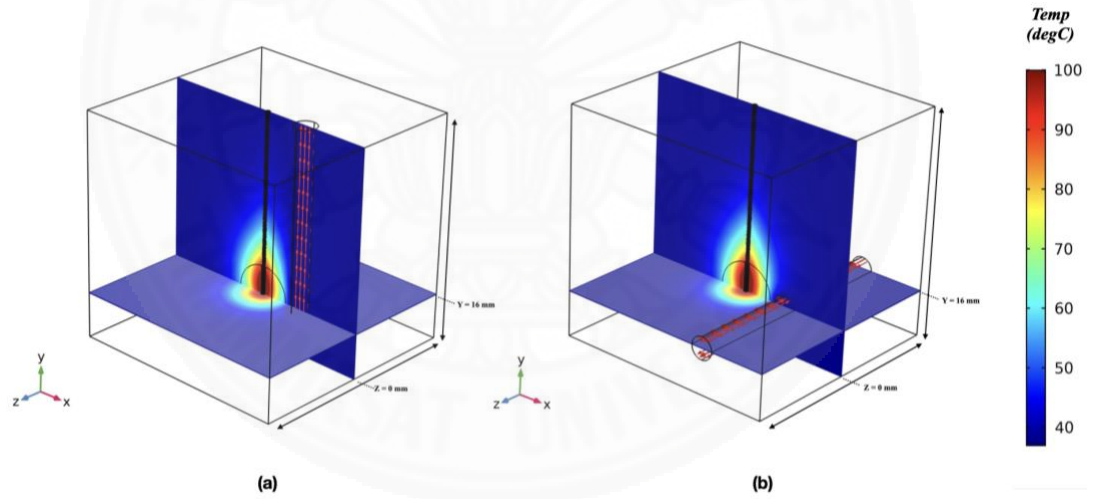

The temperature distribution on the XY plane of the model with vertical vessel, (a) the plane at Z of 10 mm, (b) the plane at Z of 0 mm, (c) the plane at Z of -10 mm.

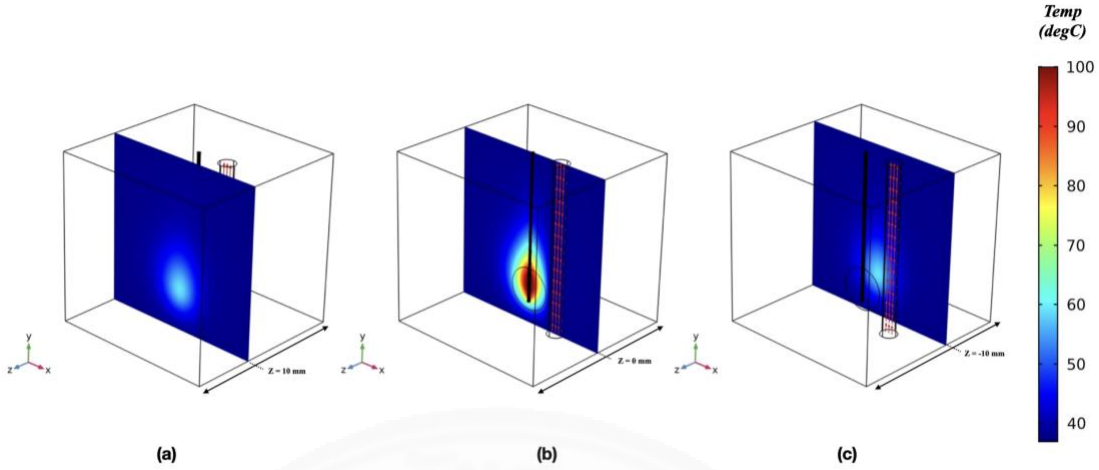

The temperature distribution on the XY plane of the model with horizontal vessel, (a) the plane at Z of 10 mm, (b) the plane at Z of 0 mm, (c) the plane at Z of -10 mm.

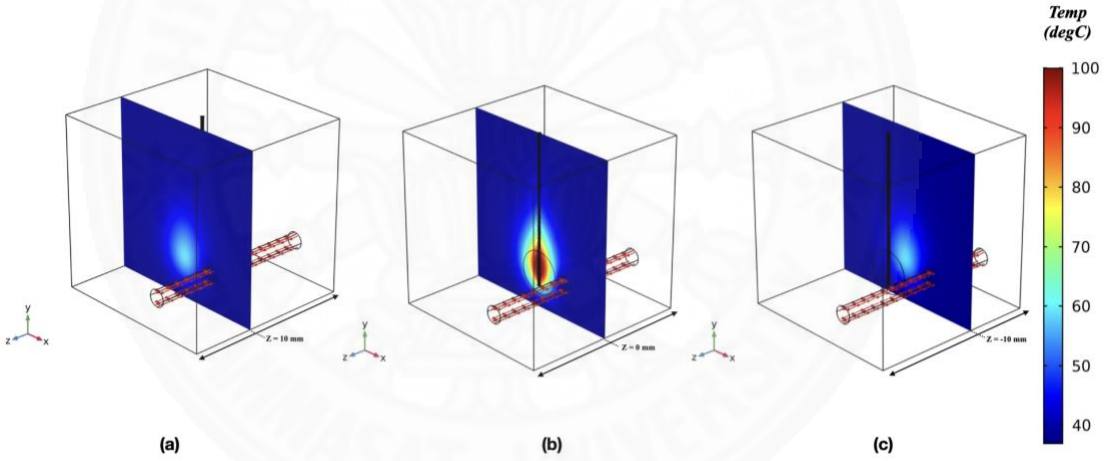

The temperature distribution on the XZ plane of the model with vertical vessel, (a) the plane at Z of 10 mm, (b) the plane at Z of 0 mm, (c) the plane at Z of -10 mm.

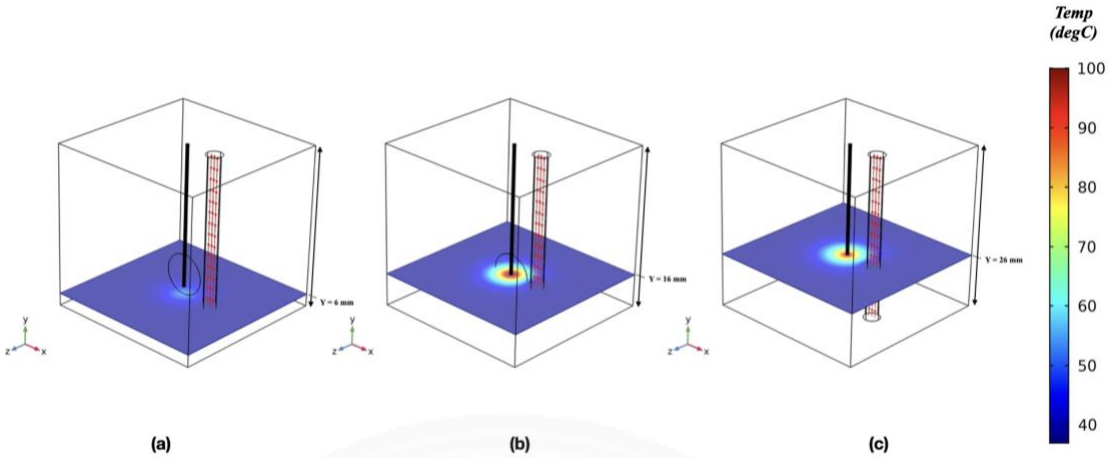

The temperature distribution on the XZ plane of the model with horizontal vessel, (a) the plane at Z of 10 mm, (b) the plane at Z of 0 mm, (c) the plane at Z of -10 mm.

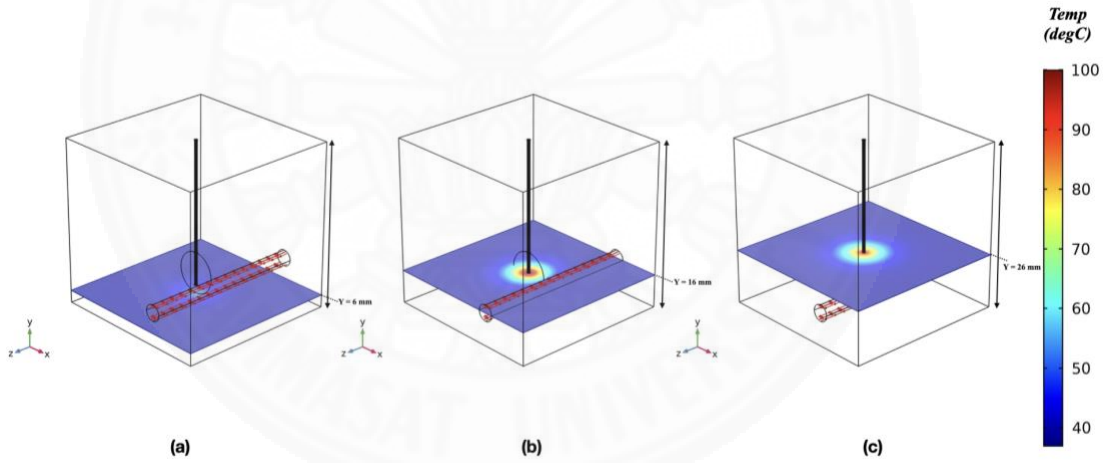

The fraction of necrotic tissue distribution on the cross-section planes between model with vertical vessel and horizontal vessel, (a) the model with vertical vessel, (b) the model with horizontal vessel.

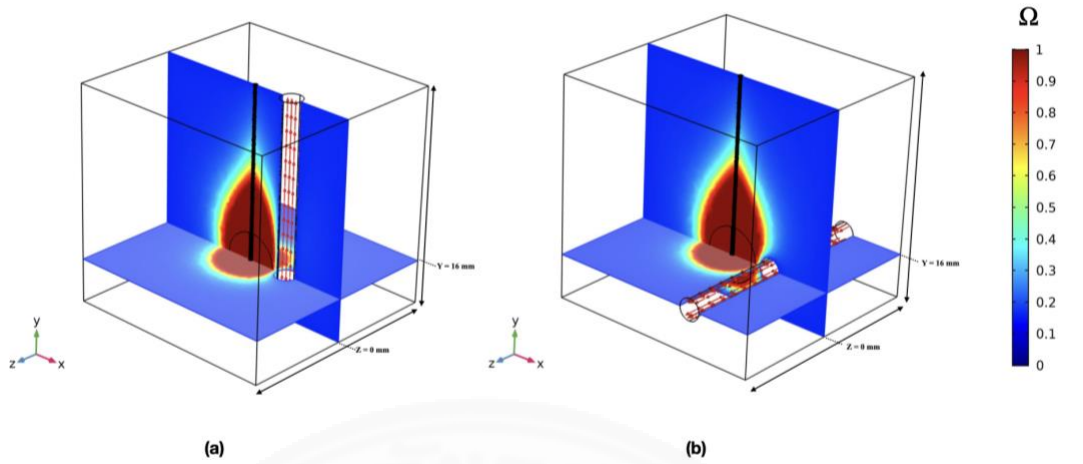

The fraction of necrotic tissue distribution on the XY plane of the model with vertical vessel, (a) the plane at Z of 10 mm, (b) the plane at Z of 0 mm, (c) the plane at Z of -10 mm.

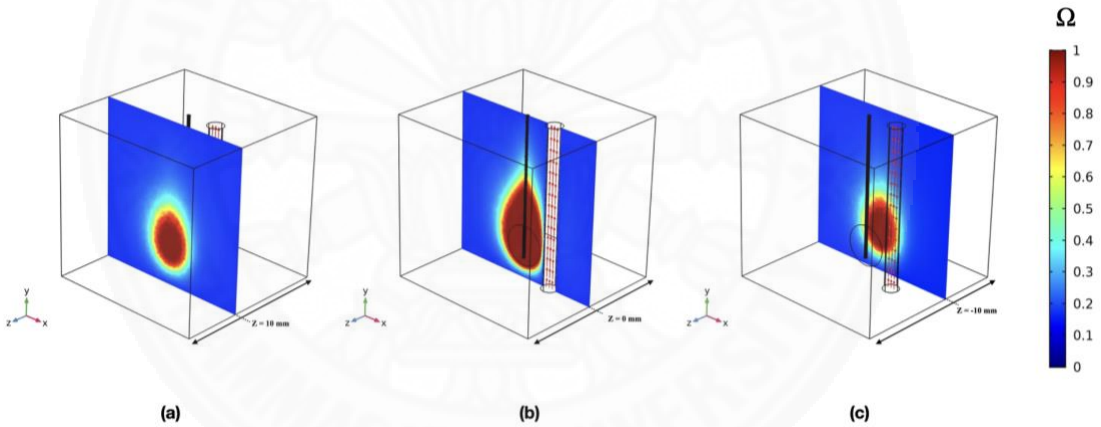

The fraction of necrotic tissue distribution on the XY plane of the model with horizontal vessel, (a) the plane at Z of 10 mm, (b) the plane at Z of 0 mm, (c) the plane at Z of -10 mm.

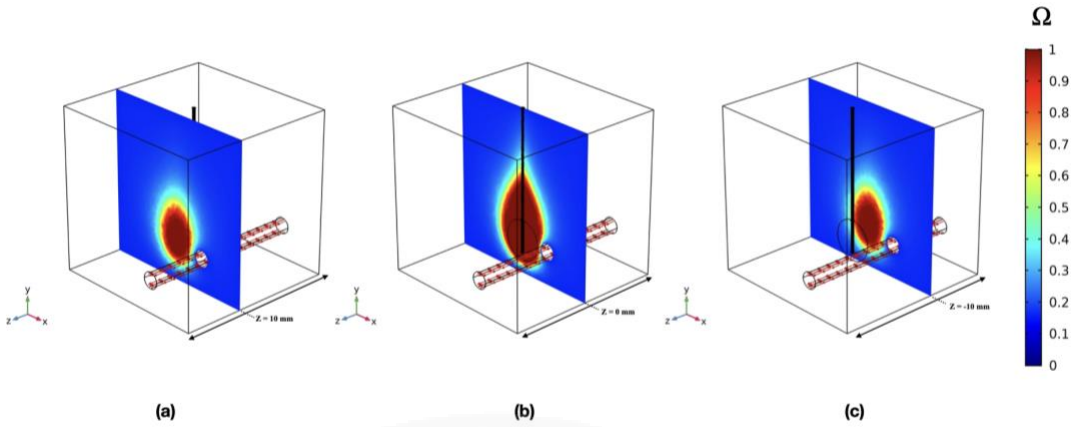

The fraction of necrotic tissue distribution on the XZ plane of the model with vertical vessel, (a) the plane at Z of 10 mm, (b) the plane at Z of 0 mm, (c) the plane at Z of -10 mm.

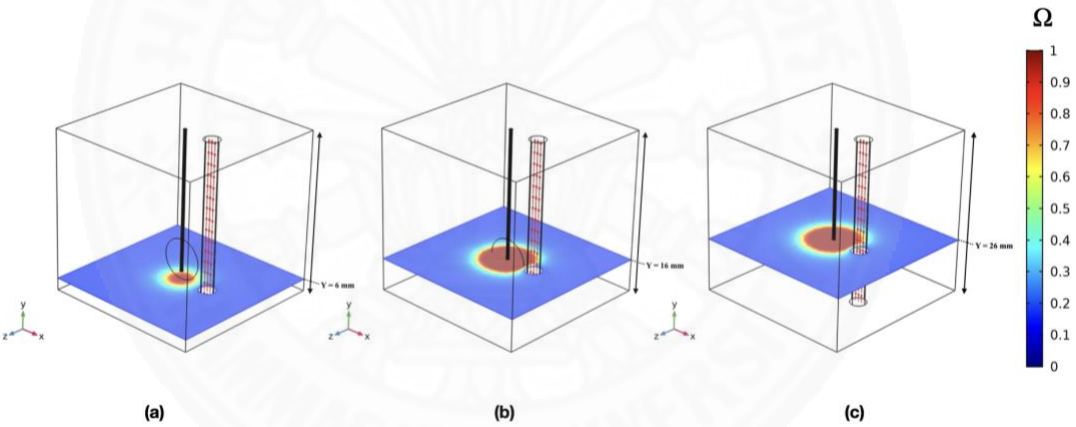

The fraction of necrotic tissue distribution on the XZ plane of the model with horizontal vessel, (a) the plane at Z of 10 mm, (b) the plane at Z of 0 mm, (c) the plane at Z of -10 mm.

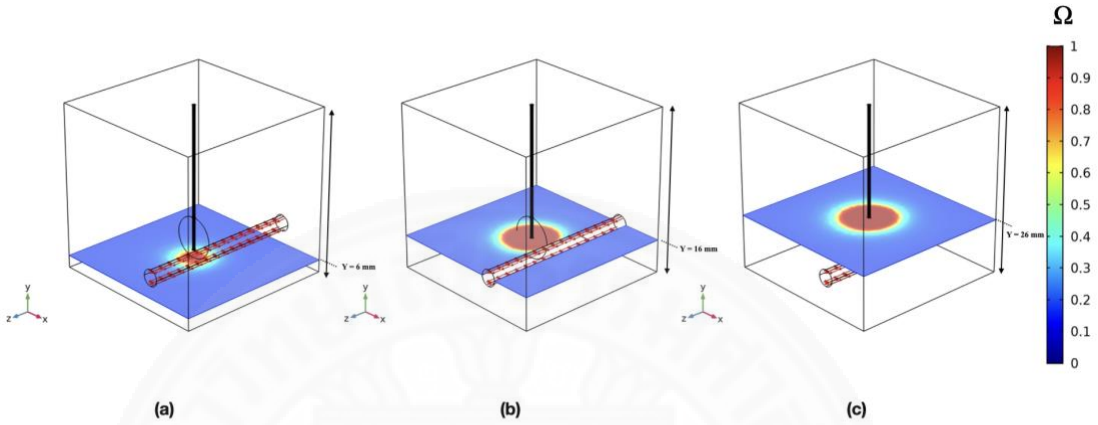

BIOGRAPHY

Name	Mr. Wutipong Preechaphonkul
Date of Birth	July 11, 1992
Educational Attainment	2014: Bachelor of Mechanical Engineering (The Second-Class Honours, B.Eng.)
Work Position	Researcher
Scholarship	Thailand Science Research and Innovation (TSRI) under the Royal Golden Jubilee Ph.D. Program (โครงการปริญญาเอกกาญจนาภิเษก, คปก.) contract No. PHD/0055/2558

PUBLICATIONS

Preechaphonkul, W., & Rattanadecho, P. (2021). The comparative of the performance for predicted thermal models during microwave ablation process using a slot antenna. Case Studies in Thermal Engineering, 100908.

Pongpakpien, S., Preechaphonkul, W., & Rattanadecho, P. (2020). Effects of Thermal and Electrical Properties on Porous Liver During Microwave Ablation Using Microwave Coaxial Slot Antenna. Journal homepage: http://iieta. org/journals/ijht, 38(2), 361-370.

Preechaphonkul, W., & Rattanadecho, P. (201). 3D Numerical Analysis of Focused Microwave Ablation for the Treatment of Patients with Localized Liver Cancer embedded with a Vertical and Horizontal Blood Vessel. Science & Technology Asia (Submitted).

AWARDS

Special Prize on Stage from Inventions Hong Kong & Invention Geneva, 47th, International Exhibition and Invention of Geneva 2019, Switzerland.

Silver medal, 47th International Exhibition and Invention of Geneva 2019, Switzerland.

Fig. 7.1 The granted award from International Exhibition and Invention of Geneva 2019

Work Experiences

2016-2020: Teaching Assistant in heat-transfer and special topic: numerical heat transfer courses in faculty of engineering, Thammasat University, Thailand